THE RADIO AND ELECTRONIC ENGINEER

The Journal of the Institution of Electronic and Radio Engineers

FOUNDED 1925 INCORPORATED BY ROYAL CHARTER 1961

"To promote the advancement of radio, electronics and kindred subjects by the exchange of information in these branches of engineering."

VOLUME 30 NOVEMBER 1965 NUMBER 5

IS TELEVISION DEVELOPMENT STAGNANT?

ONE of the criteria which may be used to indicate the rate of technical advance in any branch of engineering is the number of papers in the journals of learned societies and in the technical press. Some interesting statistics on the rapidly increasing flow of papers and articles following the invention of the laser were presented by Professor A. D. Booth in the February 1963 issue of *The Radio and Electronic Engineer* under the heading "New light on an old subject". Professor Booth's subsequent deductions were concerned mainly with the problem of information retrieval, but his data on the publication of papers in a very clearly defined field may be taken as confirming the validity of the criterion stated above.

What do other fields of electronic and radio engineering reveal when judged in this way? Certainly computer and control systems engineering are extremely active and in radio communication, too, there is much new work under way in many quarters. Papers on the semiconductor device and its engineering have come to preponderate over electron devices and circuits, although it would be a bold prophet who would foretell a complete 'take-over' in the foreseeable future.

It is, however, surprising to note that television engineering appears to be one of the least active of the many applications of electronics at the present time. Apart from judging the level of activity by the absolute number of papers published in *The Radio and Electronic Engineer*, the Institution's Papers Committee has another, supplementary guide, namely the number of outstanding papers which are reviewed each year when the award of Premiums is under consideration. From 1949 to 1958 the Sir Louis Sterling Premium for papers on television techniques was awarded without fail; its successor, the Rediffusion Television Premium, with only slightly more restricted terms of award confining it to papers on television broadcasting, has been awarded twice in six years, being withheld in 1960–61 and 1963–64. At the beginning of this year a new award was established, the P. Perring Thoms Premium for outstanding papers on advances in television reception, but here again no paper of high enough standard could be recommended.

Brief consideration of the plethora of papers in the 'fifties seems to indicate that innovations in television engineering were many and reference to the titles of award-winning papers which are listed in the Institution's *Year Book* bears this out. What has caused the apparent stagnation since 1960? Possibly there has been consolidation of the advances of the previous decade and consolidation is often a dull and not very 'newsworthy' process. More likely is it that the great new field, in Western Europe at any rate, of colour television has been inhibited by that continual uncertainty, the controversy of the systems—the technical press of other European countries appears to be similarly lacking in papers on television. The extension of television broadcasting in Europe to the u.h.f. bands—the subject of a recent joint conference in London—is of course a considerable engineering achievement but in many of its aspects represents development rather than true innovation.

As far as Great Britain is concerned, at the time of writing it seems probable that a Government pronouncement on colour television is imminent. As a corollary we may then hope and expect that there will be a spate of papers of high technical quality submitted to the Institution which will merit the award of these two Premiums. The substantial values of the television Premiums should provide incentives to television engineers from Great Britain and also from other countries to demonstrate that the pace of development in their chosen professional activity is anything but stagnant.

F. W. S.

INSTITUTION NOTICES

Conference on U.H.F. Television

The volume containing the twenty-eight contributions given at the Joint Conference on U.H.F. Television (held in London on 22nd and 23rd November) is now available for sale, price £2 10s. per copy. Remittances should be sent to the I.E.R.E. Publications Department, 8–9 Bedford Square, London, W.C.1.

C.E.I. Reception

The Chairman and Board Members of the Council of Engineering Institutions were hosts at a reception in the presence of Her Majesty The Queen and H.R.H. Prince Philip, Duke of Edinburgh, held at the Science Museum in London on 10th November last. Her Majesty was introduced to the thirteen presidents of Institutions and chairmen of the standing committees of the C.E.I. by Sir Robert Wynn-Edwards, Chairman of the Council. A short ceremony then followed when Her Majesty presented the Royal Charter granted to the Council to His Royal Highness as its Founder President.

Her Majesty then made a progress round the galleries of the Museum so that members of the Institutions could be introduced to her and to His Royal Highness by their Presidents. Colonel G. W. Raby presented to Her Majesty the Immediate Past-President of the Institution, Mr. J. Langham Thompson, and Mrs. Thompson, Professor Emrys Williams (Vice-President), Major-General L. H. Atkinson (Member of Council) and Mrs. Atkinson, and the Secretary, Mr. Graham D. Clifford, and Mrs. Clifford.

Each Institution was represented by approximately 50 members accompanied by their ladies, and there were some 300 official guests, including members of the Government and Opposition, representatives of the Armed Forces and Civil Service, industry, scientific and engineering bodies, universities, schools, local authorities and the Press.

Conference on 'Electronic Engineering in Oceanography'

The Institution is organizing what is believed to be the first Conference to be held in Europe on the applications of electronic engineering to oceanography. The Conference will be held at the University of Southampton between 19th and 22nd September 1966.

The enormous potentialities in this discipline for the ingenuity of electronic and radio engineers may readily be appreciated when it is realized that we probably know less about the deep oceans which extend over nearly three-quarters of the Earth's surface, than we do about outer space! In space research, light or radio waves are the principal means of investigation—in the oceans sound waves, or sonar, provide a valuable tool and one which will feature extensively in the programme. There are however many other techniques which can be employed as may be seen from the following list of subjects on which the Organizing Committee invites offers of papers:

Physical properties and conditions of seawater;

Unattended oceanographic stations—including sensors, recording, radio telemetering and mounting platforms;

Wave measurements and ocean current measurements;

Navigation problems (survey and position fixing);

Geophysical sensors (magnetometers, gravimeters, seismographs);

Automatic recording and analysis of data on ships;

Acoustic devices (for biological research, geological and geophysical research, and telemetering and other applications).

A feature of the Conference will be the opportunity which it will provide for oceanographers to state their problems as users and for electronic engineers to put forward means of solution, and papers will therefore be welcomed from both points of view.

Requests for further information and offers of papers preferably accompanied by a 200-word synopsis) should be sent to the Secretary of the Conference on Electronic Engineering in Oceanography, I.E.R.E., 8–9 Bedford Square, London, W.C.1.

Institution Visit to R.E.M.E., Arborfield

The Institution's Technical Committee is pleased to announce that, by kind permission of the Commandant, Colonel H. G. Frost, A.M.I.E.R.E., a visit has been arranged to the School of Electronic Engineering, R.E.M.E., Arborfield, Berkshire.

The School, which trains all R.E.M.E. officers and technicians in electronics technology and equipments, has recently been rebuilt and is probably one of the most modern schools of its type in the country. Instruction given includes all levels from basic recruit training in electronics fundamentals, to post-graduate-level courses for officers holding university degrees in engineering. Equipment training covers communications, radar, guided weapons and miscellaneous electronic equipments.

The visit will take place on Friday, 17th December and will occupy a whole day, transport being arranged from appropriate railway stations. Members will be entertained to lunch and tea in the Headquarters Officers' Mess.

Members wishing to take part in this visit are asked to apply without delay to the Institution at 8-9 Bedford Square, London, W.C.1, as the size of the Institution party will necessarily be restricted.

U.D.C. 621.372.853.1

Dielectric Loaded Waveguides—a Review of Theoretical Solutions

Part II: Propagation Through Dielectric Loaded Waveguides (*continued*)†

By

S. K. CHATTERJEE, M.Sc. AND (Mrs.) R. CHATTERJEE, Ph.D., M.S.E., M.Sc.

10. Circular Cylindrical Guide Filled Coaxially with Two Different Dielectrics

The propagation of microwaves through a circular cylindrical metallic guide filled completely with two different dielectrics (Fig. 21) has been treated as a boundary value problem.[24–26, 29, 30]‡ The characteristic equation for the H_{mn} and E_{mn} modes are respectively as follows

$$\frac{J'_m(k_2r_2)Y'_m(k_1r_1)J'_m(k_1r_2)-J'_m(k_2r_2)J'_m(k_1r_1)Y'_m(k_1r_2)}{J'_m(k_1r_2)Y'_m(k_1r_1)-J'_m(k_1r_1)Y'_m(k_1r_2)} = J'_m(k_2r_2)\frac{\sin\beta_2 z}{\sin\beta_1 z}\exp(j\beta z) \quad \text{.....(145a)}$$

and

$$\frac{J'_m(k_2r_2)}{J_m(k_2r_2)}\left[\frac{Y_m(k_1r_1)J_m(k_1r_2)-Y_m(k_1r_2)J_m(k_1r_1)}{J'_m(k_1r_2)Y_m(k_1r_1)}\right] = -\frac{k_2^2\varepsilon}{k^1\beta^1}\exp(j\beta z) \quad \text{.....(145b)}$$

where $k=\sqrt{\omega^2\mu\varepsilon+\gamma^2}$, $k'=k_2/k_1$, $\beta'=\beta_1/\beta_2$. k_1 and k_2 are the values of k in the two dielectric media. The values of k_2 and k_1 found from the above equation yield the other propagation characteristics of the two modes in the two media. For instance, in the case of H_{01} and E_{11} modes, the ratio of the phase velocities in the two media are

$$\left(\frac{c_{p1}}{c_{p2}}\right)_{H_{01}} = \sqrt{\frac{\mu_2\varepsilon_2}{\mu_1\varepsilon_1}}\left[1-\frac{9\pi^2}{16\omega^2\mu_2\varepsilon_2 r_2^2}\right]^{\frac{1}{2}} \simeq \sqrt{\frac{\varepsilon_2}{\varepsilon_1}}\left[1-\frac{9\pi^2}{32\omega^2\mu_2\varepsilon_2 r_2^2}\right] \quad \text{.....(146a)}$$

$$\left(\frac{c_{p1}}{c_{p2}}\right)_{E_{11}} \simeq \sqrt{\frac{\varepsilon_2}{\varepsilon_1}}\frac{\left[1-\frac{81\pi^2}{32\omega^2\mu_2\varepsilon_2 r_2^2}\right]}{\left[1-\frac{\pi^2}{2\omega^2\mu_1\varepsilon_1(r_1-r_2)^2}\right]} \quad \text{.....(146b)}$$

In the case of both the H and E modes, the phase velocities can be adjusted by adjusting the values of ε_1 and ε_2. For example by increasing ε_2 compared to ε_1, the velocity of the wave in the second medium may be considerably lowered. It is also observed that in the case of the H_{01} wave, the ratio of the phase velocities in the two media is independent of the radius of the outer dielectric and depend only on the radius of the inner dielectric. But in the case of the E_{11} wave, the ratio depends on the radii of both the media. The equations also show that the relative phase velocities in the two media can be adjusted to a preassigned value by a suitable choice of the dielectric constants and radii of the two dielectrics.

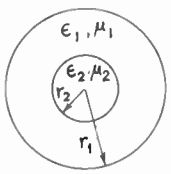

Fig. 21. Circular cylindrical guide filled coaxially with two dielectrics.

The characteristic equations for the E_{01} and H_{01} modes are

$$\frac{J_1(k_2r_2)}{k_2r_2J_0(k_2r_2)} = \frac{\varepsilon_1}{\varepsilon_2}\frac{1}{k_1r_2}\frac{J_0\left(\frac{r_1}{r_2}k_1r_2\right)Y_1(k_1r_2)-J_1(k_1r_2)Y_0\left(\frac{r_1}{r_2}k_1r_2\right)}{J_0\left(\frac{r_1}{r_2}k_1r_2\right)Y_0(k_1r_2)-J_0(k_1r_2)Y_0\left(\frac{r_1}{r_2}k_1r_2\right)} \quad \text{.....(147)}$$

for the E_{01} mode and

$$\frac{J_1(k_2r_2)}{k_2r_2J_0(k_2r_2)} = \frac{1}{k_1r_2}\frac{J_1(k_1r_2)Y_1\left(\frac{r_1}{r_2}k_1r_2\right)-J_1\left(\frac{r_1}{r_2}k_1r_2\right)Y_1(k_1r_2)}{J_0(k_1r_2)Y_1\left(\frac{r_1}{r_2}k_1r_2\right)-J_1\left(\frac{r_1}{r_2}k_1r_2\right)Y_0(k_1r_2)} \quad \text{.....(148)}$$

for the H_{01} mode

† The first three sections of Part II were published in the October issue of *The Radio and Electronic Engineer* (30, No. 4, pp. 195–205).

‡ References will be found at the end of Part III of the paper.

where

$$k_1^2 r_2^2 = k_2^2 r_2^2 - \left(\varepsilon_2 - \frac{\varepsilon_1}{\varepsilon_0}\right)\frac{4\pi^2 r_2^2}{\lambda_0^2}$$

$$k_1^2 = k_2^2 - \left(\varepsilon_2 - \frac{\varepsilon_1}{\varepsilon_0}\right)\frac{4\pi^2}{\lambda_0^2} \qquad \text{.....(149)}$$

The wavelength λ_g in the guide is found from the relation

$$\frac{4\pi^2 r_2^2}{\lambda_g^2} = \frac{\varepsilon_1}{\varepsilon_0}\frac{4\pi^2 r_2^2}{\lambda_0^2} - k_1^2 r_2^2 \qquad \text{.....(150)}$$

By determining k_2 and k_1 from (147), (148) and (149), λ_g can be found from eqn. (150). Figure 22 shows the variation of λ_g/r_2 vs. λ_0/r_2 for different values of $\varepsilon_2/\varepsilon_0$ and r_1/r_2 and with $\varepsilon_1 = \varepsilon_0$ for the E_{01} mode.

Bucholz[55] has also treated the same case. The variation of $\lambda_g/2\pi r_1$ vs. $\lambda_0/2\pi r_1$ for $\varepsilon_2/\varepsilon_0 = 16$ and $r_1/r_2 = 5$ has been plotted for the H_{10} and H_{20} modes in Fig. 23. The variation for $r_1/r_2 = 5$ for the E_{10} and E_{20} modes is shown in Fig. 24. Treating the case of E_{01} mode in the same structure, Frankel[14] also has derived the characteristic equation which gives k_1 and k_2.

The peak power transmitted through the composite guide is

$$P_M = \int_0^{r_1}\int_0^{2\pi} E_r H_\theta^* r\,d\theta\,dr \qquad \text{.....(151)}$$

The maximum value of the electric field at the axis is given by the following expression[14]

$$E_{z0} = \left|\frac{k_2}{\omega\varepsilon_2}\left(\frac{P_M\omega\varepsilon_1}{2\pi\beta F}\right)^{\frac{1}{2}}\right| \qquad \text{.....(152)}$$

where $\beta_1 = \beta = \beta_2$ the phase constant and

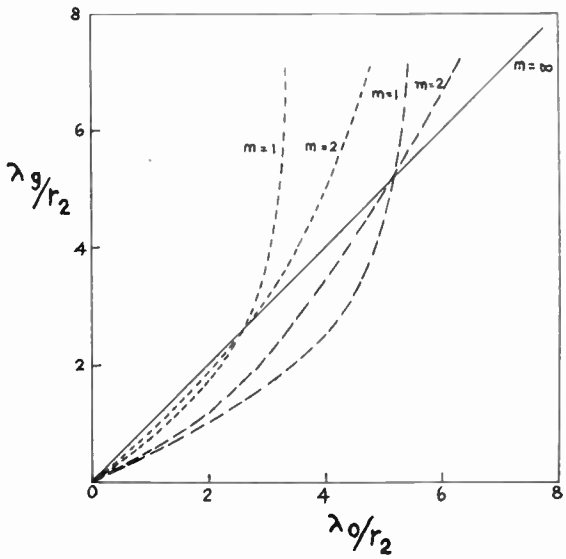

Fig. 22. Guide wavelength for E_{01} mode as a function of λ_0 for different values of dielectric constant of the slab. (Ref. 13.)

The following example will give an idea about the dimensions of the guide when a E_{01} wave of angular frequency $\omega = 3\times10^{10}$ radians per second is required to travel at a phase velocity of 3×10^7 metres per second. If the outer dielectric possesses a dielectric constant $k_{e1} = 200$ and the inner dielectric is air and r_2 is taken to be 2 mm, then it is found that $\beta = 10^3$ per metre, $k_1 = 10^3$, $k_2 = j10^3$ and $k_1 r_1 =$ 0·73, 3·78, 6·89, . . . So, r_1 = 0·7, 3·8, 6·9 . . . mm. Considering $r_1 = 3{\cdot}8$ mm as the smallest available value of $r_1 > r_2$, $K_A = j153{\cdot}3$, $K_B = j812{\cdot}5$.

$$F = F(r_1, r_2, \varepsilon_1, \varepsilon_2) = \frac{1}{k_2^2}F_1(k_2 r_2) + \frac{K_A^2}{k_1^2}[F_1(k_1 r_1) - F_1(k_1 r_2)] +$$

$$+ \frac{2K_A K_B}{k_1^2}[F_3(k_1 r_1) - F_3(k_1 r_2)] + \frac{K_B^2}{k_1^2}[F_2(k_1 r_1) - F_2(k_1 r_2)] \qquad \text{.....(153)}$$

where

$$F_1(s) = \frac{s^2}{2}\{[J_1(s)]^2 - J_0(s)J_2(s)\}$$

$$F_2(s) - F_2(u) = \frac{s^2}{2}\{[Y_1(s)]^2 - Y_0(s)Y_2(s)\} - \frac{u^2}{2}\{[Y_1(u)]^2 - Y_0(u)Y_2(u)\}$$

$$F_3(s) = \tfrac{1}{2}\{s^2[Y_1(s)J_1(s) + Y_2(s)J_2(s)] - s[Y_1(s)J_2(s) + Y_2(s)J_1(s)]\} \qquad \text{.....(154)}$$

$$K_A = -\frac{\pi\varepsilon_1 r_2}{2}\begin{vmatrix} \frac{k_2}{\varepsilon_2}J_0(r_2 k_2) & \frac{k_1}{\varepsilon_1}Y_0(k_1 r_2) \\ J_1(k_2 r_2) & Y_1(k_1 r_2) \end{vmatrix} \qquad \text{.....(155)}$$

$$K_B = -\frac{\pi\varepsilon_1 r_2}{2}\begin{vmatrix} \frac{k_1}{\varepsilon_1}J_0(k_1 r_2) & \frac{k_2}{\varepsilon_2}J_0(k_2 r_2) \\ J_1(k_1 r_2) & J_1(k_1 r_2) \end{vmatrix} \qquad \text{.....(156)}$$

The field components for the above example are given by the following expressions[14]

$$E_{z1} = A_2\,2842[J_0(k_1 r)+5{\cdot}30\,Y_0(k_1 r)]\exp(-j\beta z)$$
$$E_{r1} = jA_2\,2892[J_1(k_1 r)+5{\cdot}30\,Y_1(k_1 r)]\exp(-j\beta z)$$
$$H_{\phi 1} = jA_2\,153{\cdot}3[J_1(k_1 r)+5{\cdot}30\,Y_1(k_1 r)]\exp(-j\beta z)$$
$$E_{z2} = A_2\,3703\,J_0(k_2 r)\exp(-j\beta z) \qquad \text{.....(157)}$$
$$E_{r2} = A_2\,3774\,J_1(k_2 r)\exp(-j\beta z)$$
$$H_{\phi 2} = A_2 J_1(k_2 r)\exp(-j\beta z)$$

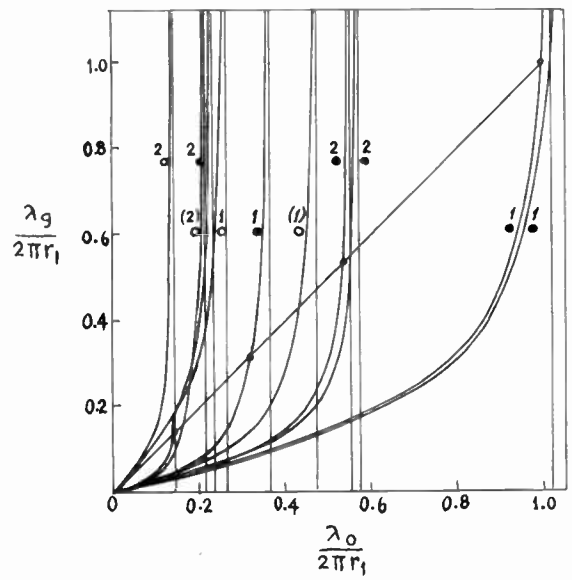

Fig. 23. Guide wavelengths as a function of λ_0 for H_{10} and H_{20} modes. (Ref. 55.)

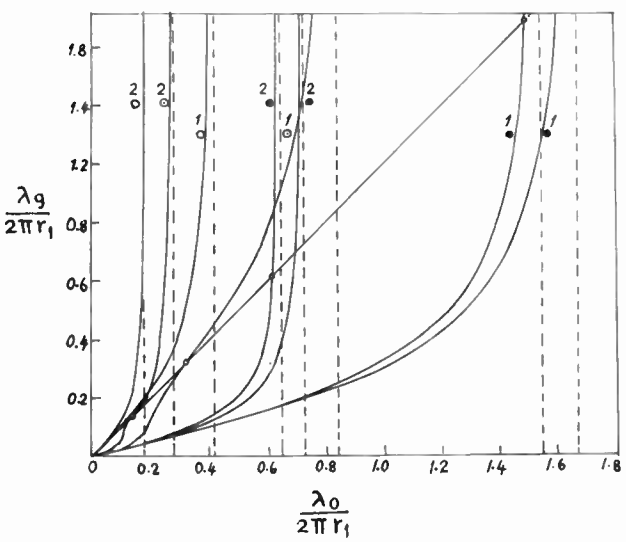

Fig. 24. Guide wavelength as a function of λ_0 for E_{10} and E_{20} modes. (Ref. 55.)

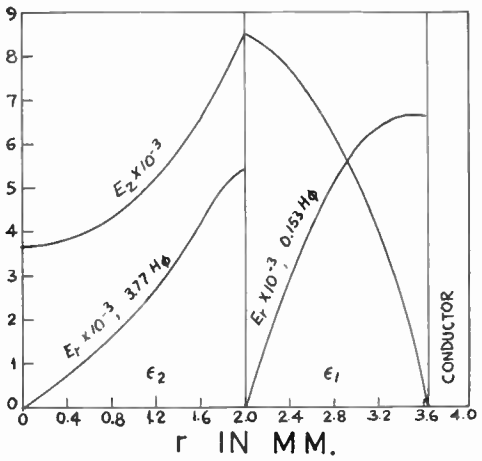

Fig. 25. Distribution of field. (Ref. 14.)

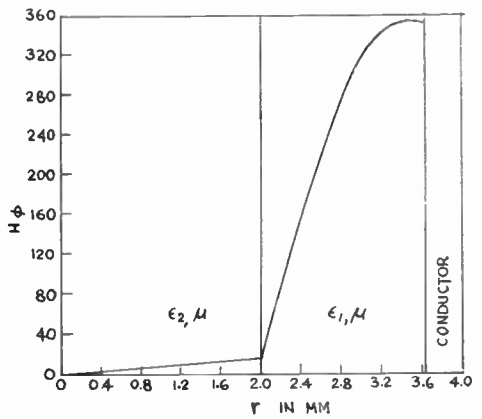

Fig. 26. Distribution of magnetic field intensity. (Ref. 14.)

The field components are plotted in Figs. 25 and 26. It is evident that the electric vectors have the same order of magnitude in both dielectrics, while the magnetic vector is very small in the central dielectric. This shows that most of the power is propagated in the outer dielectric. The value of the parameter F has been calculated in the above example and is

$$F = -0{\cdot}00037-0{\cdot}3475 = -0{\cdot}3479$$

Since, the transmitted power is related linearly to F, it is obvious that only about 0·1% of the total power is propagated in the central region. Using the above value of F, the value of the axial electric field intensity is

$$E_{z0} = 5{\cdot}77(P_M)^{\frac{1}{2}} \text{ volts per cm.}$$

Banos, Saxon and Gruen[18] have studied the frequency dependence of the phase velocity in the guide for the lowest E mode. The power flow and the field distribution curves are same as given by Frankel.[14] The following two typical cases serve as examples.

(i) $r_1/r_2 = 3$, $k_{e2} = 1$, $k_{e1} = 100$. It is found that the inner radius (r_2 in metres) required to produce a

phase velocity $c_p = 0{\cdot}8c$ of E_{01} wave can be calculated from $\omega^2 r_2^2 = 8{\cdot}55 \times 10^{14}$ for any given ω. The total power flow in this case is computed from the following relation

$$P = 0{\cdot}0156|E_{0z}|^2 r_2^2 \text{ watts} \qquad \text{.....(158)}$$

The power ratio in the two media is $P_2/P_1 = 0{\cdot}0038$, or the power flow in the inner media (2) is about 0·4%, i.e. most of the power flows through the outer dielectric.

(ii) In the converse case, $k_{e1} = 1$, $k_{e2} = 100$, $r_1/r_2 = 3$, to produce a phase velocity $c_p = 0{\cdot}8c$ of the E_{01} wave, the inner dielectric radius is calculated from

$$\omega^2 r_2^2 = 1{\cdot}10 \times 10^{16}$$

for any given ω. The total power flow is given by the relation

$$P = 0{\cdot}0344|E_{0z}|^2 r_2^2 \text{ watts} \qquad \text{.....(159)}$$

The ratio of power flowing in the two media is $P_2/P_1 =$ 0·031 or the power flow in the inner media is about 3%, which again shows that most of the power flows in the outer dielectric. The application of such a guide for producing slow wave by adjusting dielectric constants and relative dimensions of the two media was also suggested by Bruck and Wicher.[16]

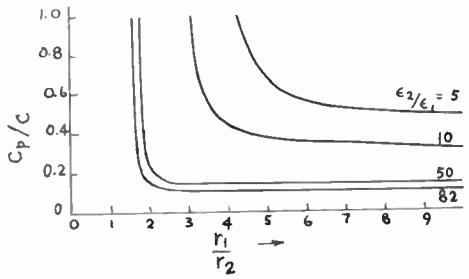

Fig. 27. Phase velocity as a function of r_1/r_2 for different values of the dielectric constant of the slab. (Ref. 17.)

Teasdale and Higgins[17] have also studied the same problem by field theory approach. Figure 27 shows the variation of c_p/c as a function of r_1/r_2 for different values of $k_{e2} = \varepsilon_2/\varepsilon_0$ for $\omega r_2/c = 0{\cdot}3$ for E_{01} wave. It is concluded that in any guide for sufficiently high frequencies, most of the energy propagates in the medium with higher value of $\mu\varepsilon$. Teasdale and Crawford[20] have also studied the same problem by the field theory and have derived the characteristic equation to determine the cut-off frequency for E_{01} wave. The characteristic equation is

$$\phi\left(\sqrt{\frac{k_{e2}}{k_{e1}}}\, k_1 r_2\right) = ct(k_1 r_2, k_1 r_1) \qquad \text{.....(160)}$$

which governs resonance. For a specified value of r_1/r_2 and k_{e2}/k_{e1} the above equation can be solved for

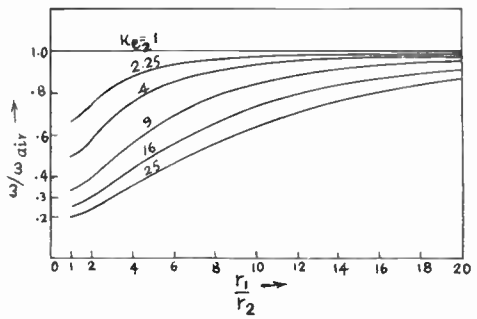

Fig. 28. Variation of cut-off frequency with respect to r_1/r_2 for different values of k_{e2}. (Ref. 20.)

$k_1 r_2$ for which k_1 is determined. Hence, the resonant frequency ω can be calculated from the relation

$$\omega = \frac{k_1 c}{\sqrt{k_{e1}}} = \frac{\frac{r_1}{r_2} k_1 r_2 c}{r_1 \sqrt{k_{e1}}} \qquad \text{.....(161)}$$

The lowest cut-off frequency of the same guide containing air only is given by the relation

$$\omega_{air} = k_1 c = \frac{2{\cdot}405c}{r_1} \qquad \text{.....(162)}$$

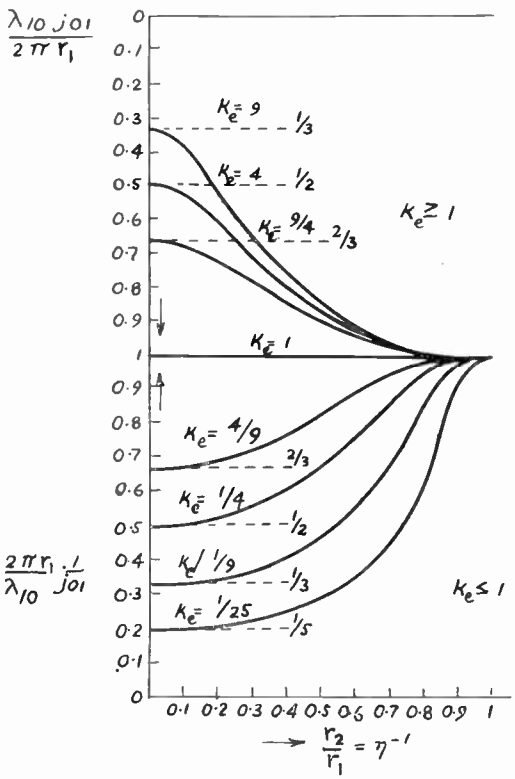

Fig. 29. Variation of cut-off frequency for E_{01} wave with r_2/r_1 for different values of $\varepsilon_2/\varepsilon_1$. (Refs. 54 and 55.)

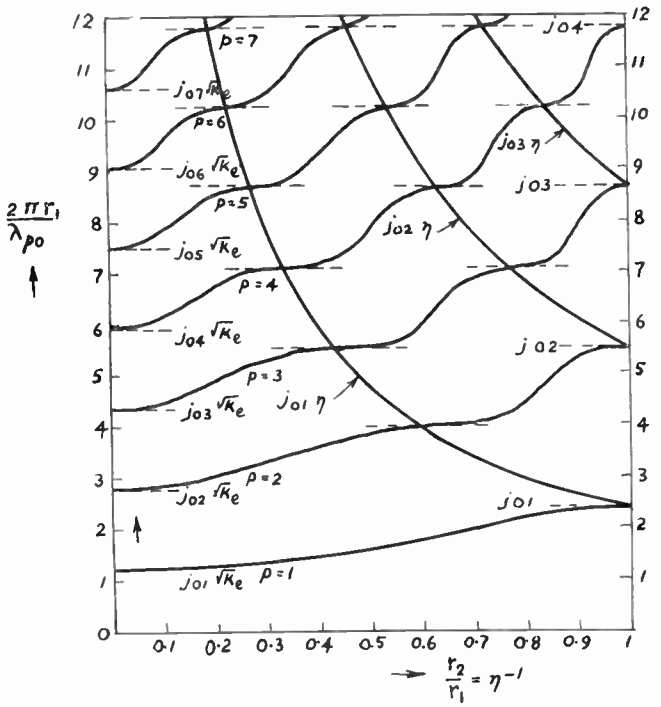

Fig. 30. Variation of cut-off frequency for E_{0p} wave with respect to r_2/r_1. (Refs. 54 and 55.)

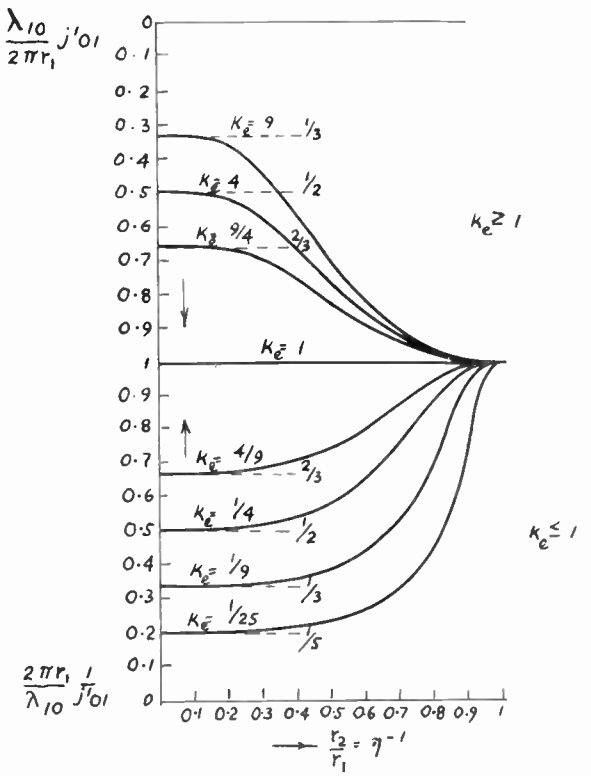

Fig. 31. Variation of cut-off frequency for H_{01} wave with respect to r_2/r_1. (Refs. 54 and 55.)

Thus the normalized resonant frequency is[20]

$$\frac{\omega}{\omega_{air}} = \frac{(r_1/r_2)k_1 r_2}{2{\cdot}405\sqrt{k_{e1}}} \qquad \text{.....(163)}$$

Figure 28 shows the variation of ω/ω_{air} with r_1/r_2 for various values of k_{e2} when medium 1 is air ($k_{e1} = 1$). Chambers[54] has also discussed the same problem and has given graphs showing the cut-off frequencies for H and E modes as shown in Fig. 29. The cut-off frequency is defined in terms of the wavelength to which it corresponds in an unbounded space composed of medium 2 where j_{0p} and j'_{0p} are defined by the roots of the relations

$$\begin{aligned} J_0(j_{0p}) &= 0 \\ J'_0(j'_{0p}) &= 0 \end{aligned} \qquad \text{.....(164)}$$

Figure 30 shows the cut-off frequency for E_{0p} waves for varying values of r_2/r_1 with $\varepsilon_1 = 4\varepsilon_2$. Figures 31 and 32 give the corresponding results for the H_{01} and H_{0q} waves respectively.

It can be shown[25] that a guide filled with two coaxial dielectrics can support a pure E or H mode if it is circularly symmetric. For the propagation of higher order modes it is necessary that both the E and H waves coexist in order that the boundary conditions may be satisfied. This means that both the longitudinal components E_z and H_z should be present.

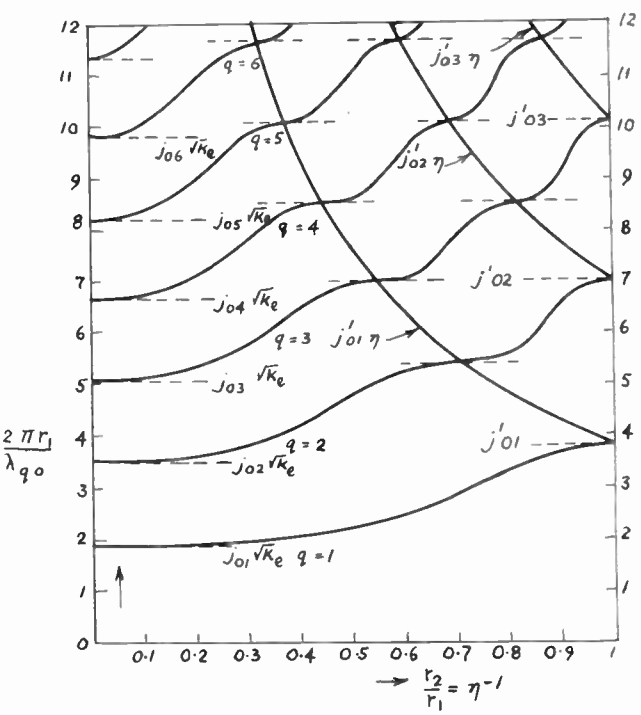

Fig. 32. Variation of cut-off frequency for H_{0q} wave with respect to r_2/r_1. (Refs. 54 and 55.)

The resultant wave is $(HE)_{mn}$ or $(EH)_{mn}$ according as H wave predominates over E wave or vice versa respectively. By rewriting the field components (eqn. (28)) for the two media and applying proper boundary conditions at the two interfaces inside the guide, all the constants in the equations for field components are expressed in terms of A_2 and A_2' as follows

$$\begin{aligned} A_1 &= A_2 k_3^2 \exp(\gamma_3 z) f(k_1, k_2, r_1, r_2) \\ B_1 &= A_2 k_3^2 \exp(\gamma_3 z) g(k_1, k_2, r_1, r_2) \\ A_1' &= A_2' k_4^2 \exp(\gamma_3 z) f(k_1, k_2, r_1, r_2) \\ B_1' &= A_2' k_4^2 \exp(\gamma_3 z) g(k_1, k_2, r_1, r_2) \end{aligned} \quad \text{.....(165)}$$

where

$$k_3^2 = \frac{k_2^2}{k_1^2}, \quad k_4^2 = \frac{k_2^2 - \dfrac{2m^2}{r_2^2}}{k_1^2 - \dfrac{2m^2}{r_2^2}}, \quad \gamma_3 = \gamma_1 - \gamma_2 \quad \text{.....(166)}$$

$$\begin{aligned} f &= \frac{J_m(k_2 r_2) Y_m(k_1 r_1)}{J_m(k_1 r_2) Y_m(k_1 r_1) - J_m(k_1 r_1) Y_m(k_1 r_2)} \\ g &= \frac{J_m(k_2 r_2) J_m(k_1 r_1)}{J_m(k_1 r_1) Y_m(k_1 r_2) - J_m(k_1 r_2) Y_m(k_1 r_1)} \end{aligned} \quad \text{.....(167)}$$

The values of A_2 and A_2' are found in terms of the peak power flow through the guide from the following equation:

$$\hat{P}_z = \int_{r=r_2}^{r=r_1} \int_{\theta=0}^{2\pi} [E_{r1}^{e,h} H_{\theta 1}^{e,h*} - E_{\theta 1}^{e,h} H_{r1}^{e,h*}] r \, d\theta \, dr + \int_{r=0}^{r_2} \int_{\theta=0}^{2\pi} [E_{r2}^{e,h} H_{\theta 2}^{e,h*} - E_{\theta 2}^{e,h} H_{r2}^{e,h*}] r \, d\theta \, dr \quad \text{.....(168}$$

This yields the field components in the two media in terms of known factors as follows[29]

$$E_{r1}^{e,h} = jP \left[k_3^2 \gamma_1 k_1 \{ g Y_m'(k_1 r) - f J_m'(k_1 r) \} + C_m k_4^2 \omega \mu_1 \frac{m}{r} \{ g Y_m(k_1 r) - f J_m(k_1 r) \} \right] \cos m\theta \exp(-\gamma_2 z)$$

$$E_{\theta 1}^{e,h} = P \left[k_3^2 \gamma_1 \frac{m}{r} \{ f J_m(k_1 r) + g Y_m(k_1 r) \} + jC_m \omega \mu_1 k_1 k_4^2 \{ f J_m'(k_1 r) + g Y_m'(k_1 r) \} \right] \sin m\theta \exp(-\gamma_2 z)$$

$$E_{z1}^{e,h} = P[k_1^2 k_3^2 \{ f J_m(k_1 r) + g Y_m(k_1 r) \}] \cos m\theta \exp(-\gamma_2 z)$$

$$H_{r1}^{e,h} = -P \left[jk_1 k_3^2 \omega \varepsilon_1 \{ f J_m'(k_1 r) + g Y_m'(k_1 r) \} + C_m \gamma_1 k_4^2 \frac{m}{r} \{ f J_m(k_1 r) + g Y_m(k_1 r) \} \right] \cos m\theta \exp(-\gamma_2 z)$$

$$H_{z1}^{e,h} = C_m P k_4^2 \left(k_1^2 - \frac{2m^2}{r^2} \right) [f J_m(k_1 r) + g Y_m(k_1 r)] \sin m\theta \exp(-\gamma_2 z)$$

$$E_{r2}^{e,h} = -jP \left[\gamma_2 k_2 J_m'(k_2 r) + C_m \omega \mu_2 \frac{m}{r} J_m(k_2 r) \right] \cos m\theta \exp(-\gamma_2 z)$$

$$E_{\theta 2}^{e,h} = P \left[-\gamma_2 \frac{m}{r} J_m(k_2 r) + jC_m \omega \mu_2 k_2 J_m'(k_2 r) \right] \sin m\theta \exp(-\gamma_2 z)$$

$$E_{z2}^{e,h} = P[k_2^2 J_m(k_2 r)] \cos m\theta \exp(-\gamma_2 z)$$

$$H_{r2}^{e,h} = -P \left[\omega \varepsilon_2 \frac{m}{r} J_m(k_2 r) + C_m \gamma_2 k_2 J_m'(k_2 r) \right] \sin m\theta \exp(-\gamma_2 z)$$

$$H_{\theta 2}^{e,h} = -P \left[j\omega \varepsilon_2 k_2 J_m'(k_2 r) + C_m \gamma_2 \frac{m}{r} J_m(k_2 r) \right] \cos m\theta \exp(-\gamma_2 z)$$

$$H_{z2}^{e,h} = PC_m \left(k_2^2 - \frac{2m^2}{r^2} \right) [J_m(k_2 r)] \sin m\theta \exp(-\gamma_2 z) \quad \text{.....(169)}$$

where C_m represents a constant involving the electrical properties and radial dimensions of the two media and is given by the following expression.

$$C_m = \frac{-\varepsilon_1 \gamma_1 k_1 k_3^2 [f J_m'(k_1 r_2) + g Y_m'(k_1 r_2)] - \varepsilon_2 \gamma_2 k_2 J_m'(k_2 r_2)}{\omega \mu_1 \varepsilon_1 \dfrac{m}{r_2} k_4^2 [f J_m(k_1 r_2) + g Y_m(k_1 r_2)] - \omega \mu_2 \varepsilon_2 \dfrac{m}{r_2} J_m(k_2 r_2)} \quad \text{.....(170)}$$

and P represents the peak power flow through the guide. By applying proper boundary conditions, the characteristic equation for the $(EH)_{mn}$ mode is obtained from eqns. (169) as follows

$$\frac{Y_m(k_1 r_1)}{Y'_m(k_1 r_1)} = \frac{Y_m(k_1 r_2)J_m(k_1 r_1)\left\{\mu_1\varepsilon_1 - \frac{\mu_2\varepsilon_2}{k_3^2}\right\} + \frac{\mu_2\varepsilon_2}{k_3^2}\, Y_m(k_1 r_1)J_m(k_1 r_2)}{Y_m(k_1 r_2)J'_m(k_1 r_1)\left\{\mu_1\varepsilon_1 - \frac{\mu_2\varepsilon_2}{k_4^2}\right\} + \frac{\mu_2\varepsilon_2}{k_4^2}\, Y'_m(k_1 r_1)J_m(k_1 r_2)} \qquad \text{.....(171)}$$

The propagation of this mode requires that $\gamma_1 = \gamma_2$. The above equation (171) in conjunction with the relation

$$k_1^2 - k_2^2 = \omega^2(\mu_1\varepsilon_1 - \mu_2\varepsilon_2) \qquad \text{.....(172)}$$

can be solved graphically for some definite modes to give k_1 and k_2 in terms of the radial dimensions and the electrical constants of the two dielectrics. The validity of the above equation can be tested as follows.

For a single dielectric (say air) bounded by perfectly conducting boundaries

$$\mu_1 = \mu_2 = \mu_0 \qquad \varepsilon_1 = \varepsilon_2 = \varepsilon_0$$
$$k_3 = k_4 = 1 \qquad r_1 = r_2 = r_0$$

Hence eqn. (171) reduces to the following identity

$$\frac{Y_m(k_1 r_0)}{Y'_m(k_1 r_0)} = \frac{Y_m(k_1 r_0)}{Y'_m(k_1 r_0)} \qquad \text{.....(173)}$$

which shows that the general equation is correct.

The propagation characteristics of a circular waveguide containing an axial dielectric rod have also been investigated by Clarricoats.[125] Approximate and exact graphical methods have been used to establish the mode spectrum. The phase change coefficients of bounded and unbounded dielectric rod exhibit close correlation over a wide range of rod diameter. The table below shows $2r_1/\lambda_0$ for cut-off ($\bar{\beta} = 0$) for H and E modes as computed by Clarricoats.[125] The propagating and nonpropagating modes are denoted respectively by P and NP over the range $0 < r_1/r_0 < 1$ and $\bar{\varepsilon} = 10$ where r_0 represents the radius of the circular guide.

Table 5

Normalized dielectric rod diameter for $\bar{\beta} = 0$ for H and E modes

	$2r_0/\lambda_0 = 0{\cdot}685$			$2r_0/\lambda_0 = 0{\cdot}8$		
Mode	$\bar{\mu} = 0{\cdot}25$	$\bar{\mu} = 1{\cdot}0$	$\bar{\mu} = 1{\cdot}6$	$\bar{\mu} = 0{\cdot}25$	$\bar{\mu} = 1{\cdot}0$	$\bar{\mu} = 1{\cdot}6$
H_{11}	P	P	P	P	P	P
H_{12}	NP	0·440	0·325	NP	0·395	0·31
H_{13}	NP	NP	0·6	NP	NP	0·60
E_{11}	0·490	0·240	0·205	0·460	0·230	0·195
E_{12}	NP	0·585	0·465	NP	0·66	0·445
E_{13}	NP	NP	NP	NP	NP	0·78

The distribution of power between the inside and outside of the rod has also been calculated by Clarricoats[125] and is given by the following expression:

$$\frac{P_i}{P_o} = -\left(\frac{k_1}{k}\right)^4 \frac{(\bar{\varepsilon} + \bar{\mu}\bar{A}^2)T_1 + \bar{\Lambda}\left(\frac{1}{\bar{\beta}}\,\bar{\mu}\bar{\varepsilon} + \bar{\beta}\right)}{(\bar{\varepsilon}_1 T_3 + \bar{\mu}_1 \bar{\Lambda}^2 T_4) + \bar{\Lambda}\left(\frac{1}{\bar{\beta}}\,\bar{\mu}_1\bar{\varepsilon}_1 + \bar{\beta}\right)} \qquad \text{.....(174)}$$

$$T_3 = \left[\frac{2}{\pi}\frac{J_1(k_1 r_0)Y_1(k_1 r_0) + \frac{2}{\pi^2}}{\sigma^2(k_1 r_1)} + \frac{J_1(k_1 r_0)Y_1(k_1 r_1)S(k_1 r_1)}{\sigma(k_1 r_1)} - \frac{k_1 r_1 J'_1(k_1 r_1)Y_1(k_1 r_0)}{\sigma(k_1 r_1)} - \right.$$
$$\left. - \tfrac{1}{2}S^2(k_1 r_1) - \tfrac{1}{2}(k_1^2 r_1^2 - 1)\right]$$

$$T_4 = \left[\frac{2}{\pi}\frac{J'_1(k_1 r_0)Y'_1(k_1 r_0) + \frac{2}{\pi^2}\left(1 - \frac{1}{k_1^2 r_0^2}\right)}{\rho^2(k_1 r_1)} + \frac{J'_1(k_1 r_0)Y_1(k_1 r_1)R(k_1 r_1)}{\rho(k_1 r_1)} - \right.$$
$$\left. - \frac{k_1 r_1 J'_1(k_1 r_1)Y'_1(k_1 r_0)}{\rho(k_1 r_1)} - \tfrac{1}{2}R^2(k_1 r_1) - \tfrac{1}{2}(k_1^2 r_1^2 - 1)\right] \qquad \text{.....(175)}$$

where

$$\sigma(k_1 r_1) = J_1(k_1 r_1)Y_1(k_1 r_0) - Y_1(k_1 r_1)J_1(k_1 r_0)$$
$$\rho(k_1 r_1) = J_1(k_1 r_1)Y'_1(k_1 r_0) - Y_1(k_1 r_1)J'_1(k_1 r_0)$$
$$R(k_1 r_1) = (k_1 r_1)\frac{J'_n(k_1 r_1)Y'_n(k_1 r_0) - J'_n(k_1 r_0)Y'_n(k_1 r_1)}{J_n(k_1 r_1)Y'_n(k_1 r_0) - J'_n(k_1 r_0)Y_n(k_1 r_1)}$$

$$S(k_1 r_1) = (k_1 r_1)\,\frac{J_n'(k_1 r_1)Y_n(k_1 r_0) - J_n(k_1 r_0)Y_n'(k_1 r_1)}{J_n(k_1 r_1)Y_n(k_1 r_0) - J_n(k_1 r_0)Y_n(k_1 r_1)}$$

k = wavenumber within the dielectric rod

k_1 = wavenumber external to dielectric rod

For H modes $1/\bar{\Lambda} = 0$, $\bar{\Lambda}\bar{\beta}$ is finite when $\bar{\beta} = 0$, while for E modes $\bar{\Lambda} = 0$, $\bar{\Lambda}/\bar{\beta}$ is finite at $\bar{\beta} = 0$.

$$\frac{P_i}{P_o} = -\left(\frac{k_1}{k}\right)^4 \frac{\bar{\mu}T_1 + 1/\bar{\Lambda}\bar{\beta}\bar{\mu}\bar{\varepsilon}}{\bar{\mu}_1 T_4 + 1/\bar{\Lambda}\bar{\beta}\bar{\mu}_1\bar{\varepsilon}_1} \qquad \text{for H modes at } \bar{\beta} = 0 \qquad \text{.....(176}$$

and

$$\frac{1}{\bar{\Lambda}\bar{\beta}} = \frac{[1-(k_1/k)^2]}{\bar{\varepsilon}F(kr_1)(k_1/k)^2 - \bar{\varepsilon}_1 S(k_1 r_1)}; \qquad \left(\frac{k_1}{k}\right)^2 = \frac{\mu_1\varepsilon_1}{\mu\varepsilon} \qquad \text{.....(177)}$$

$$\frac{P_i}{P_o} = -\left(\frac{k_1}{k}\right)^4 \frac{\bar{\varepsilon}T_1 + \bar{\Lambda}/\bar{\beta}\bar{\mu}\bar{\varepsilon}}{\bar{\varepsilon}_1 T_3 + \bar{\Lambda}/\bar{\beta}\bar{\mu}_1\bar{\varepsilon}_1} \qquad \text{for E modes when } \bar{\beta} = 0 \qquad \text{.....(178)}$$

$$\frac{\bar{\Lambda}}{\bar{\beta}} = \frac{[1-(k_1/k)^2]}{\bar{\mu}F(kr_1)(k_1/k)^2 - \bar{\mu}_1 R(k_1 r_1)} \qquad \text{.....(179)}$$

The expressions enable the determination of the distribution of power at cut-off. In the above expressions

$$\bar{\Lambda} = \frac{\bar{\varepsilon}_1 S(k_1 r_1)/(k_1 r_1)^2 - \bar{\varepsilon}F(kr_1)/(kr_1)^2}{n\bar{\beta}[1/(kr_1)^2 - 1/(k_1 r_1)^2]} \qquad \text{.....(180)}$$

μ_1 = permeability of the surrounding medium

μ = permeability of the rod

ε_1 = permittivity of the surrounding medium

ε = permittivity of the rod

$$F(x) = \frac{xJ_1'(x)}{J_1(x)}$$

$$T_1 = \tfrac{1}{2}F^2(kr_1) + F(kr_1) + \tfrac{1}{2}[(kr_1)^2 - 1] \qquad \text{.....(181)}$$

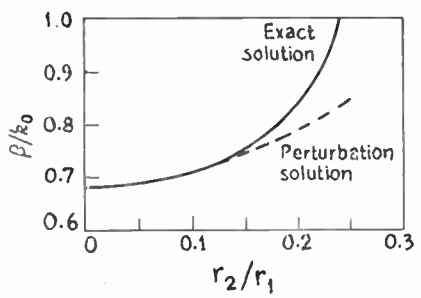

Fig. 33. Variation of the propagation constant with respect to r_2/r_1. Comparison of the results obtained by perturbational solution with that obtained by exact solution. (Ref. 95.)

The perturbation method can be applied to find the change in the propagation constant $\gamma_0 = j\beta_0$, when the dielectric is introduced. It may be noted that γ_0 represents the propagation constant in an empty guide considered as lossless and enclosing a lossless dielectric (air). If $\mathbf{E}_0$, $\mathbf{H}_0$ represent the field of the unperturbed guide and $\mathbf{E}$, $\mathbf{H}$ represent the field of the perturbed guide (i.e. with the dielectric) and $\gamma = j\beta$ represents the propagation constant of the perturbed guide, then the change in the propagation constant is given by the following relation[95]

$$\beta - \beta_0 = \omega \frac{\iint_s (\Delta\varepsilon\hat{\mathbf{E}}.\hat{\mathbf{E}}_0^* + \Delta\mu\hat{\mathbf{H}}.\hat{\mathbf{H}}_0^*)\,ds}{\iint_s (\hat{\mathbf{E}}_0^* \times \hat{\mathbf{H}} + \hat{\mathbf{E}} \times \hat{\mathbf{H}}_0^*).\mathbf{i}_z\,ds} \qquad \text{.....(182)}$$

where ω represents the resonant frequency of the perturbed guide, treated as a two-dimensional resonator at cut-off frequency ω_c. The unperturbed field of the dominant mode H_{11} for the circular guide is given by the following expressions

$$E_r = \frac{1}{r} J_1\left(1{\cdot}841\,\frac{r}{r_2}\right)\sin\theta$$

$$E_\theta = \frac{1{\cdot}841}{r_1} J_1'\left(1{\cdot}841\,\frac{r}{r_2}\right)\cos\theta \qquad \text{.....(183)}$$

$$H_r = -\frac{E_\theta}{Z_0}$$

$$H_\theta = \frac{E_r}{Z_0}$$

where Z_0 is the characteristic impedance of the unperturbed guide. Putting $\Delta\mu = 0$ and making the quasi-static assumption[123] that

$$E_{\text{int}} = \frac{2}{1+k_{e2}} E_{\text{ext}} \qquad \text{.....(184)}$$

the change in the propagation constant (eqn. (183)) reduces for the H mode to the following:

$$\frac{\beta - \beta_0}{k_0} = \frac{2{\cdot}146}{\sqrt{1-(\omega_c/\omega)^2}} \frac{k_{e2}-1}{k_{e1}+1}\left(\frac{r_2}{r_1}\right)^2 \qquad \text{.....(185)}$$

β/k_0 is plotted vs. r_2/r_1 in Fig. 33, where $k_{\epsilon 2} = 10$ and $r_1 = 0{\cdot}4\lambda_0$. The exact solution obtained by the field theory is also shown by the solid curve for the sake of comparison.

Waldron[68–70, 85] has made a comprehensive study of the propagation of electromagnetic waves in a cylindrical guide containing gyromagnetic media. Treating this as a boundary value problem, Waldron[68] has not only derived the characteristic equation for a cylindrical guide of radius a containing a concentric ferrite rod of radius b, but also a characteristic equation for a cylindrical guide containing a concentric dielectric rod of radius b. By putting the normalized phase constant $\bar{\beta} = 0$ in the characteristic equation for the guide with ferrite rod, the cut-off equations[69] as follows are obtained

$$J_p(B\chi)\Delta_1 - \left\{PJ'_p(B\chi) - \frac{pQ}{B}J_p(B\chi)\right\}\Delta_2 = 0 \quad \text{.....(186)}$$

and

$$J_p(B\sqrt{\varepsilon})\Delta_3 - \frac{J'_p(B\sqrt{\varepsilon})}{\sqrt{\varepsilon}}\Delta_4 = 0 \quad \text{.....(187)}$$

where

$$\Delta_1 = \begin{vmatrix} J_p(A) & Y_p(A) \\ J'_p(B) & Y'_p(B) \end{vmatrix}; \quad \Delta_2 = \begin{vmatrix} J_p(A) & Y_p(A) \\ J_p(B) & Y_p(B) \end{vmatrix}$$

$$\Delta_3 = \begin{vmatrix} J'_p(A) & Y'_p(A) \\ J'_p(B) & Y'_p(B) \end{vmatrix}; \quad \Delta_4 = \begin{vmatrix} J'_p(A) & Y'_p(A) \\ J_p(B) & Y_p(B) \end{vmatrix}$$

$$A = \frac{2\pi a}{\lambda_0} \qquad B = \frac{2\pi b}{\lambda_0}$$

$$P = \sqrt{\frac{\varepsilon}{\mu(1-\alpha^2/\mu^2)}} \qquad Q = \frac{\alpha}{\mu^2(1-\alpha^2/\mu^2)}$$

$$\chi = \sqrt{\varepsilon\mu(1-\alpha^2/\mu^2)}$$

μ and α are the diagonal and off-diagonal elements of the relative permeability tensor and ε is the relative permittivity of the ferrite rod. These quantities are relative to the properties of the medium surrounding the ferrite in the guide

$$\bar{\beta} = \beta/\omega\sqrt{\mu_0\varepsilon_0} = \lambda_0\beta/2\pi = \lambda_0/\lambda_g$$

λ_g = guide wavelength

p = integer giving the θ-dependence of electromagnetic fields.

The loci of points in β-space satisfying the cut-off condition $\bar{\beta} = 0$ are given by the eqns. (186) and (187), which involve a/λ_0, b/a, ε, μ and α. In the five dimensional space with dimensions a/λ_0, b/a, ε, μ and α, if the cut-off equations are satisfied by a given set of these values, the set is referred to as a cut-off point. This five dimensional space is called β-space. It is to be noted that the values of a/λ_0 and ε are restricted to positive values and b/a lies in the range of 0 to 1, whereas, μ and α may assume any values in the β-space. A study of the relations between the above parameters when $\bar{\beta} = 0$ for all modes leads to the proper understanding of the mode spectrum. A given set of values of the above parameters will enable the modes to be identified as propagating or non-propagating. The normal modes are divided into two sets according as the condition $\bar{\beta} = 0$ is satisfied by a solution of eqn. (186) or of eqn. (187). These sets of modes are related to the E and H modes respectively of the guide filled with homogeneous isotropic dielectric. The modes may be designated as E_{pq} and H_{pq} where q refers to the qth zero of equations

$$J_p(A\sqrt{\varepsilon}) = 0$$

and .....(188)

$$J'_p(A\sqrt{\varepsilon}) = 0$$

and p is an integer including zero. An exhaustive study of the mode spectrum has been made from the solutions of eqns. (186) and (187). The results presented both graphically and in tabular forms yield valuable information about the variation of b/a vs. ε for different values of a/λ_0, μ and α. The results include the case of $\mu = 1$ and $\alpha = 0$ which is the case of a guide containing a dielectric rod and also $\mu = 1$, $\varepsilon = 1$, $\alpha = 0$, $b/a = 0$, the condition existing in a guide containing air only.

An expression for the total power flow through a cylindrical guide containing a concentric dielectric rod has been derived by Waldron.[70] The total power flow through the guide consists of two parts, namely the power P_1 flowing through the central dielectric and the power P_2 flowing in the medium surrounding the dielectric rod. The expressions for P_1 and P_2 are as follows[70]

$$P_1 = \omega\beta k_1^2[\varepsilon_0\varepsilon A'^2_p - \mu_0 B'^2_p]U_p(k_1 b) - jpk_1^2 A'_p B'_p V_p(k_1 b) \quad \text{.....(189)}$$

where

$$U_0(k_1 b) = b^2\left[J_0^2(k_1 b) - \frac{2}{k_1 b}J_0(k_1 b)J_1(k_1 b) + J_1^2(k_1 b)\right]$$

$$U_1(k_1 b) = \frac{b^2}{2}[J_0^2(k_1 b) + J_1^2(k_1 b)] + \frac{1}{k_1^2}[J_0^2(k_1 b) - 1]$$

$$U_p(k_1 b) = \frac{b^2}{2}\left[J^2_{p-2}(k_1 b) - \frac{2(p-1)}{k_1 b} J_{p-2}(k_1 b) J_{p-1}(k_1 b) + J^2_{p-1}(k_1 b)\right] + \\ + \frac{p}{k_1^2}[J_0^2(k_1 b) - 1] + \frac{2p}{k_1^2}\sum_{q=1}^{p-1} J_q^2(k_1 b) \qquad \text{.....(190)}$$

and

$$V_p(k_1 b) = J_p^2(k_1 b) \qquad \text{for} \quad p \geqq 1$$
$$V_0(k_1 b) = 2J_0^2(k_1 b)$$

$$P_2 = \omega\beta k_0^2\{(\varepsilon_0 C_p^2 - \mu_0 F_p^2)[U_p(k_0 a) - U_p(k_0 b)] + (\varepsilon_0 D_p^2 - \mu_0 G_p^2)[U_p'(k_0 a) - U_p'(k_0 b)] + \\ + 2(\varepsilon_0 C_p D_p - \mu_0 F_p G_p)[U_p''(k_0 a) - U_p''(k_0 b)]\} - jpk_0^2 \times \\ \times \{F_p C_p[V_p(k_0 a) - V_p(k_0 b)] + D_p G_p[V_p'(k_0 a) - V_p'(k_0 b)] + (F_p D_p + C_p G_p)[V_p''(k_0 a) - V_p''(k_0 b)]\} \\ \text{.....(191)}$$

where U_p', V_p' are obtained from eqns. (190) by replacing J everywhere by Y and U_p'', V_p'' are obtained from the equations by replacing J_n^2 everywhere with $J_n Y_n$ and $J_n J_{n-1}$ everywhere with $0{\cdot}5(J_{n-1}Y_n + J_n Y_{n-1})$

$k_0^2 = \omega^2\mu_0\varepsilon_0 - \beta^2 = \omega^2\mu_0\varepsilon_0(1 - \bar{\beta}^2)$

$k_1^2 = \omega^2\mu_0\varepsilon_0\mu\varepsilon - \beta^2 = \omega^2\mu_0\varepsilon_0(\mu\varepsilon - \bar{\beta}^2)$

A_p, B_p, A_p', B_p', C_p, D_p, F_p, G_p are arbitrary constants.

The behaviour of the field components and power distributions in relation to the phase constant has been discussed thoroughly in a much more general way and the results of computations have been presented graphically and in tabular form by Waldron.[85] It has been concluded that certain aspects of the theory of conventional waveguides filled homogeneously with isotropic lossless scalar media are inadequate in handling inhomogeneous guides containing more than one medium or a tensor or lossy medium. The reader is referred to the original literatures[68–70, 85] for further details on mode spectrum, distribution of power, field components, etc.

It may be of interest to discuss briefly in this connection the propagation characteristics of electromagnetic waves through the two coaxial dielectric media when they are unbounded, i.e. if the metallic wall of the guide is absent. In this case, the guide with two coaxial dielectrics is reduced to a dielectric rod guide having dielectric constant ε_2 and immersed in a medium of dielectric constant ε_1. The field components (eqn. (28)) in this case are to be modified for the first medium by replacing the function J_m's, Y_m's and their first derivatives J_m''s, Y_m''s by the Hankel functions $H_m^{(1)}$, $H_m^{(2)}$ and their derivatives $H_m^{(1)\prime}$, $H_m^{(2)\prime}$ respectively in order to account for the decay of the field intensity to a vanishingly small value at infinity. Introducing the above changes in eqn. (28) and applying continuity conditions at the interface of the two media, the following eqns. (192) are obtained

$$A_1\left[\varepsilon_1\gamma_1 k_1 H_m^{(1)\prime}(k_1 r_2) - \frac{\varepsilon_2\gamma_2 k_2}{k_3^2}\frac{J_m'(k_2 r_2)}{J_m(k_2 r_2)} H_m^{(1)}(k_1 r_2)\right] + \\ + B_1\left[\varepsilon_1\gamma_1 k_1 H_m^{(2)\prime}(k_1 r_2) - \frac{\varepsilon_2\gamma_2 k_2}{k_3^2}\frac{J_m'(k_2 r_2)}{J_m(k_2 r_2)} H_m^{(2)}(k_1 r_2)\right] + \\ + A_1'\left[\omega\mu_1\varepsilon_1 \frac{m}{r_2} H_m^{(1)}(k_1 r_2) - \frac{\omega\mu_2\varepsilon_2}{k_4^2}\frac{m}{r_2} H_m^{(1)}(k_1 r_2)\right] + \\ + B_1'\left[\omega\mu_1\varepsilon_1 \frac{m}{r_2} H_m^{(2)}(k_1 r_2) - \frac{\omega\mu_2\varepsilon_2}{k_4^2}\frac{m}{r_2} H_m^{(2)}(k_1 r_2)\right] = 0 \qquad \text{(a)}$$

$$A_1\left[\omega\mu_1\varepsilon_1 \frac{m}{r_2} H_m^{(1)}(k_1 r_2) - \frac{\omega\mu_2\varepsilon_2}{k_3^2}\frac{m}{r_2} H_m^{(1)}(k_1 r_2)\right] + \\ + B_1\left[\omega\mu_1\varepsilon_1 \frac{m}{r_2} H_m^{(2)}(k_1 r_2) - \frac{\omega\mu_2\varepsilon_2}{k_3^2}\frac{m}{r_2} H_m^{(2)}(k_1 r_2)\right] + \\ + A_1'\left[\mu_1\gamma_1 k_1 H_m^{(1)\prime}(k_1 r_2) - \frac{\mu_2\gamma_2 k_2}{k_4^2}\frac{J_m'(k_2 r_2)}{J_m(k_2 r_2)} H_m^{(1)}(k_1 r_2)\right] + \\ + B_1'\left[\mu_1\gamma_1 k_1 H_m^{(2)\prime}(k_1 r_2) - \frac{\mu_2\gamma_2 k_2}{k_4^2}\frac{J_m'(k_2 r_2)}{J_m(k_2 r_2)} H_m^{(2)}(k_1 r_2)\right] = 0 \qquad \text{(b)}$$

$$A_1\left[j\omega\varepsilon_1 k_1 H_m^{(1)\prime}(k_1 r_2)-j\omega\varepsilon_2\frac{k_2}{k_3^2}\frac{J_m'(k_2 r_2)}{J_m(k_2 r_2)}H_m^{(1)}(k_1 r_2)\right]-$$
$$-B_1\left[j\omega\varepsilon_1 k_1 H_m^{(2)\prime}(k_1 r_2)+j\omega\varepsilon_2\frac{k_2}{k_3^2}\frac{J_m'(k_2 r_2)}{J_m(k_2 r_2)}H_m^{(2)}(k_1 r_2)\right]+$$
$$+A_1'\left[\gamma_1\frac{m}{r_2}H_m^{(1)}(k_1 r_2)-\gamma_2\frac{m}{r_2}\frac{1}{k_4^2}H_m^{(1)}(k_1 r_2)\right]-$$
$$-B_1'\left[\gamma_1\frac{m}{r_2}H_m^{(2)}(k_1 r_2)+\gamma_2\frac{m}{r_2}\frac{1}{k_4^2}H_m^{(2)}(k_1 r_2)\right]=0 \qquad (c)$$

$$A_1\left[\omega\mu_1\varepsilon_1\frac{m}{r_2}H_m^{(1)}(k_1 r_2)-\omega\mu_2\varepsilon_2\frac{m}{r_2}\frac{1}{k_3^2}H_m^{(1)}(k_1 r_2)\right]-$$
$$-B_1\left[\omega\mu_1\varepsilon_1\frac{m}{r_2}H_m^{(2)}(k_1 r_2)+\omega\mu_2\varepsilon_2\frac{m}{r_2}\frac{1}{k_3^2}H_m^{(2)}(k_1 r_2)\right]+$$
$$+A_1'\left[\mu_1\gamma_1 k_1 H_m^{(1)\prime}(k_1 r_2)-\gamma_2 k_2\frac{\mu_2}{k_4^2}\frac{J_m'(k_2 r_2)}{J_m(k_2 r_2)}H_m^{(1)}(k_1 r_2)\right]-$$
$$-B_1'\left[\mu_1\gamma_1 k_1 H_m^{(2)\prime}(k_1 r_2)+\gamma_2 k_2\frac{\mu_2}{k_4^2}\frac{J_m'(k_2 r_2)}{J_m(k_2 r_2)}H_m^{(2)}(k_1 r_2)\right]=0 \qquad (d) \quad \text{.....(192)}$$

where

$$A_2=\frac{1}{k_3^2}\exp(-\gamma_3 z)\left[A_1\frac{H_m^{(1)}(k_1 r_2)}{J_m(k_2 r_2)}+B_1\frac{H_m^{(2)}(k_1 r_2)}{J_m(k_2 r_2)}\right]$$
$$A_2'=\frac{1}{k_1^2}\exp(-\gamma_3 z)\left[A_1'\frac{H_m^{(1)}(k_1 r_2)}{J_m(k_2 r_2)}+B_1'\frac{H_m^{(2)}(k_1 r_2)}{J_m(k_2 r_2)}\right]$$

In order that A_1, B_1, A_1', B_2' may not vanish, the following condition must hold good

$$\begin{vmatrix} A_1^{(a)} & B_1^{(a)} & A_1'^{(a)} & B_1'^{(a)} \\ A_1^{(b)} & B_1^{(b)} & A_1'^{(b)} & B_1'^{(b)} \\ A_1^{(c)} & -B_1^{(c)} & A_1'^{(c)} & -B_1'^{(c)} \\ A_1^{(d)} & -B_1^{(d)} & A_1'^{(d)} & -B_1'^{(d)} \end{vmatrix}=0 \quad \text{.....(193)}$$

where A's and B's refer to their coefficients in the respective eqns. (192). By solving the above determinant, making some approximations and simplification, the propagation constant is found to be

$$\gamma_1=j\left\{\omega^2\mu_1\varepsilon_1-\frac{1}{r_2^2}\left[\frac{\pi}{2}(m+n)+\frac{\pi}{4}\right]^2\right\}^{\frac{1}{2}} \quad \text{.....(194)}$$

γ_1 becomes zero, real or imaginary according as r_2 is equal, less or greater than

$$\left[\frac{\left\{\frac{\pi}{2}(m+n)+\frac{\pi}{4}\right\}}{\omega\sqrt{\mu_1\varepsilon_1}}\right] \quad \text{.....(195)}$$

This signifies that there will be no energy flow in the first medium unless r_2 is greater than the above expression. Similarly, it can be derived that there can be no propagation in the second medium unless

$$r_2>\frac{s_{mn}}{\omega\sqrt{\mu_2\varepsilon_2}} \quad \text{.....(196)}$$

where s_{mn} is the root of $J_m(k_2 r_2)=0$. If γ_1 (eqn. (194)) is substituted in the expressions for field components, it will be observed that there will be a spreading-out of the field to a great distance, which amounts to a dielectric rod acting as a dielectric aerial. This leads to the conclusion that the dielectric rod will behave as a guide or as an aerial depending on the radius of the rod. The limiting values of the radii of the rod in the above two cases are found from the following expressions:

$$r_2=\frac{\left[\frac{\pi}{2}(m+n)+\frac{\pi}{4}\right]}{\omega\sqrt{\mu_1\varepsilon_1}} \quad \text{and} \quad r_2=\frac{s_{mn}}{\omega\sqrt{\mu_2\varepsilon_2}} \quad \text{.....(197)}$$

The limiting values of radii of the dielectric rod for some of the modes are indicated in Table 6.

Table 6

Limiting values of the radii of the dielectric rod for several modes

Modes	$(EH)_{11}$	$(EH)_{22}$	$(EH)_{12}$	$(EH)_{21}$
First medium	$0{\cdot}625\,\lambda_1$	$1{\cdot}125\,\lambda_1$	$0{\cdot}875\,\lambda_1$	$0{\cdot}875\,\lambda_1$
Second medium	$0{\cdot}61\,\lambda_2$	$1{\cdot}34\,\lambda_2$	$1{\cdot}12\,\lambda_2$	$0{\cdot}82\,\lambda_2$
	$(0{\cdot}386\,\lambda_1)$	$(0{\cdot}848\,\lambda_1)$	$(0{\cdot}708\,\lambda_1)$	$(0{\cdot}591\,\lambda_1)$

If the second medium possesses a dielectric constant 2·5 and if the first medium is air, then $\lambda_2 \simeq 0{\cdot}64\,\lambda_1$

and the critical dimensions of the rod for several modes are given in the above table inside brackets. The following conclusions may be drawn from the above table.

(i) If $r_2 < \lambda_1/4$ none of the above modes can be propagated inside the rod.

(ii) The energy flow is wholly concentrated in the second medium when r_2 lies between $0{\cdot}386\,\lambda_1$ and $0{\cdot}625\,\lambda_1$ in the case when the rod is excited by $(E\,H)_{11}$ mode and so on.

(iii) When the rod is excited in the $(EH)_{11}$ mode, if the radius of the rod is increased beyond $0{\cdot}625\,\lambda_1$, the energy flow will be distributed in both the media. Similarly, for the $(EH)_{22}$ mode, when $r_2 > 1{\cdot}125\,\lambda_1$ and so on for the other modes, the energy will flow in both the media.

The radial spread of the field in the case of the dielectric rod can be obtained[29] from the radial components of the electric and magnetic fields. These components, when modified by the introduction of Hankel functions, so as to ensure the proper decrease of the field at infinity and also to give the proper direction of energy flow when k becomes complex are

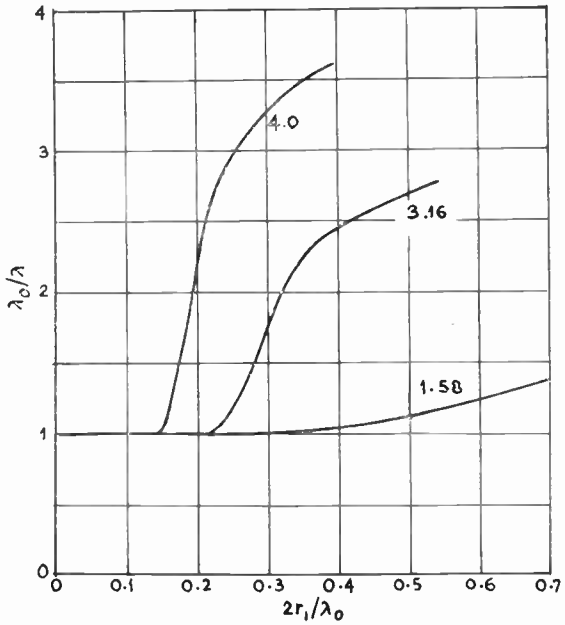

Fig. 34. $\bar{\beta}$ as a function of $2r_1/\lambda_0$ for HE_{11} mode. $(\bar{\mu}/\bar{\varepsilon})^{1/2} = 0{\cdot}17$ $(\bar{\mu}\bar{\varepsilon})^{1/2} = 1{\cdot}58,\ 3{\cdot}16,\ 4{\cdot}0$. (Ref. 124.)

$$E_r = \mathrm{j}P\left[k_3^2 k_1 \gamma_1 \{gH_m^{(2)\prime}(k_1 r) - fH_m^{(1)\prime}(k_1 r)\} + C_m k_4^2 \omega\mu_2 \frac{m}{r}\{gH_m^{(2)}(k_1 r) - fH_m^{(1)}(k_1 r)\}\right]\cos m\theta \exp(-\gamma_2 z)$$

$$H_r = -P\left[\omega\varepsilon_1 k_3^2 \frac{m}{r}\{fH_m^{(1)}(k_1 r) + gH_m^{(2)}(k_1 r)\} + C_m \gamma_1 k_1 k_4^2\{fH_m^{(1)\prime}(k_1 r) + gH_m^{(2)\prime}(k_1 r)\}\right]\sin m\theta \exp(-\gamma_2 z) \quad \ldots\ldots(198)$$

where f, g and C_m are given by the following expressions

$$= \frac{\mathrm{J}_m(k_2 r_2)H_m^{(2)}(k_1 r_1)}{H_m^{(1)}(k_1 r_2)H_m^{(2)}(k_1 r_1) - H_m^{(1)}(k_1 r_1)H_m^{(2)}(k_1 r_2)}$$

$$g = \frac{\mathrm{J}_m(k_2 r_2)H_m^{(1)}(k_1 r_1)}{H_m^{(1)}(k_1 r_1)H_m^{(2)}(k_1 r_2) - H_m^{(1)}(k_1 r_2)H_m^{(2)}(k_1 r_2)}$$

$$C_m = -\frac{\varepsilon_1 \gamma_1 k_1 k_3^2[fH_m^{(1)\prime}(k_1 r_2) + gH_m^{(2)\prime}(k_1 r_2)] - \varepsilon_2 \gamma_2 k_2 \mathrm{J}_m'(k_2 r_2)}{\omega\mu_1\varepsilon_1 \frac{m}{r_2} k_4^2[fH_m^{(1)}(k_1 r_2) + gH_m^{(2)}(k_1 r_2)] - \omega\mu_2\varepsilon_2 \frac{m}{r_2}\mathrm{J}_m(k_2 r_2)}$$

$$k_3^2 = k_2^2/k_1^2; \qquad k_4^2 = [k_2^2 - 2m^2/r_2^2]/[k_1^2 - 2m^2/r_2^2]$$

The values of k_1, γ_1, k_2 and γ_2 being known, the radial field at any point can be calculated in terms of the total power flow P along the guide.

The propagation of electromagnetic waves through an unbounded dielectric rod guide has been studied by Clarricoats.[124] In this paper a graphical method for evaluating the propagation coefficient was described in which the method of solution enables the complete mode spectrum to be identified. A study of the higher order modes reveals that they are degenerate, in the sense that a pair of modes has the same genesis value of the normalized radius (r_1/λ_0) of the rod, though there is a difference in the dependence on r_1/λ_0 of the phase change coefficients of the modes. It has also been established that the product $\mu\varepsilon$ of the rod primarily determines the propagation characteristics and the distribution of power between the inside and outside of the rod. The variation of the normalized phase coefficient $\bar{\beta} = \lambda_0/\lambda$ with respect to

the ratio of the diameter of the rod to the free space wavelength ($2r_1/\lambda_0$) for different values of $\bar{\mu}\bar{\varepsilon} = \mu\varepsilon/\varepsilon_0^2$ for HE_{11} mode is shown in Fig. 34. The variation of $\bar{\beta}$ as a function of $2r_1/\lambda_0$ for various values of $(\bar{\mu}/\bar{\varepsilon})^{\frac{1}{2}}$ is shown in Fig. 35. These figures show that the phase change coefficient of the modes depends primarily on r_1/λ_0 and $\bar{\mu}\bar{\varepsilon}$ and very little on the actual

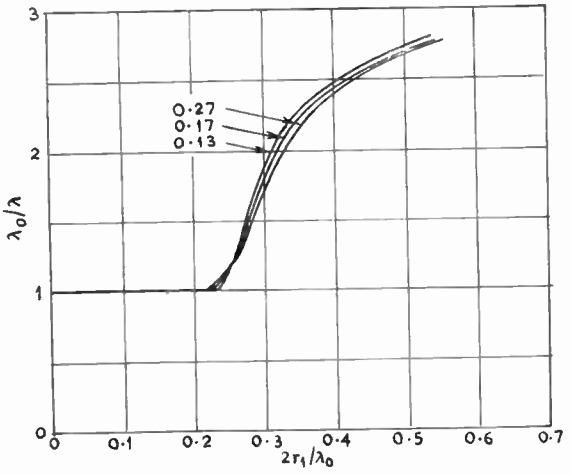

Fig. 35. $\bar{\beta}$ as a function of $2r_1/\lambda_0$ for HE_{11} mode propagating in a dielectric guide. $(\bar{\mu}\bar{\varepsilon})^{1/2} = 3{\cdot}16$. $(\bar{\mu}/\bar{\varepsilon})^{1/2} = 0{\cdot}13, 0{\cdot}17, 0{\cdot}27$. (Ref. 124.)

values of $\bar{\mu}$ and $\bar{\varepsilon}$. An expression for the ratio of power flowing through the guide (P_i) and outside (P_0) has also been derived by Clarricoats.[124] The result for the HE_{11} mode is given in Fig. 36. It is observed that for HE_{11} mode $P_i/P_o \to 0$ as $r_1/\lambda_0 \to 0$. The study by Clarricoats also reveals that for any other mode P_i/P_0 remains finite for all values of r_1/λ_0 over which the mode can propagate.

When the dielectric guide is excited by an EH wave, the power flow density becomes negative under certain conditions. The power flow through a guide is usually calculated from the Poynting vector S. In a right-handed cartesian coordinate system, if propagation takes place in the positive z-direction, the Poynting vector is

$$S_z = \tfrac{1}{2}(E_x H_y^* - E_y H_x^*) \qquad \text{.....(199)}$$

Introducing the wave impedances $Z_1 = E_x/H_y$ and $Z_2 = E_y/H_x$, the Poynting vector reduces to

$$S_z = \tfrac{1}{2}(Z_1 H_y H_y^* + Z_2 H_x H_x^*)$$

The power flow derived by integrating S_z over the cross-section of the guide and taking the real parts becomes negative if either Z_1 or Z_2 or both becomes negative. It has been shown by Gillespie[126] that this condition is achieved in the case of a guide supporting a mixed mode such as EH_{11} in a dielectric guide.

For EH mode

$$H_x = H'_x + H''_x$$
$$H_y = H'_y + H''_y$$

where H'_x, H'_y represent magnetic field components of H mode and

H''_x, H''_y represent magnetic field components of E mode.

It can be easily shown[126] that for EH mode

$$Z_1 = \sqrt{\frac{\bar{\mu}}{\bar{\varepsilon}}}\left[\frac{\lambda_g}{\lambda} + b\left(\frac{\lambda}{\lambda_g} - \frac{\lambda_g}{\lambda}\right)\right]$$
$$Z_2 = \sqrt{\frac{\bar{\mu}}{\bar{\varepsilon}}}\left[\frac{\lambda_g}{\lambda} + c\left(\frac{\lambda}{\lambda_g} - \frac{\lambda_g}{\lambda}\right)\right] \qquad \text{.....(200)}$$

For a dielectric guide, $\lambda = \lambda_0/\sqrt{\varepsilon_r}$ in the dielectric region, so $\lambda_g > \lambda$. Consequently, Z_1 and Z_2 can become negative if $b > 1$, $c > 1$. For the region outside the rod $\lambda = \lambda_0$, so $\lambda > \lambda_g$ and Z_1 and Z_2 can be negative if b and c are negative. It can also be shown that for EH or HE modes the transverse electric and magnetic fields are not orthogonal to each other, so $Z_1 \neq Z_2$.

Figure 37 shows the ratio of power flow outside the rod P_o to the total power flow P_t as function of the dielectric constant of the rod for different values of the normalized diameter $2a/\lambda_0$ of the rod. It is ob-

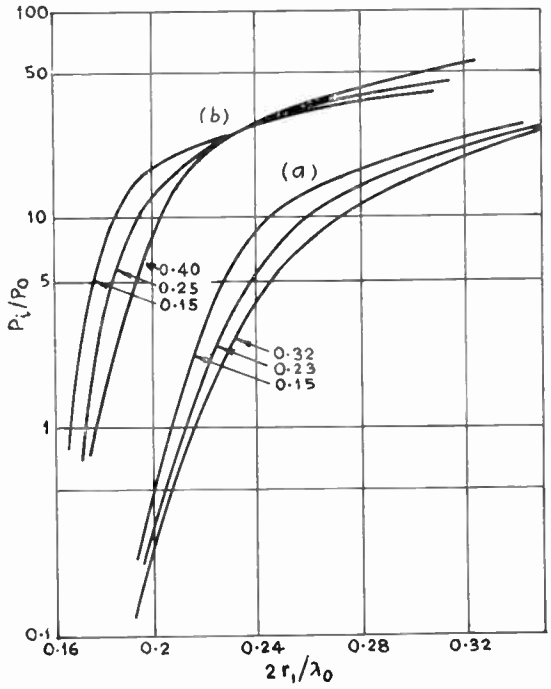

Fig. 36. P_i/P_o as a function of $2r_1/\lambda_0$ for HE_{11} mode propagating in an unbounded dielectric rod. (a) $(\bar{\mu}\bar{\varepsilon})^{1/2} = 3{\cdot}16$; (b) $(\bar{\mu}\bar{\varepsilon})^{1/2} = 4{\cdot}0$. Parameter $(\bar{\mu}/\bar{\varepsilon})^{1/2}$. (Ref. 124.)

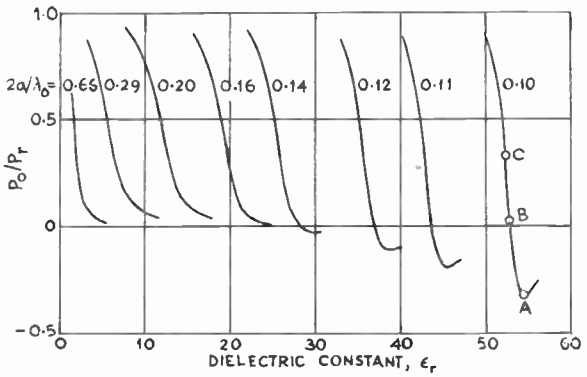

Fig. 37. Ratio of power flow outside to the total power flow as a function of the dielectric constant of the rod for different values of $2a/\lambda_0$. (Ref. 126.)

served that the ratio, i.e. P_0, is negative under certain conditions. By calculating S_z for $r < a$ and for $r \geqq a$, the equations for the loci of zero power density can be obtained.[126] Figure 38 shows a plot of loci of zero power density. The curves correspond to a total energy flow outside the rod which is negative at A, approximately zero at B and positive at C for $2a/\lambda_0 = 0{\cdot}10$. The power density everywhere inside the loops formed by these loci is negative and conversely, is positive outside. The limiting values of radius of the rod for the three cases A, B and C (Fig. 37) are given in Table 7.

Table 7

Limiting values of radius of the rod for the three cases A, B and C (after reference 126)

	Point A	Point B	Point C
Upper limit of $2r/\lambda_0$	0·460	0·368	0·325
Lower limit of $2r/\lambda_0$	0·0846	0·0836	0·0835
Approximate lower limit of $2r/\lambda_0$	0·0825	0·0823	0·0824

Though the power flow is negative at certain restricted parts of the cross-section of the guide, it may be remarked that the total power flow is positive.

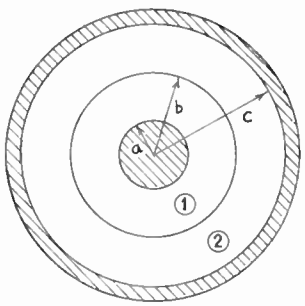

Fig. 39. Transverse section of the duo-dielectric coaxial guide.

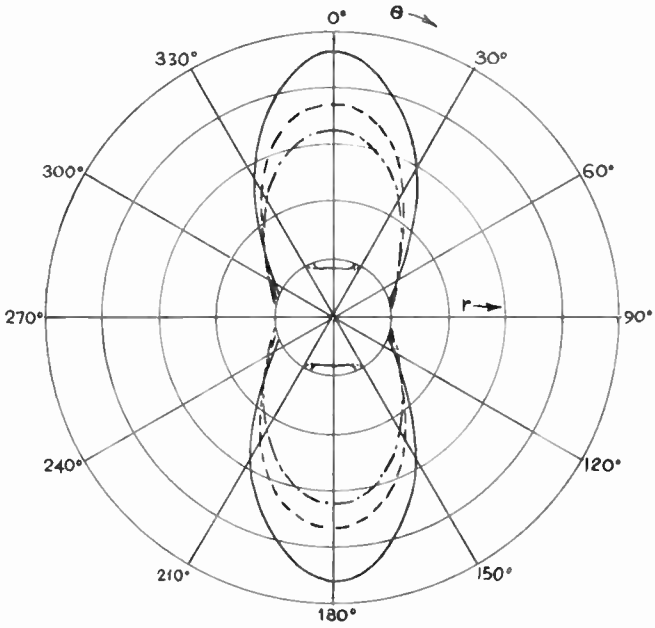

Fig. 38. Loci of zero power density. (Ref. 126.)
— Total power outside rod negative.
— — — Total power outside rod ≃ 0.
— o — Total power outside rod positive.

11. Coaxial Guide with Two Concentric Dielectrics

Beam and Dobson[21] have studied the propagation of electromagnetic waves in a coaxial line having two different dielectric regions (Fig. 39). Treating this as a boundary value problem, the characteristic equation derived is

$$n^2 \frac{T^2}{Q^2} - (F_1 - F_2)(G_1 - G_2) = 0 \quad \text{.....(201)}$$

where

$$F_i = \frac{1}{k_i}\left[\frac{J_n'(k_i)Y_n'(c_i k_i) - J_n'(c_i k_i)Y_n'(k_i)}{J_n(k_i)Y_n'(c_i k_i) - J_n'(c_i k_i)Y_n(k_i)}\right]$$

$$G_i = \frac{\varepsilon_i}{k_i}\left[\frac{J_n'(k_i)Y_n(c_i k_i) - J_n(c_i k_i)Y_n'(k_i)}{J_n(k_i)Y_n(c_i k_i) - J_n(c_i k_i)Y_n(k_i)}\right]$$

$$Q = \left(\frac{\lambda_g}{\lambda}\right)^2 = \frac{k_1^2 - k_2^2}{\varepsilon_2 k_1^2 - \varepsilon_1 k_2^2}$$

$$c_1 = \frac{a}{b}; \quad c_2 = \frac{c}{b}; \quad T^2 = \left(\frac{1}{k_1^2} - \frac{1}{k_2^2}\right)^2, \quad i = 1, 2$$

$$k_1^2 = b^2(\omega^2 \mu_0 \varepsilon_0 \varepsilon_1 - \beta_g^2) \quad \text{.....(202)}$$

$$k_2^2 = b^2(\omega^2 \mu_0 \varepsilon_0 \varepsilon_2 - \beta_g^2)$$

which yields

$$\left(\frac{b}{\lambda}\right)^2 = \frac{k_1^2 - k_2^2}{4\pi^2(\varepsilon_1 - \varepsilon_2)} \quad \text{.....(203)}$$

since

$$\omega^2 \mu_0 \varepsilon_0 = 4\pi^2/\lambda^2$$

In order that b/λ may be real, $k_1 > k_2$ when both k_1 and k_2 are real. Also, $k_1 > k_2\sqrt{\varepsilon_1/\varepsilon_2}$ for real λ/λ_g. When $k_1 \to k_2\sqrt{\varepsilon_1/\varepsilon_2}$, $\lambda_g \to \infty$ and cut-off occurs when $k_1 = k_2\sqrt{\varepsilon_1/\varepsilon_2}$. If k_2 is imaginary, modified Bessel functions should be used in the expressions for F_i and G_i in place of J's and Y's. The transition between the regions where k_2 is real and when it is imaginary occurs when $k_2 = 0$ and $\lambda = \lambda_g\sqrt{\varepsilon_2}$. Between this point and cut-off k_2 is real. The above reasoning holds only in the case when $\varepsilon_1 > \varepsilon_2$. If $\varepsilon_2 > \varepsilon_1$, then k_2 is always real and k_1 maybe real or imaginary, and k_2 must be greater than $k_1\sqrt{\varepsilon_2/\varepsilon_1}$ and cut-off occurs, when $k_2 = k_1\sqrt{\varepsilon_2/\varepsilon_1}$. Since at cut-off $k_1 = k_2\sqrt{\varepsilon_1/\varepsilon_2}$ the cut-off wavelength λ_c is given by the relation

$$\lambda_c = \frac{2\pi b\sqrt{\varepsilon_1}}{k_1} = \frac{2\pi b\sqrt{\varepsilon_2}}{k_2} \qquad \text{.....(204)}$$

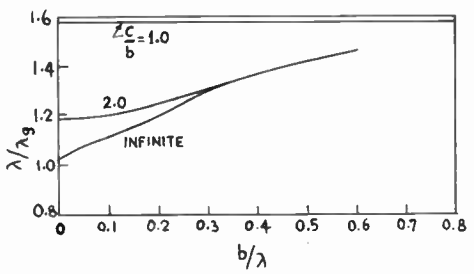

Fig. 40. Variation of λ/λ_g with respect to b/λ. (Ref. 21.)

The values of k_1 and k_2 at cut-off are determined by substituting $k_1\sqrt{\varepsilon_2/\varepsilon_1}$ for k_2 in the characteristic eqn. (201). For a fixed n there will be an infinite number of values of k_1 which will satisfy the characteristic equation. The modes corresponding to the cut-off frequencies determined by n and m will be designated as E_{nm} or H_{nm} and HE_{nm} or EH_{nm}.

For E_{00} mode the guide wavelength is given by the relation

$$\left(\frac{\lambda}{\lambda_g}\right)^2 = \frac{\ln(c_1/c_2)}{\dfrac{\ln c_1}{\varepsilon_1} - \dfrac{\ln c_2}{\varepsilon_2}} = \frac{\varepsilon_1\varepsilon_2 \ln(c_1/c_2)}{\varepsilon_2 \ln c_1 - \varepsilon_1 \ln c_2} \qquad \text{.....(205)}$$

The variation of λ/λ_g with b/λ for $\varepsilon_1 = 2{\cdot}5$ and $\varepsilon_2 = 1{\cdot}0$ and for $c_1 = 0{\cdot}5$ and different values of c_2 is shown in Fig. 40. The cut-off frequency curves for E_{01} and H_{01} modes are shown in Figs. 41 and 42. The characteristic equation for the HE_{11} mode is

$$\frac{\varepsilon_1+\varepsilon_2}{k_1^2} + \varepsilon_2\left(\frac{c_2^2+1}{c_2^2-1}\right)F_1 + \left(\frac{c_2^2-1}{c_2^2+1}\right)G_1 - 2\varepsilon_2\left(\frac{c_2^4}{c_2^4-1}\right)\ln G_2 - \frac{\varepsilon_2}{2} = 0 \qquad \text{.....(206)}$$

The characteristic curves for the mode is shown in Fig. 43 for $c_2 = 2{\cdot}0$ and $c_1 = 0$, $0{\cdot}5$, $0{\cdot}7$, $0{\cdot}9$, $1{\cdot}0$. When $c_1 = 1{\cdot}0$, the waveguide reduces to an air-filled coaxial line and the curve is for H_{11} mode in this line. The variation of λ/λ_g with b/λ for various modes is

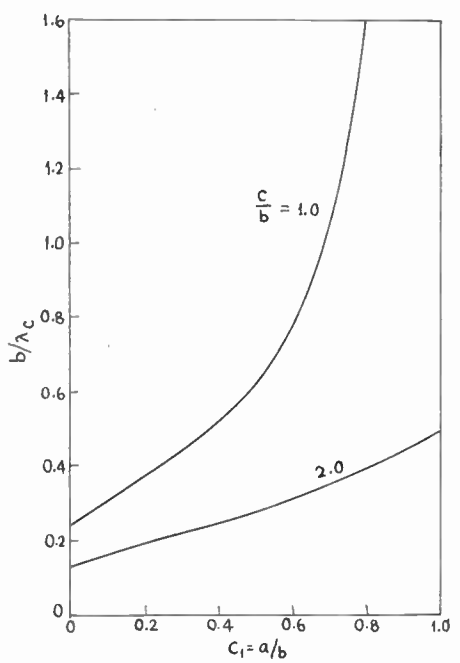

Fig. 41. Cut-off frequency of E_{01} mode as a function of a/b and $c/b = c_2$. (Ref. 21.)

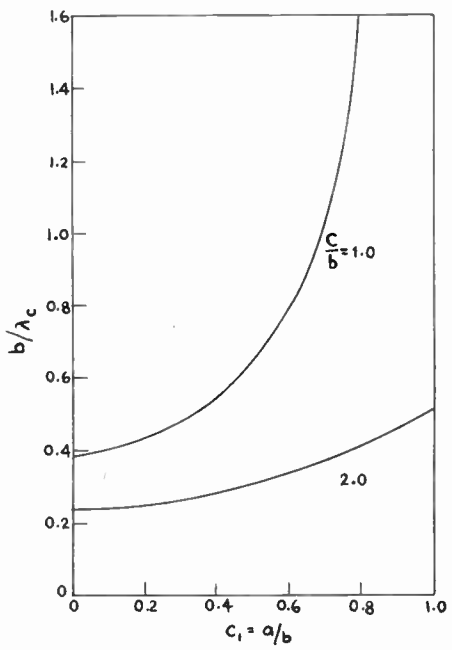

Fig. 42. Cut-off frequency of H_{01} mode as a function of a/b and c/b. (Ref. 21.)

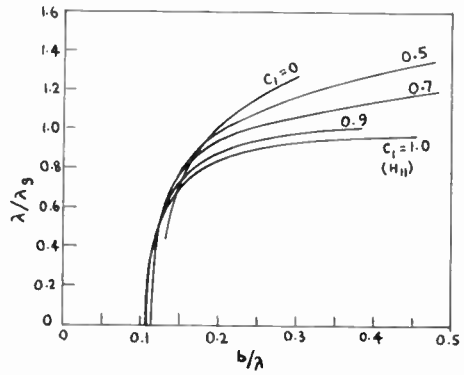

Fig. 43. Guide wavelength for HE_{11} mode as a function of b/λ and $c_1 = a/b$, $\varepsilon_1 = 2{\cdot}5$, $\varepsilon_2 = 1{\cdot}0$. (Ref. 21.)

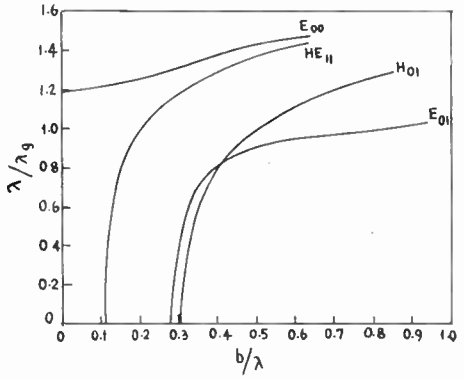

Fig. 44. Comparison of the guide wavelength for various modes as a function of b/λ, $\varepsilon_1 = 2{\cdot}5$, $\varepsilon_2 = 1{\cdot}0$, $c_1 = 0{\cdot}5$, $c_2 = 2{\cdot}0$. (Ref. 21.)

shown in Fig. 44 for the sake of comparison. Treating this as a boundary value problem Kostriza[27] has studied the propagation of electromagnetic waves in a uniform composite dielectric coaxial line of fixed ratio between conductor and dielectric radii and of specific dielectric constant ratio. The ratio of the longitudinal (E_{z1}) to the radial (E_{r1}) electric fields at the boundary ($r = b$) between the two dielectric regions is given by the following expression

$$\frac{E_{z1}(b)}{E_{r1}(b)} = \frac{1}{\gamma k_1}\,\frac{J_0(k_1 b)Y_0(k_1 a) - J_0(k_1 a)Y_0(k_1 b)}{J_1(k_1 b)Y_0(k_1 a) - J_0(k_1 a)Y_1(k_1 b)} \qquad \text{.....(207)}$$

The variation of $(E_{z1}/E_{r1})_b$ with respect to $A\omega$ is shown in Fig. 45 for E_{00} mode, where

$$A = [a(\mu_1\varepsilon_1 - \mu_2\varepsilon_2)]^{\frac{1}{2}}$$

The cut-off frequency for E_{0r} mode is determined from the equation

$$\frac{J_1(mx)Y_0(x) - J_0(x)Y_1(mx)}{J_0(x)Y_0(x) - J_0(mx)Y_0(x)} = \frac{\varepsilon_2}{\varepsilon_1}\sqrt{\frac{\varepsilon_1\mu_1}{\varepsilon_2\mu_2}} \times \frac{J_1(mpx)Y_0(mnpx) - J_0(mnpx)Y_1(mpx)}{J_0(mnpx)Y_0(mpx) - J_0(mpx)Y_0(mnpx)} \qquad \text{.....(208)}$$

where $n = c/b$, $m = b/a$, $x = k_1 a$, and $p = \sqrt{\varepsilon_2\mu_2/\varepsilon_1\mu_1}$. When $m = 2$, $n = 1{\cdot}25$, $p = 0{\cdot}5$, the first two cut-off frequencies are given by the following two roots of eqn. (208):

$$x_1 = 2{\cdot}220$$
$$x_2 = 4{\cdot}879$$

Similarly, for H_{0r} and $(E_z + H_z)_{nr}$ mixed modes, the cut-off frequency equation can be derived. The cut-off values are found from the roots

$$x_1\,(H_{0r}) = 2{\cdot}31$$
$$x_1\,(\text{mixed mode}) = 0{\cdot}775$$
$$x_2\,(\text{mixed mode}) = 2{\cdot}45$$

for the case when $m = 2$, $n = 1{\cdot}25$ and $p = 0{\cdot}5$

The composite coaxial line with two dielectrics may be treated as homogeneous coaxial structure whose effective dielectric constant ε_p may be computed from electrostatic considerations. For E_{00} mode, ε_p for the composite line in analogy with a homogeneous dielectric coaxial line is defined by the relation

$$\lambda_p/\lambda_0 = 1/\sqrt{\varepsilon_p} \qquad \text{.....(209)}$$

where λ_p is the phase wavelength in the composite dielectric. Also,

$$\lambda_p/\lambda_0 = A\omega/\sqrt{3}(\beta a) \qquad \text{.....(210)}$$

The equivalent dielectric constant ε_p is given as follows

$$\varepsilon_p = \frac{(\varepsilon_1/\varepsilon_2)\ln mn}{(\varepsilon_1/\varepsilon_2)\ln n + \ln m} \qquad \text{.....(211)}$$

The variation of λ_p/λ_0 with $A\omega$ is shown in Fig. 46, where $A = a/\sqrt{3}\times 10^{10}$ seconds and a is in centimetres.

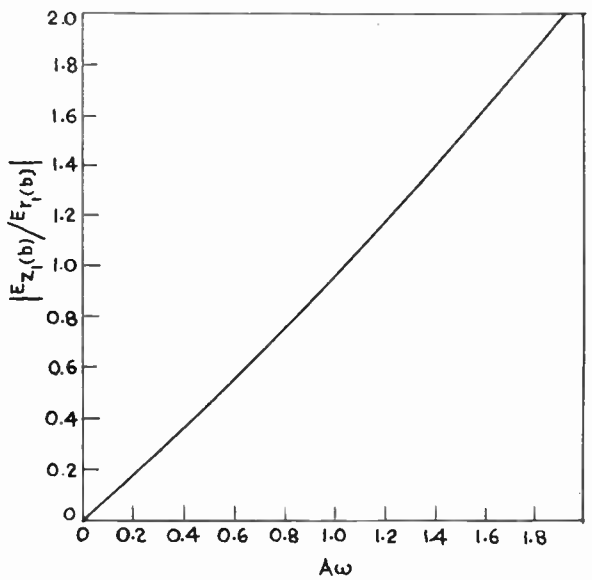

Fig. 45. Variation of $(E_{z1}/E_{r1})_b$ with respect to $A\omega$ for E_{00} mode. (Ref. 27.)

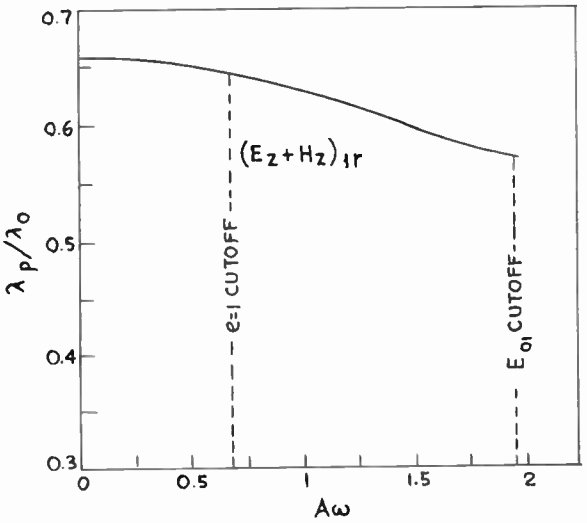

Fig. 46. Variation of phase wavelength (λ_p) of the composite guide with respect to $A\omega$. (Ref. 27.)

The same problem has been studied by the network theory approach.[97] The equivalent network consists of two short-circuited (Fig. 47) E-type radial transmission lines of characteristic admittance Y_{01} and

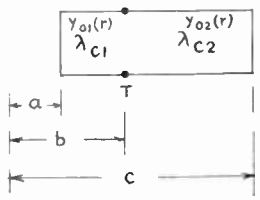

Fig. 47. Equivalent network of the composite coaxial line. (Ref. 97.)

Y_{02} and joined at the reference plane T. The transverse resonant condition yields the following relation[97]

$$Y_{01}\cot(x_2, x_1) = Y_{02}\cot(x_2', x_3') \quad \text{.....(212)}$$

which is valid for all E modes with no angular dependence. The radial cotangent function is defined as

$$\cot(x, y) = \frac{J_1(x)Y_0(y) - Y_1(x)J_0(y)}{J_0(x)Y_0(y) - Y_0(x)J_0(y)} \quad \text{.....(213)}$$

$$x_1 = \frac{2\pi a}{\lambda_{c1}}, \quad x_2 = \frac{2\pi b}{\lambda_{c1}}, \quad x_2' = \frac{2\pi b}{\lambda_{c2}}, \quad x_3' = \frac{2\pi c}{\lambda_{c2}} \quad \text{.....(214)}$$

$$\frac{Y_{02}}{Y_{01}} = \frac{k_{e2}\,\lambda_{c2}}{k_{e1}\,\lambda_{c1}} = \frac{k_{e2}}{k_{e1}}\sqrt{\frac{k_{e1} - (\lambda_0/\lambda_g)^2}{k_{e2} - (\lambda_0/\lambda_g)^2}}$$

An approximate solution of the characteristic eqn. (212) for the lowest root valid in the low-frequency range yields the following relation[97] for the wavelength (λ_g) of the principal mode

$$\left(\frac{\lambda_g}{\lambda_0}\right)^2 \simeq \frac{\frac{1}{k_{e1}}\ln\frac{b}{a} + \frac{A}{k_{e2}}\ln\frac{c}{b}}{\ln\frac{b}{a} + A\ln\frac{c}{b}} \quad \text{.....(215)}$$

when $2\pi b/\lambda_{c1} < 1$ and $2\pi c/\lambda_{c2} < 1$, where,

$$A = \frac{1 + \frac{1}{2}\left(\frac{2\pi b}{\lambda_0}\right)^2\left[k_{e1} - \left(\frac{\lambda_0}{\lambda_g}\right)^2\right]\ln\left|\frac{\gamma\pi a}{\lambda_0}\sqrt{k_{e1} - \left(\frac{\lambda_0}{\lambda_g}\right)^2}\right|}{1 + \frac{1}{2}\left(\frac{2\pi b}{\lambda_0}\right)^2\left[k_{e2} - \left(\frac{\lambda_0}{\lambda_g}\right)^2\right]\ln\left|\frac{\gamma\pi c}{\lambda_0}\sqrt{k_{e2} - \left(\frac{\lambda_0}{\lambda_g}\right)^2}\right|} \quad \text{.....(216)}$$

and $\gamma = 1{\cdot}781$. It has been assumed in deriving the relation (215) that the dielectric is lossless and the guide walls possess perfect conductivity.

12. Coaxial Lines with Non-concentric Dielectrics

Coaxial lines with non-concentric dielectrics are finding increasing use in microwave devices.[76–80, 130–135] Sullivan and Parker[132] have studied the case of a partially dielectric-loaded coaxial transmission line (Fig. 48). By applying electrostatic methods an expression for the normalized guide wave length ($\lambda g/\lambda a$) and normalized characteristic impedance (Z_g/Z_a) has been obtained

$$\frac{\lambda_g}{\lambda_a} = \frac{Z_g}{Z_a} = \frac{1}{\sqrt{\frac{\theta}{360}\left[\frac{\epsilon_2 \ln b/a}{\epsilon_1 \ln\frac{c}{a} + \epsilon_2 \ln\frac{b}{c}} - 1\right] + 1}} \quad \text{...(217)}$$

where θ represents the angular dielectric filling. The variation of λ_g/λ_a as a function of b/c with $Z_a = 50$ ohms and $\theta = 180°$, $\epsilon_1 = 1{\cdot}00$ for various values of the relative dielectric constant ϵ_2 is shown in Fig. 49. Angelakos[79] has also studied the problem of a coaxial line with non-concentric dielectric and has derived a relation for λ_g by applying resonant condition to the plane transverse to the direction of propagation. The variation of the normalized guide wavelength with angular dielectric filling and ϵ_2/ϵ_1 as a parameter

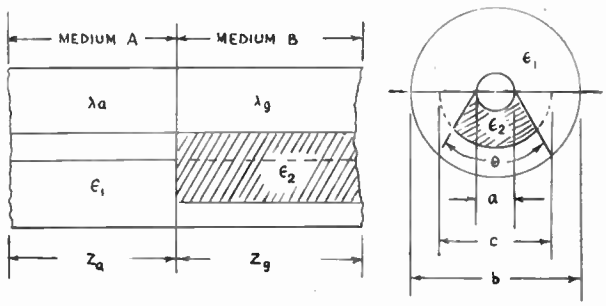

Fig. 48. Cross-section of partially filled coaxial transmission line. (Ref. 132.)

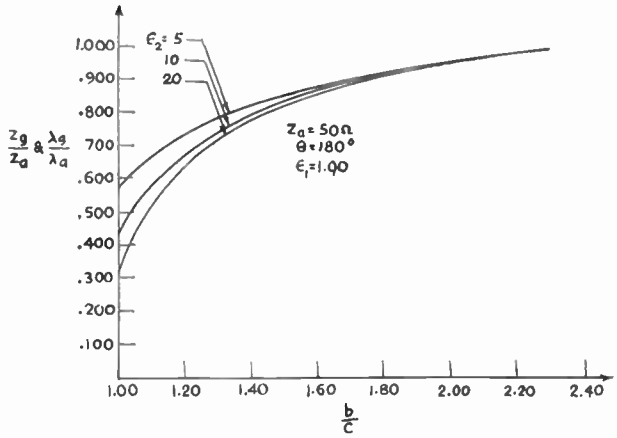

Fig. 49. Normalized guide wavelength λ_g/λ_a and characteristic impedance Z_g for partially-filled coaxial line. Parameter ε_2. (Ref. 132.)

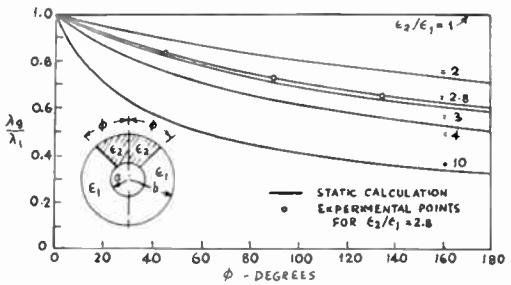

Fig. 50. Low frequency approximate guide wavelength variation as a function of angular diameter filling. Parameter $\varepsilon_2/\varepsilon_1$. (Ref. 79.)

is shown in Fig. 50, where λ_g is the propagation wavelength in the axial direction and ϕ is half the angular dielectric filling.

The characteristics of non-reciprocal microwave devices using ferrite and garnet have been considerably improved by using dielectric loading.[76–80] In order to achieve non-reciprocal propagation characteristics it is necessary that the microwave magnetic field be circularly polarized in the region of the ferrite. This condition is easily fulfilled in rectangular guide propagating the dominant mode[136–138] and in circular guide propagating the H_{11} mode. In coaxial line propagating the dominant TEM mode there is no longitudinal (H_z) component of microwave magnetic field. The only component of the H vector that exists is H_θ. So it cannot furnish a circularly or elliptically polarized microwave driving field for the ferrite spins. This means that, for a coaxial line propagating the TEM mode, the microwave magnetic field is linearly polarized at all points and so any ferrite effects will be reciprocal. If, however a ferrite-loaded coaxial line is loaded antisymmetrically with a dielectric, the transverse electric field E_r can no longer remain constant with respect to θ and so there will be a longitudinal component of the microwave magnetic field $H_z \propto \partial E_r/\partial\theta$. Thus partially filling the cross-section of coaxial line with a dielectric serves to distort[77, 80, 130] the mode pattern and create an almost true sense of circular polarization at the air-dielectric interface. This mode distortion technique by dielectric loading makes coaxial line suitable as non-reciprocal device.

Figure 51(b) shows an air-filled coaxial line with two transversely magnetized ferrites located on opposite sides of the coaxial line centre conductor, and partially filled with a low loss dielectric. In this case the wave propagates in the two dielectric media with different phase velocities and hence as discussed above, a z-component of the microwave field which is not in phase with H_θ is produced. By a proper selection and shaping of the dielectric, an almost true sense of circular polarization can be produced. The configuration of the microwave magnetic field in such a structure is shown in Fig. 52.

By using the parallel-plate analogue[131, 135] method, Button[76] has derived an expression for the differential phase shift $\beta_+ - \beta_-$, where β_+ and β_- refer to the positive and negative directions of propagation respectively. The variation of $\beta_+ - \beta_-$ as a function of the dielectric loading factor for different values of the relative dielectric constant is shown in Fig. 53.

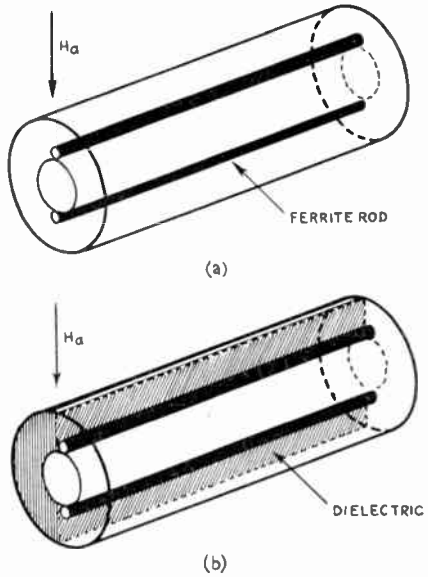

Fig. 51. Ferrite and dielectric configuration on a coaxial guide. (Ref. 80.)
(a) Ferrite coaxial line reciprocal structure.
(b) Dielectric loaded ferrite coaxial line non-reciprocal structure. One sense of circular polarization.

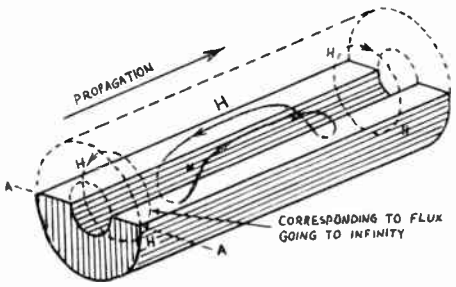

Fig. 52. Microwave H field configuration in partially dielectric loaded coaxial line. (Ref. 77.)

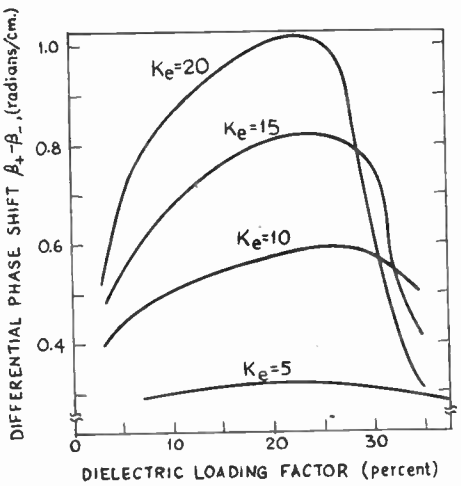

Fig. 53. Theoretical differential phase shift as a function of dielectric loading factor. Parameter: dielectric constant. Frequency 2000 Mc/s; Ferrite thickness: 4 mm in $1\frac{5}{8}$ in. diameter coaxial line. The ferrite was assumed to have 50 oersted resonance line width and was biased below resonance. (Ref. 76.)

It is observed that the coaxial line should not be filled more than twenty-five per cent except for very small dielectric constants for which the non-reciprocal property is very weak. It has been shown by Sucher and Carlin[131] that for dielectric slabs having $k_e = 100$, and having the same angular width as the ferrite slabs, the $\beta_+ - \beta_-$ exceeds 4·5 radians per cm for a convenient range of slab separation.

Coaxial lines with dielectric loading are finding extensive applications as microwave filters. Design technique for band rejection radial line coaxial filters have been studied by Loach.[78] The effects of different parameters on the resonant frequency of these filters have been investigated and a simple empirical formula for radial line coaxial filters employing teflon dielectric has been determined.[78]

13. Backward Waves

While investigating the propagation characteristics of electromagnetic waves in a circular cylindrical guide of radius a containing a coaxial dielectric rod of radius b, it has been found[71] that propagation is possible when b/a is less than that value for which the phase constant β is zero. This amounts to a negative value of the group velocity $c_g = d\omega/d\beta$. Figures 54(a) and (b) show normalized phase constant $a\beta$ as a function of normalized frequency $a\omega/c$ for different values of b/a. It is observed that the curves pass through a minimum value of $a\omega/c$, i.e. of ω for a finite value of $a\beta$, i.e. of β. The group velocity $d\omega/d\beta = 0$ at the minimum which means that the guide acts as a slow wave structure, while for smaller values of β the group velocity is negative. So β and $d\omega/d\beta$ are of opposite sign which means that the guide can support backward waves. In Fig. 54(b), $b/a = 1$ and $b/a = 0$ which represent respectively the case of dielectric-filled guide and empty guide are given for the sake of comparison. These two curves show that for homogeneous guide β is a monotonic increasing function of frequency and hence such a structure cannot support normal modes with negative $d\omega/d\beta$. This has also been discussed by Adler.[23] Examples of periodic structures, which can support backward waves are well known. But the fact that a

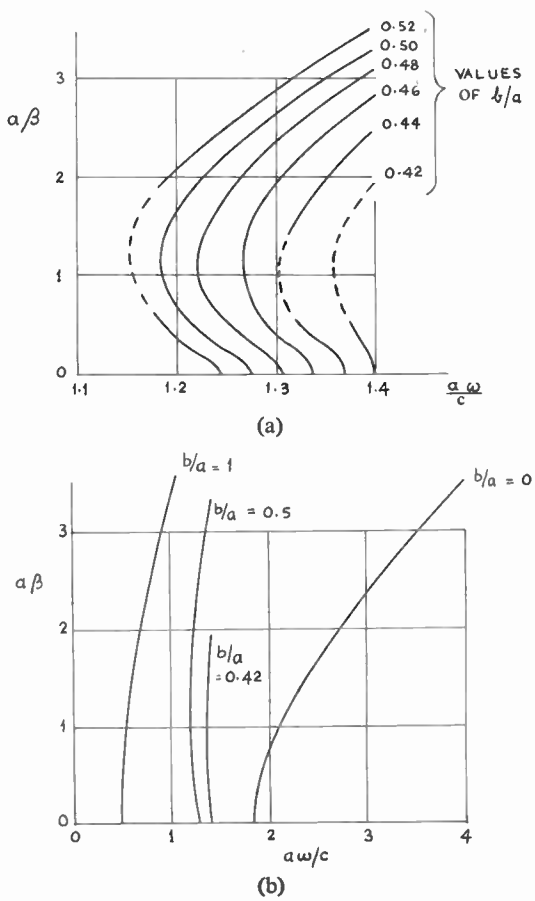

Fig. 54(a) and (b). Normalized phase constant as a function of normalized frequency for different values of b/a, $\varepsilon = 15$. (Ref. 71.)

circular waveguide partially-filled with an axial dielectric rod can also support backward waves is of recent origin.[71–73, 127, 146] Most of the backward waves supported by non-periodic structures discussed so far in the literature are hybrid modes if isotropic non-dispersive materials are used inside the guide. It has been shown by Brown[74] that the necessary and essential but not sufficient conditions for a structure to support backward waves are

$$\int_A \mathrm{Re}[\mathbf{H}_t^* . \mathbf{B}_t - E_z D_z^*]\mathrm{d}A < 0 \quad \text{.....(218)}$$

and

$$\int_A \mathrm{Re}[\mathbf{E}_t . \mathbf{D}_t^* - H_z^* B_z]\mathrm{d}A < 0 \quad \text{.....(219)}$$

where the integrals are taken over the waveguide cross-section and the subscripts t and z indicate transverse and longitudinal components respectively with respect to the guide axis. In the case of isotropic, non-dispersive material having scalar permittivity and permeability, the above equations reduce to

$$\int_A [\mu|\mathbf{H}_t|^2 - \varepsilon|E_z|^2]\mathrm{d}A < 0 \quad \text{.....(220)}$$

$$\int_A [\varepsilon|\mathbf{E}_t|^2 - \mu|H_z|^2]\mathrm{d}A < 0 \quad \text{.....(221)}$$

Since neither E_z nor H_z can be zero, it is concluded that in such a case backward wave characteristic is exhibited by hybrid waves. It may however be mentioned that if the inhomogeneous guide consists of two regions, one in which ε is negative as may happen in the case of plasma and in which $\mathbf{E}_t$ is strong and the second in which ε is positive and E_z is relatively strong, then a backward E mode can be supported by such a structure. Similarly, a backward H mode may be supported if the material in the inhomogeneous guide has a negative μ. The existence of backward waves in waveguides containing plasma has been reported recently by Thelen,[128] Trivelpiece and Gould.[128a] Analogous effects have also been predicted by Trivelpiece *et al.*,[128b] Thompson[128c] and Clarricoats *et al.*,[128d] for waveguides containing ferrites with $|\mu| < |\alpha|$. Waldron[129] has also discussed the existence of backward waves for ferrite loaded waveguides near cut-off with $|\mu| > |\alpha|$ and has pointed out that what is true for dielectric loaded waveguides is also true for the ferrite loaded guides under the above mentioned condition.

The theoretical study of a circular guide containing an axial dielectric rod by Clarricoats[72, 73, 127] and Waldron[129] determines the conditions under which the H_{11} mode of circular guide has a backward wave component. It has been shown that the cut-off conditions of H_{1m} and E_{1m} modes can become degenerate under certain conditions and that the appearance of the backward wave component is associated with the degeneracy in the cut-off conditions.

The characteristic equation for the phase change coefficient β in a lossless structure composed of a circular waveguide of radius r_0 containing an axial dielectric rod of radius r and permittivity ε for modes which possess an azimuthal dependence of unity is[73]

$$\frac{\beta^2}{\omega^2}\frac{[(k_1r_1)^2-(kr_1)^2]^2}{[(k_1r_1)^2(kr_1)^2]^2} = \left[\frac{\mu F(kr_1)}{(kr_1)^2} - \frac{\mu_1 R(k_1,r_1,r_0)}{(k_1r_1)^2}\right] \times \left[\frac{\varepsilon F(kr_1)}{(kr_1)^2} - \frac{\varepsilon_1 S(k_1,r_1,r_0)}{(k_1r_1)^2}\right] \quad \text{.....(222)}$$

where k and k_1 represent wave numbers in the rod and surrounding medium respectively

$$\left.\begin{aligned}
F(kr) &= krJ_n'(kr)/J_n(kr)\\
R(k_1,r,r_0) &= \eta(k_1,r,r_0)/\rho(k_1,r,r_0)\\
S(k_1,r,r_0) &= \xi(k_1,r,r_0)/\sigma(k_1,r,r_0)\\
\eta(k_1,r,r_0) &= (k_1r)[J_1'(k_1r)Y_1'(k_1r_0) - J_1'(k_1r_0)Y_1'(k_1r)]\\
\xi(k_1,r,r_0) &= (k_1r)[J_1'(k_1r)Y_1(k_1r_0) - J_1(k_1r_0)Y_1'(k_1r)]\\
\sigma(k_1,r,r_0) &= [J_1(k_1r)Y_1(k_1r_0) - J_1(k_1r_0)Y_1(k_1r)]\\
\rho(k_1,r,r_0) &= [J_1(kr)Y_1'(k_1r_0) - J_1'(k_1r_0)Y_1(k_1r)]
\end{aligned}\right\} \quad \text{.....(223)}$$

For $\beta = 0$, $\mu = \mu_1 = \mu_0$, $\varepsilon_1 = \varepsilon_0$ (permittivity of the medium surrounding the rod), equations (223) reduce to the cut-off equation

$$\left[F(kr_1) - \frac{\varepsilon}{\varepsilon_0}R(k_1,r_1,r_0)\right][F(kr_1) - S(k_1,r_1,r_0)] = 0 \quad \text{.....(224)}$$

which has two sets of solutions corresponding to modes which at cut-off have either $E_z = 0$ or $H_z = 0$. It can be shown[127] that under certain condition the two roots can be degenerate and the condition for degeneracy is given by

$$F(kr_1) = \bar{\varepsilon}R(k_1,r_1,r_0) = S(k_1,r,r_0) \quad \text{.....(225)}$$

where $\bar{\varepsilon} = \varepsilon/\varepsilon_1$. This degeneracy at cut-off is associated with backward wave propagation above cut-off. If the degeneracy takes place, when the relative permittivity of the rod is $\bar{\varepsilon}_p$ and if $\bar{\varepsilon} > \bar{\varepsilon}_p$, the backward wave mode has $H_z = 0$ at cut-off, while the backward wave mode has $E_z = 0$ at cut-off if $\varepsilon < \bar{\varepsilon}_p$.

The normalized phase change coefficient $\bar{\beta} = \beta/\omega(\mu_1\varepsilon_1)^{\frac{1}{2}}$ is obtained from the solution of eqn. (223). The variation of $\bar{\beta}$ for H_{11} and E_{11} modes with respect to r_1/r_0 for different values of $\bar{\varepsilon} = \varepsilon/\varepsilon_1$ when $\bar{r}_0 = (2\pi r_0/\lambda_0\,\varepsilon_1^{\frac{1}{2}}) = 1$ is shown in Fig. 55. It has been shown[127] that when $\bar{r}_0 = 1$, the condition for a backward wave to exist is $\bar{\varepsilon} > 9{\cdot}85$, while for this value of $\bar{r}_0$, $\bar{\varepsilon}_p = 18{\cdot}3$. It is observed from Fig. 55 that in a backward wave device, there cannot be interference between the hybrid H_{11} and E_{11} modes provided r_1/r_0 is chosen to correspond with the

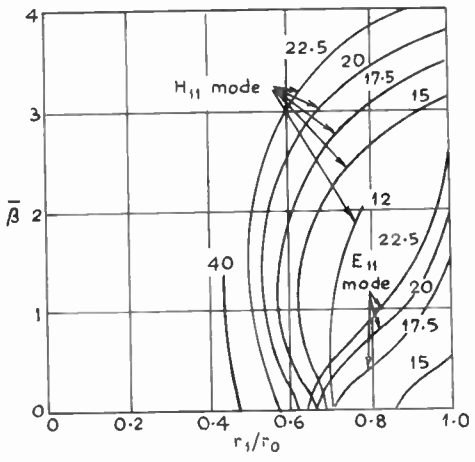

Fig. 55. $\bar{\beta}$ as a function of r_1/r_0 for H_{11} and E_{11} hybrid modes for different values of $\bar{\varepsilon}$, $\bar{r}_0 = 1$. (Ref. 73.)

backward wave region. Figure 56 shows the variation of the normalized ratio $\bar{\Lambda}$ of longitudinal electric fields with respect to r_1/r_0 for different values of $\bar{\varepsilon}$ when $\bar{r}_0 = 1$. It is seen that for the hybrid H_{11} mode,

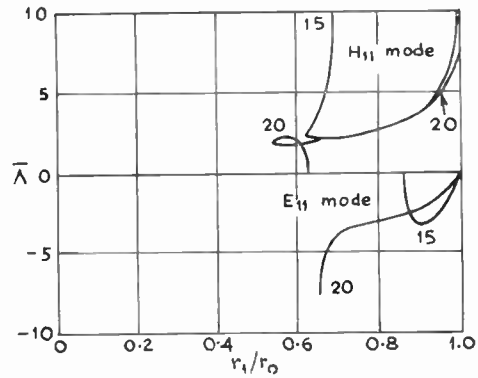

Fig. 56. $\bar{\Lambda}$ as a function of r_1/r_0 for hybrid H_{11} and E_{11} modes for different values of $\bar{\varepsilon}$, $\bar{r}_0 = 1$.

the ratio $\bar{\Lambda}$ is almost unity in the region of maximum bulge and the mode is truly hybrid. Waldron has suggested the nomenclature 'submode' to describe the hybrid mode which possesses a backward wave region.

The ratio of the time average power flow within (P_i) and outside (P_o) the rod has also been calculated by Clarricoats.[124, 125] Figure 57 shows a plot of P_i/P_o vs. r_1/r_0 for hybrid H_{11} and E_{11} modes for various values of $\bar{\varepsilon}$, when $\bar{r}_0 = 1$. It is observed that for $P_i/P_o < 0$ and $|P_i/P_o| < 1$, propagation of backward wave takes place. When $|P_i/P_o| > 1$, propagation of forward wave occurs. The figure also exhibits a difference for the ratio P_i/P_o in the case of the backward and forward waves, other than in the immediate vicinity of the maximum bulge of $\bar{\beta}$. Most of the time average power flows within the rod for the forward wave, whereas, for the backward wave, most of the power flows outside the rod. It has been reported that the largest backward wave region occurs when $\bar{\varepsilon} = \bar{\varepsilon}_p$. Computations for hybrid H_{12}, E_{12}, H_{13} and E_{13} modes over a sufficient range of $\bar{\beta}$ have been made when $\bar{\varepsilon} \simeq \bar{\varepsilon}_p$ to find whether the modes possess backward wave properties. It is found that for hybrid H_{12} mode, the backward wave region lies very close to cut-off, whereas for the hybrid H_{13} mode, it is still closer to cut-off. It is also shown that for these higher modes, although a backward wave region exists when $\bar{\varepsilon} > \bar{\varepsilon}_p$, the extent of the region is very small unless $\bar{\varepsilon} \simeq \bar{\varepsilon}_p$. This may limit the utility of these higher modes in the field of backward wave devices.

It has been shown by Lavik and Unger[146] that backward waves in rectangular and trough guides have more favourable characteristics than in circular guides. The relative permittivity of the dielectric may be as low as 4 as compared to 9·1 in round waveguides. The widest frequency range of a backward wave in rectangular waveguides with optimum size and insert is 11·7% of the cut-off frequency as compared to 9·5% in circular waveguides. The relative permittivity for widest frequency range is 15 as compared to 16·5 in circular waveguides.

14. Imperfect Inhomogeneous Waveguides

The discussions made so far relate to the propagation of electromagnetic waves through inhomogeneous guides having lossless dielectrics enclosed in metallic guides having infinitely conducting walls. If the metallic walls are considered to have finite conductivity and the dielectric to be lossy, the propagating

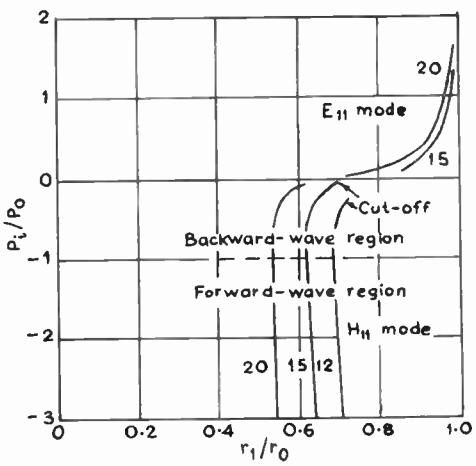

Fig. 57. P_i/P_o as a function of r_1/r_0 for H_{11} and E_{11} modes. Parameter $\bar{\varepsilon}$, $\bar{r}_0 = 1$. (Ref. 73.)

wave will suffer attenuation. If the losses are assumed to be small, the attenuation can be determined in two steps, one due to the dielectric and the other due to the finite conductivity of the metal surface. A brief discussion of the theory of dielectrics is given in Appendix 1.

The attenuation contributed by the finite conductivity of the metallic walls can be determined approximately from the relation

$$\alpha_m = P_L/2P_T \qquad \text{.....(226)}$$

which gives the ratio between the power lost (P_L) per unit length of the metallic wall and the power transmitted (P_T). P_L and P_T can be found in the usual way from the field components. In the power loss method (eqn. (226)), the field distribution is assumed to be the same as when the conductivity of the walls is assumed to be infinite. In this method, no information is available about the change in the imaginary part of the propagation constant, i.e., change in phase change coefficient caused by imperfectly conducting walls. It is known[145] that the wall loss per unit length is not necessarily additive when two or more modes are present simultaneously so the result found by this method is valid only when the propagating modes are non-degenerate. In other words, the result obtained by this method is correct when there is no degeneracy between the mode under consideration and any other propagating modes along the perfectly conducting walls of the guide. If there is degeneracy, energy may be continuously coupled from the desired mode to other degenerate modes via the surface impedance presented by the waveguide walls. Thus the mode pattern is no longer stable. This is the case for example, with H_{mn} and E_{mn} modes ($m \neq 0$; $n \neq 0$) in a lossy rectangular guide since these modes are always degenerate. The attenuation caused by the losses in the dielectric can be determined by using complex dielectric constant k_c^* instead of k_c. This method of substituting k_c^* for k_c in the term for phase constant and using the first term of the binomial expansion is not accurate in the region of low loss. A more correct approach is to expand the characteristic equation in a Taylor's series about the point determined by the solution of the characteristic equation for lossless dielectric and set it equal to zero. The attenuation constant is then determined by solving[56, 140] this expression. Theoretical study of imperfect waveguides has been made by Karbowiak,[57] Papadopoulos,[58] Chatterjee[56] and other authors.[15, 59–67, 143, 144]

14.1. *Cylindrical Guide with Imperfectly Conducting Walls*

The propagation of electromagnetic waves in cylindrical waveguides of arbitrary cross-section and having imperfectly conducting walls enclosing free space has been studied by Papadopoulos[58] by using the perturbation method and approximate boundary conditions at the walls. The principle of this method is based on the assumption that there exists an eigenvalue in the imperfect guide corresponding to each eigenvalue in a perfect guide and the difference between corresponding eigenvalues is of the order of η where $\eta = \frac{1}{2}\delta\omega(1+j)$ and δ is the skin depth.

The field $\mathbf{E}'$ in the perturbed guide can be expressed in terms of the field $\mathbf{E}_r$ in the unperturbed guide as

$$\mathbf{E}' = \sum_{r=1}^{m} a_{0r}\mathbf{E}_{0r} + 0(\eta) \qquad \text{.....(227)}$$

The electric field $\mathbf{E}$ represents the transverse components and satisfies the equation

$$-\nabla(\nabla . \mathbf{E}) + \mathbf{k} \wedge \nabla(\nabla . \nabla \wedge \mathbf{E}) = \rho\mathbf{E} \qquad \text{.....(228)}$$

and the boundary conditions

$$\left.\begin{aligned} \mathbf{E} . \mathbf{s} &= \frac{\eta}{j\omega} \nabla . \mathbf{k} \wedge \mathbf{E} \\ \nabla . \mathbf{E} &= \eta\left[\frac{j\omega}{c^2}\mathbf{E} . \mathbf{n} + \mathbf{s} . \nabla(\nabla . \mathbf{k} \wedge \mathbf{E})\right] \end{aligned}\right\} \qquad \text{.....(229)}$$

where $\mathbf{k}$ is the unit vector in the z direction, $\mathbf{n}$ is the unit vector in the direction of the outward normal to the boundary S of the cross-section A of the guide and $\mathbf{s}$ is a unit vector forming a right-handed system with the vectors $\mathbf{n}$ and $\mathbf{k}$ in the order $\mathbf{n}, \mathbf{s}, \mathbf{k}$. ρ is a constant given by $\rho = \gamma^2 + \omega^2/c^2$ and

$$a_{0r} = \iint_A \mathbf{E}' . \mathbf{E}_{0r}\, ds \qquad \text{.....(230)}$$

If ρ' corresponding to a mode in an imperfect guide has a value close to a particular eigenvalue ρ_0 of the perfect guide of the set of values ρ_r, then the following set of m linear homogeneous equations in which ρ' is a parameter yield the complex propagation constant γ

$$(\rho' - \rho_0)a_{0r'} = \eta \oint_s \sum_{r=1}^{m} a_{0n}\left\{\frac{(\nabla . \mathbf{k} \wedge \mathbf{E}_{0r'})(\nabla . \mathbf{k} \wedge \mathbf{E}_{0r'})}{j\omega} - (\mathbf{E}_{0r'} . \mathbf{n})\left[\frac{j\omega}{c^2}\mathbf{E}_{0r} . \mathbf{n} + \frac{1}{j\omega}\mathbf{s} . \nabla(\nabla . \mathbf{k} \wedge \mathbf{E}_{0r})\right]\right\} ds \qquad \text{.....(231)}$$

$$r' = 1, 2, 3, \ldots, m$$

The equations have a solution for those values of ρ' for which the determinant of the coefficient of a_{0r} vanishes.

In the case of a non-degenerate mode in a guide having infinitely conducting walls

$$\mathbf{E}' = a_{01}\mathbf{E}_{01} + 0(\eta)$$

$$(\rho' - \rho_0) = \eta \oint_s \left\{\frac{(\nabla . \mathbf{k} \wedge \mathbf{E}_{01})(\nabla . \mathbf{k} \wedge \mathbf{E}_{01})}{j\omega} - (\mathbf{E}_{01} . \mathbf{n}) \times \left[\frac{j\omega}{c^2}(\mathbf{E}_{01} . \mathbf{n}) + \frac{\mathbf{s} . \nabla(\nabla . \mathbf{k} \wedge \mathbf{E}_{01})}{j\omega}\right]\right\} ds \qquad \text{.....(232)}$$

Using Maxwell's equations to express **B** (transverse components) and B_z in terms of $\mathbf{E}_{01}$, the following equation is obtained[58]

$$(\rho'-\rho_0)=\eta\oint_s\{j\omega B_z^2+\gamma_0(\mathbf{E}_{01}\,.\,\mathbf{n})(\mathbf{B}\,.\,\mathbf{s})\}\,ds \qquad \text{.....(233)}$$

where γ_0 represents the propagation constant in the perfect guide. Above cut-off $\omega^2 > \rho_0 c^2$ and $\gamma_0 = j\beta_0$, so

$$\alpha = \mathrm{Re}\,(\gamma) = \frac{1}{2\beta_0}\,\mathrm{Im}\,(\rho'-\rho_0)$$

Hence,

$$\alpha=\frac{1}{2\beta_0}\,\mathrm{Im}\left[\eta\oint_s\{j\omega B_z^2+j\beta_0(\mathbf{E}_{01}\,.\,\mathbf{n})(\mathbf{B}\,.\,\mathbf{s})\}\,ds\right]$$

As .....(234)

$$\mathbf{B}=\frac{j\omega}{\gamma c^2}\,\mathbf{k}\wedge\mathbf{E} \qquad \text{for E mode}$$

and .....(235)

$$\mathbf{B}=\frac{\gamma}{j\omega}\,\mathbf{k}\wedge\mathbf{E} \qquad \text{for H mode}$$

Therefore, from eqns. (234) and (235)

$$\alpha=\frac{1}{2\beta_0}\,\mathrm{Im}\left[\frac{j\eta\beta_0^2c^2}{\omega}\oint_s(\mathbf{B}\,.\,\mathbf{s})^2\,ds\right] \qquad \text{for E modes}$$

and

$$\alpha=\frac{1}{2\beta_0}\,\mathrm{Im}\left[j\eta\omega\oint_s\{\mathbf{B}_z^2+(\mathbf{B}\,.\,\mathbf{s})^2\}\,ds\right] \qquad \text{for H modes}$$

Papadopoulos[58] and Kurokawa[143] have also clarified how the removal of degeneracy takes place when the wall loss is finite. In a circular cylindrical guide with perfectly conducting walls for all modes except those which are circularly symmetric there are two modes corresponding to each eigenvalue. Such a degeneracy will not be resolved in an imperfect circular guide. In a rectangular guide E_{mn} and H_{mn} modes have the same eigenvalue, so there is twofold degeneracy. In this case,

$$\mathbf{E}=-a_1\nabla\phi-a_2\mathbf{k}\wedge\nabla\psi+0(\eta) \qquad \text{.....(236)}$$

where ϕ and ψ satisfy respectively

$$(\nabla^2+\rho_r^{(1)})\phi_r=0$$
$$(\nabla^2+\rho_r^{(2)})\psi_r=0$$

and

$E_r^{(1)}=-\nabla\phi_r$ corresponds to the E mode
$E_r^{(2)}=-\mathbf{k}\wedge\nabla\psi_r$ corresponds to the H mode

The propagation equations in this case reduce to

$$(\rho'-\rho_0)a_1=-\eta\oint_s\frac{j\omega}{c^2}\frac{\partial\phi}{\partial n}\left(a_1\frac{\partial\phi}{\partial n}+a_2\frac{\partial\psi}{\partial s}\right)ds \qquad \text{for E modes}$$

$$(\rho'-\rho_0)a_2=\eta\oint_s\left\{\frac{a_2(\rho_0\psi)^2}{j\omega}-\frac{\partial\psi}{\partial s}\left(a_1\frac{j\omega}{c^2}\frac{\partial\phi}{\partial n}+a_2\frac{\gamma^2}{j\omega}\frac{\partial\psi}{\partial s}\right)\right\}ds \qquad \text{for H modes} \qquad \text{.....(237)}$$

Using the expressions for ϕ_{mn} and ψ_{mn} given by Marcuvitz[97] and the eigenvalue

$$\rho_0=\frac{m^2\pi^2}{a^2}+\frac{n^2\pi^2}{b^2} \qquad \text{.....(238)}$$

the equations for propagation above the cut-off frequency ($\omega > \omega_c$) are

$$\left[\frac{\omega^2}{c^2}\left(\frac{n^2\pi^2a^2}{b^2}+\frac{m^2\pi^2b^2}{a^2}\right)-\lambda\right]a_1+\left[\frac{\omega^2mn\pi^2}{c^2ab}(a-b)\right]a_2=0 \qquad \text{.....(239)}$$

and

$$\left[\frac{\omega^2mn\pi^2}{c^2ab}(a-b)\right]a_1+\left[\beta_0^2\left(\frac{m^2\pi^2}{a^2}+\frac{n^2\pi^2}{b^2}\right)+(a+b)\frac{\omega_0^4}{c^4}-\lambda\right]a_2=0$$

where

$$\lambda=\frac{jab\omega_0^2\,\omega(\rho'-\rho_0)}{4c^2\eta}, \qquad \gamma_0=j\beta_0=\text{propagation constant in the perfect guide}$$

Hence,

$$\gamma^2+\beta_0^2=\frac{4c^2(1-j)}{\omega_0^2ab}\sqrt{\frac{\mu\lambda}{2\mu_0\omega\sigma}}$$

It follows from the above equation that when $a = b$ (square guide), pure E and H modes are propagated with different propagation constants, i.e. there is no coupling between E and H modes. For $a \neq b$, the equations determine a solution for a_1 and a_2, provided the determinant of the coefficients vanishes. The vanishing of the determinant leads to two roots of γ^2. For one root $a_1 > a_2$ and this is the propagation constant for a mode corresponding to a perturbed mode H. The other root corresponds to a perturbed E mode for which $a_2 > a_1$.

Robson[64] and Kurokawa[143] have studied the same problem by using the variational principle. The variational expression[64] for the complex propagation coefficient of a cylindrical waveguide of arbitrary cross-section and having inperfectly conducting walls is

$$j\gamma = \frac{\iint (\omega\mu \mathbf{H}_- . \mathbf{H}_+ - \omega\varepsilon \mathbf{E}_+ . \mathbf{E}_- - j\mathbf{H}_- . \nabla_t \times \mathbf{E}_+ - j\mathbf{E}_+ . \nabla_t \times \mathbf{H}_-) ds + j \oint \mathbf{H}_- . (\mathbf{n} \times \mathbf{E}_+ - Z_s \mathbf{H}_+ (\tan)) dl}{2 \iint \mathbf{E}_+ \times \mathbf{H} . \mathbf{k}\, ds} \quad \ldots\ldots(240)$$

where the subscripts + and − indicate propagation in the positive and negative z direction respectively, and Z_s represents the surface impedance of the guide wall. This equation is used to determine the nature of the stable modes that may be propagated in a lossy rectangular waveguide. The propagation equation is

$$-(\beta - \beta_{mn}) + j\alpha = \frac{2jZ_s(k_{mn}^2 - 1)^{\frac{1}{2}}}{abZ_0 k_{mn}[(k_{mn}^2 - 1) + \delta_{mn}^2 k_{mn}^2][m^2 b^2 + n^2 a^2]} \left[k_{mn}^2 (m^2 ab^2 + n^2 a^2 b) + \right.$$
$$\left. + (m^2 b^3 + n^2 a^3) + 2k_{mn}^2 \delta_{mn} (mn)(ab)(b-a) + \frac{k_{mn}^4 \delta_{mn}^2}{(k_{mn}^2 - 1)} (a^3 n^2 + m^2 b^3) \right] \quad \ldots\ldots(241)$$

where $Z_0 = 120\pi$ ohms free space impedance and

$$k_{mn} = \frac{k}{k_{cmn}}$$
$$k_{cmn}^2 = (m\pi/a)^2 + (n\pi/b)^2$$
$$\beta_{mn}^2 + k_{cmn}^2 = k^2 = \omega^2 \mu\varepsilon$$

δ_{mn} determines the ratio in which H_{mn} and E_{mn} modes combine and is given by the following equation

$$\left(\frac{mn}{ab}\right)(b-a)[k_{mn}^2 \delta_{mn}^2 - (k_{mn}^2 - 1)] + \delta_{mn} \left[k_{mn}^2 (b-a) \left(\frac{m^2}{a^2} - \frac{n^2}{b^2} \right) - \left(\frac{n^2 a}{b^2} + \frac{m^2 b}{a^2} \right) \right] = 0 \quad \ldots\ldots(242)$$

The two roots of δ_{mn} can be found from the solution of eqn. (242). These two roots define the ratio in which H_{mn} and E_{mn} normal modes combine to form the two possible stable modes that might exist in the lossy rectangular guide. The values of δ_{mn} substituted in eqn. (241) will yield the change in phase change coefficient $(\beta - \beta_{mn})$ and the attenuation constant α. It has been shown by Kurokawa[143] that the results obtained by the perturbation method in a slightly modified form from that used by Papadopoulos[58] is identical with that obtained by the variational principle.

14.2. *Parallel Plane Guide with Imperfectly Conducting Walls and Imperfect Dielectric*

By following the power loss method, the attenuation constant of a parallel plane guide having walls of finite conductivity and filled with a lossy dielectric has been computed for even and odd order H modes and the results are[41]

$$\alpha_{me} b\sqrt{\lambda_0} = \frac{0{\cdot}0291}{\sqrt{\sigma_m}} \frac{\left[\pi^2 \frac{\varepsilon_1}{\varepsilon_0} \left(\frac{d}{\lambda_0} \right)^2 - \frac{(k_{1e}a)^2 \cot k_{1e}a}{k_{1e}a + \cot k_{1e}a} \right]}{\left(\frac{d}{\lambda_0} \right) \sqrt{\pi^2 \frac{\varepsilon_1}{\varepsilon_0} \left(\frac{d}{\lambda_0} \right)^2 - (k_{1e}a)^2}} \quad \ldots\ldots(243)$$

$$\alpha_{mo} b\sqrt{\lambda_0} = \frac{0{\cdot}0291}{\sqrt{\sigma_m}} \frac{\left[\pi^2 \frac{\varepsilon_1}{\varepsilon_0} \left(\frac{d}{\lambda_0} \right)^2 (k_{1o}a - \tan k_{1o}a) + (k_{1o}a)^2 \tan k_{1o}a \right]}{\left(\frac{d}{\lambda_0} \right) (k_{1o}a - \tan k_{1o}a) \sqrt{\pi^2 \frac{\varepsilon_1}{\varepsilon_0} \left(\frac{d}{\lambda_0} \right)^2 - (k_{1o}a)^2}} \quad \ldots\ldots(244)$$

$\sigma_m = 5{\cdot}80 \times 10^7$ mho/m. b is the height of the guide, d is the thickness of the dielectric and $a = d/2$. α_{me} and α_{mo} represent the attenuation due the finite conductivity of the walls for the even and odd order modes respectively.

The expressions for dielectric attenuation α_{de} and α_{do} in the case of even and odd order H modes are respectively

$$\alpha_{de}\lambda_0 = \frac{\pi^2 \frac{\varepsilon_1}{\varepsilon_0}\phi_d\left(\frac{d}{\lambda_0}\right)}{\sqrt{\pi^2 \frac{\varepsilon_1}{\varepsilon_0}\left(\frac{d}{\lambda_0}\right)^2 - (k_{1e}a)^2}} \left[\frac{k_{1e}a + \sin k_{1e}a \cos k_{1e}a}{k_{1e}a + \cot k_{1e}a}\right] \qquad \text{.....(245)}$$

$$\alpha_{do}\lambda_0 = \frac{\pi^2 \frac{\varepsilon_1}{\varepsilon_0}\phi_d\left(\frac{d}{\lambda_0}\right)}{\sqrt{\pi^2 \frac{\varepsilon_1}{\varepsilon_0}\left(\frac{d}{\lambda_0}\right)^2 - (k_{1o}a)^2}} \left[\frac{k_{1o}a - \sin k_{1o}a \cos k_{1o}a}{k_{1o}a - \tan k_{1o}a}\right] \qquad \text{.....(246)}$$

ϕ_d = dielectric loss tangent.

Figure 58 represents the variation of α_{me} with respect to d/λ_0 for different values of $\varepsilon_1/\varepsilon_0$. Figure 59 represents the variation of α_{de} with respect to d/λ_0 for different values of $\varepsilon_1/\varepsilon_0$. In both the cases, the mode is dominant and the medium outside the dielectric is air.

14.3. *Imperfectly Conducting Rectangular Guide Partially Filled with an Imperfect Dielectric*

Treating this as a boundary value problem Woodward[15] has derived the following relation for the attenuation constant when the guide (Fig. 18) is excited by an H_{01} wave, by assuming σ_1 to be sufficiently small so that β has the same value given by eqn. (142) for $\sigma_1 = 0$:

$$\frac{\alpha\beta}{\mu_2}\left[\frac{\varepsilon_2^2-\varepsilon_0^2}{(\varepsilon_0^2-\beta^2)\sqrt{\varepsilon_2^2-\beta^2}}\cot\{d\sqrt{\varepsilon_2^2-\beta^2}\} + \frac{\mu_2}{\mu_0}(\tfrac{1}{2}a-d) + d + \tfrac{1}{2}\left\{(\tfrac{1}{2}a-d)\frac{\mu_0}{\mu_2}\frac{\varepsilon_2^2-\beta^2}{\varepsilon_0^2-\beta^2} + d\right\}\cot^2\{d\sqrt{\varepsilon_2^2-\beta^2}\}\right]$$

$$= \tfrac{1}{2}\sigma_2\omega\left[d + d\cot^2\{d\sqrt{\varepsilon_2^2-\beta^2}\} - \frac{\cot\{d\sqrt{\varepsilon_2^2-\beta^2}\}}{\sqrt{\varepsilon_2^2-\beta^2}}\right] \qquad \text{.....(247)}$$

The attenuation is due to the losses in the dielectric as given in Fig. 60, where

$$\mu_1 = \mu_2 = \mu_0 = 4\pi \times 10^{-9} \text{ H/cm}$$
$$\sigma_2 = 1{\cdot}9 \times 10^{-6} \text{ mho/cm} \quad \text{for polyethylene}$$
$$\varepsilon_2 = 2{\cdot}3\varepsilon_0 = \frac{2{\cdot}3 \times 10^{-11}}{36\pi} \text{ F/cm}$$

It is noted that as the frequency increases indefinitely the attenuation tends to the same value. The attenuation due to losses in the walls of the guide can be found by the usual power loss method.

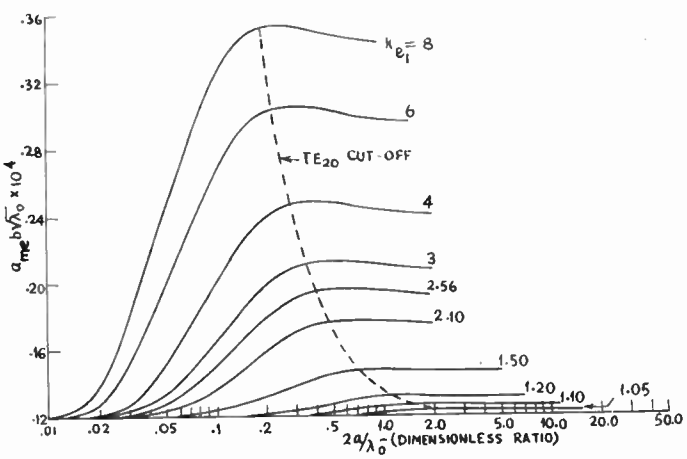

Fig. 58. Attenuation constant (nepers per metre) due to imperfect conductivity of walls as a function of normalized dielectric slab width for dominant mode. Outer region: air ($\sigma_{cn} = 5{\cdot}80 \times 10-7$ mho/m). (Ref. 41.)

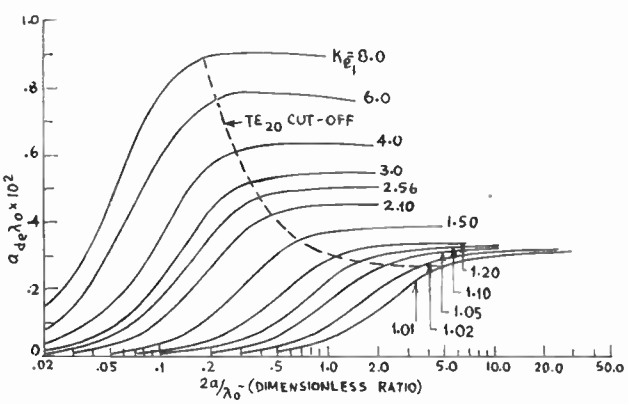

Fig. 59. Attenuation constant (nepers per metre) due to dielectric loss as a function of normalized dielectric slab width for dominant mode. Outer region: air. Loss tangent $\phi_d = 0{\cdot}001$. (Ref. 41.)

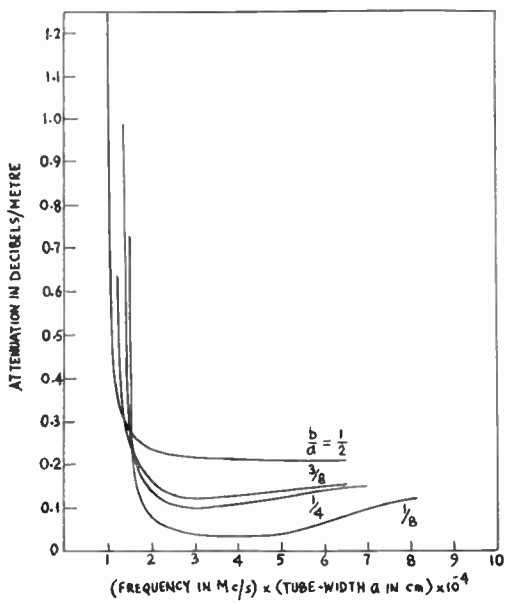

Fig. 60. Variation of attenuation in dB per metre vs. the product of frequency in Mc/s and tube width in cm for various values of b/d for H_{01} mode. (Ref. 15.)

14.4. *Imperfectly Conducting Cylindrical Guide Filled with an Imperfect Dielectric*

The guide with imperfectly conducting walls may be considered to consist of infinitely conducting walls with a coating of resistance sheet of thickness greater than the skin depth. The problem then reduces to the case of an inhomogeneously-filled guide in which case, the propagation of a pure E or H mode is not possible except E_{01} or H_{01} mode.

The propagation of the EH_{11} mode through such a guide has been studied as a boundary value problem. Applying proper boundary conditions at the interface between the walls of the guide and the dielectric enclosed, the following characteristic equation[56] is obtained

$$\frac{\chi_1''}{\chi_2''}\frac{H_1^{(1)\prime}(\chi_2'' a)}{H_1^{(1)}(\chi_2'' a)} = \frac{J_1'(\chi_1'' a)}{J_1(\chi_1'' a)} \qquad \text{.....(248)}$$

Using recurrence relations and asymptotic expansions for the Hankel functions, the following equation is obtained

$$\frac{J_0(\chi_1'' a)}{J_1(\chi_1'' a)} = \frac{1}{\chi_1'' a} - \frac{\chi_1''}{\chi_1''^2 a} - j\frac{\chi_1''}{\chi_2''} \qquad \text{.....(249)}$$

Expanding J's in the above equation by complex Taylor series, substituting the values in (249), using the relation

$$\chi_2''^2 = \chi_1''^2 - k_1^2 + k_2^2 \qquad \text{.....(250)}$$

rearranging the terms and separating the real and imaginary parts, the following two equations are obtained

$$a^2 r_{01}\chi_1''^4 - a r_{01}^2 \chi_1''^3 + \\ + (a^2 r_{01} k_2^2 - a^2 r_{01} k_1^2 - 2a r_{01} + 2r_{01})\chi_1''^2 + \\ + (a r_{01}^2 k_1^2 - a r_{01}^2 k_2^2 + a k_1^2 - a k_2^2)\chi_1'' + \\ + 2r_{01}(k_2^2 - k_1^2) = 0 \qquad \text{.....(251)}$$

and

$$a^2 \chi_1''^2 [\chi_1'' - 2r_{01}][\chi_1''^2 - k_1^2 + k_2^2]^{\frac{1}{2}} = 0 \qquad \text{.....(252)}$$

where $r_{01} = 2{\cdot}4048$

The above equations have been solved for the propagation constant χ_1''. The following conclusions are arrived at from the solution of eqn. (252):

(i) $\chi_1''^2 = 0$, which gives the propagation constant as $h'' = jk_1$ which yields the attenuation constant as $\alpha = 0$.

(ii) $\chi_1'' - 2r_{01} = 0$, which yields

$$h'' = j\sqrt{k_1^2 - 4r_{01}^2}$$

or

$$h'' = -\sqrt{4r_{01}^2 - k_1^2}$$

In the former case, $\alpha = 0$ and $\beta = \sqrt{k_1^2 - 4r_{01}^2}$. In the latter case, α is negative and $\beta = 0$.

(iii) $\chi_1''^2 = k_1^2 - k_2^2$ or $h'' = jk_2$ which gives $\alpha = 0$. So the solution of the eqn. (252) for χ_1'' is physically inadmissible in the present case. The eqn. (251) which is quartic in χ_1'' has been solved by the usual Ferrari's method.[142] The solution yields four values of χ_1''. It is found that ${}^1\chi_1''$ and ${}^3\chi_1''$ and hence h_1'' and h_2'' give rise to the existence of either a backward wave of decreasing amplitude or a forward wave of increasing amplitude. As we are concerned with a forward wave of decreasing amplitude, the two propagation constants being physically inadmissible are discarded. The root ${}^2\chi_1''$ is found to be vanishingly small and therefore does not yield a valid solution. The other root ${}^4\chi_1''$ yields the following values of the attenuation constant α and the phase constant β

$$\alpha = \frac{1}{\sqrt{2}}\left[\left\{\left(k_1^2 + \frac{e^2}{2}\right)^2 - \tfrac{3}{4}e^4\right\}^{\frac{1}{2}} - k_1^2 - \frac{e^2}{2}\right]^{\frac{1}{2}} \qquad \text{.....(253)}$$

$$\beta = \frac{1}{\sqrt{2}}\left[\left\{\left(k_1^2 + \frac{e^2}{2}\right)^2 - \tfrac{3}{4}e^4\right\}^{\frac{1}{2}} + k_1^2 + \frac{e^2}{2}\right]^{\frac{1}{2}}$$

where the factor e depends on the electrical properties of the boundary wall of the guide and the enclosed dielectric.

14.5. *Circular Cylindrical Waveguide containing a Coaxial Dielectric Rod*

Assuming that the loss is contributed by only the dielectric rod and that the power lost per wavelength along the rod is small compared to the total power flowing and β is not too near cut-off, the following expression for the attenuation coefficient α per unit

length of the dielectric-rod-waveguide structure has been derived by Clarricoats[125]

$$\alpha = \frac{\bar{\mu}''\left[(\bar{\varepsilon}^2+\bar{\Lambda}^2\bar{\beta}^2)T_1+2\bar{\Lambda}\bar{\varepsilon}\bar{\beta}+\left(\frac{\lambda_0}{2\pi}\right)^2\bar{\Lambda}^2k^4T_5\right]+ +\bar{\varepsilon}''\left\{[\bar{\beta}^2+(\bar{\Lambda}\bar{\mu})^2]T_1+2\bar{\Lambda}\bar{\mu}\bar{\beta}+\left(\frac{\lambda_0}{2\pi}\right)^2k^4T_5\right\}}{\{[(\bar{\varepsilon}+\bar{\mu}\bar{\Lambda}^2)T_1+\bar{\Lambda}(\bar{\mu}\bar{\varepsilon}/\bar{\beta}+\bar{\beta})]+ +(k/k_1)^4[(\bar{\varepsilon}_1T_3+\bar{\mu}_1\bar{\Lambda}^2T_4-\bar{\Lambda}(\bar{\mu}_1\bar{\varepsilon}_1/\bar{\beta}+\bar{\beta})]\}} \quad \ldots\ldots(254)$$

where

$$T_5 = \tfrac{1}{2}r_1^2\left\{\left[1-\frac{1}{(kr_1)^2}\right]+\frac{J_1'(kr_1)^2}{J_1(kr_1)^2}\right\}$$

For other symbols see section 10. Near cut-off $\bar{\beta}\to 0$, eqn. (254) reduces to

$$\alpha = \frac{\left[\bar{\mu}''\left(\frac{\lambda_0}{2\pi}\right)^2k^4T_5+\bar{\varepsilon}''\bar{\mu}^2T_1\right]\left(\frac{\pi\lambda}{\lambda_0^2}\right)}{(\bar{\mu}T_1+\bar{\mu}\bar{\varepsilon}/\bar{\Lambda}\bar{\beta})+(k/k_1)^4(\bar{\mu}_1T_4-\bar{\mu}_1\bar{\varepsilon}_1/\bar{\Lambda}\bar{\beta})} \quad \ldots\ldots(255)$$

for H_{1m} limit mode, and

$$\alpha = \frac{[\bar{\mu}''\varepsilon^{-2}T_1+\bar{\varepsilon}''(\lambda_0/2\pi)^2k^4T_5]\left(\frac{\pi\lambda}{\lambda_0^2}\right)}{(\bar{\varepsilon}_1T_1+\bar{\mu}\bar{\varepsilon}/\bar{\Lambda}\bar{\beta})+(k/k_1)^4(\bar{\varepsilon}_1T_3-\bar{\Lambda}\bar{\mu}_1\bar{\varepsilon}_1/\bar{\beta})} \quad \ldots(256)$$

for E_{1m} limit modes. The above equations for α are valid under the restrictions.

(i) $\bar{\beta}$ must be small so that terms containing $\bar{\beta}^2$ may be neglected compared to those terms which do not contain $\bar{\beta}$.

(ii) As $\bar{\beta}\to 0$, the value of $\bar{\mu}''/\bar{\mu}'$ and $\bar{\varepsilon}''/\bar{\varepsilon}'$ must be of order $\bar{\beta}^2$ or less.

(iii) In the limit $\bar{\beta}\to 0$, the wall losses cannot be ignored.

By using perturbation method, it has been shown by Suhl and Walker[148] that the change in propagation constant $\delta\gamma = \alpha+j\delta\beta$ due to the introduction of a thin rod with permeability μ and permittivity ε into a waveguide is given by the following expression, when $\bar{\mu}=1$

$$\delta\gamma = \frac{j\omega}{2\int_{S_0}\mathbf{E}_{t,nm}\times\mathbf{H}_{t,nm}\cdot d\mathbf{s}} \times \left\{\int_{S_1}[(\mu-\mu_0)\mathbf{H}.\mathbf{H}_{nm}^*+(\varepsilon-\varepsilon_0)\mathbf{E}.\mathbf{E}_{nm}^*]d\mathbf{s}\right\} \quad \ldots\ldots(257)$$

where $\mathbf{H}$ and $\mathbf{E}$ represent perturbed fields and $\mathbf{H}_{nm}$, $\mathbf{E}_{nm}$ the fields inside the guide before the rod is inserted. S_1 and S_0 represent the cross-section surfaces of the rod and waveguide respectively.

The above expression (257) leads to the following expression for the attenuation constant for the H_{11} mode in the dielectric-rod-waveguide structure when the rod is thin:

$$\alpha = \frac{u_1^2}{J_1^2(u_1)(u_1^2-1)}\frac{2\pi}{\lambda_0}\left(\frac{r_1}{r_0}\right)^2 \times \times\left[\bar{\beta}_0\frac{\bar{\mu}''}{(\bar{\mu}'+1)^2+\bar{\mu}''^2}+\frac{1}{\bar{\beta}_0}\frac{\bar{\varepsilon}''}{(\bar{\varepsilon}'+1)^2+\bar{\varepsilon}''^2}\right] \quad \ldots\ldots(258)$$

where u_1 is the first root of $J_1(x)$ and $\bar{\beta}_0$ is the phase change coefficient in the unperturbed guide.

The attenuation constant α of a waveguide completely filled with a lossy dielectric is given by the expression[125]

$$\alpha = \frac{\sqrt{2}\pi}{\lambda_0}\left[\left\{\left(\frac{\lambda_0}{\lambda_c}\right)^2+\bar{\varepsilon}''\bar{\mu}''-\bar{\varepsilon}'\bar{\mu}'\right\}+ +\left\{\left[\left(\frac{\lambda_0}{\lambda_c}\right)^2+\bar{\varepsilon}''\bar{\mu}''-\bar{\varepsilon}'\bar{\mu}'\right]^2+(\bar{\varepsilon}''\bar{\mu}'+\bar{\mu}''\bar{\varepsilon}')^2\right\}^{\frac{1}{2}}\right]^{\frac{1}{2}} \quad \ldots\ldots(259)$$

Clarricoats[125] has also derived a relation for the attenuation coefficient of the structure in terms of the attenuation factors F_M and F_D for magnetic and dielectric loss respectively. Using the general expression (Appendix 2), the attenuation constant of a guide of diameter 0·875 inches and containing a dielectric rod whose parameters are $\bar{\mu}=1{\cdot}6$, $\bar{\varepsilon}=11{\cdot}4$, $2r_0/\lambda_0=0{\cdot}685$ has been determined at 9·25 Gc/s and their variations with the normalized rod diameter $(2r_1/\lambda_0)$ are shown in Fig. 61. The difference between the

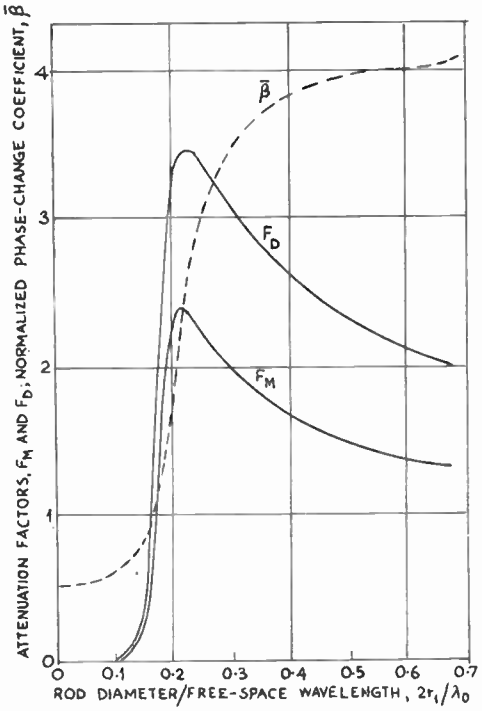

Fig. 61. $\bar{\beta}$ and attenuation factors F_M and F_D as a function of $2r_1/\lambda_0$. Scale factor for F_D multiplied by a factor of 10. Ref. 125.)

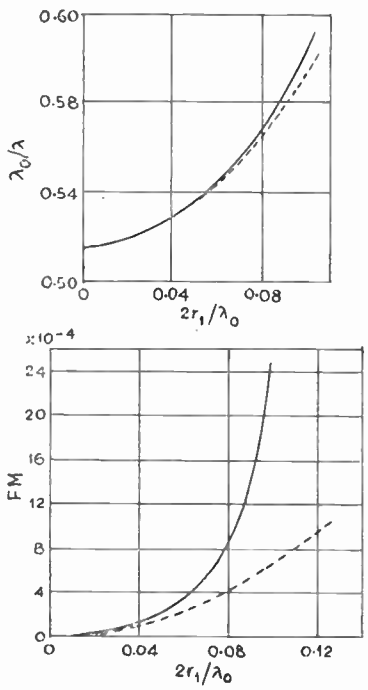

Fig. 62. $\bar{\beta}$ and attenuation factor F_M for H_{11} limit mode as a function of $2r_1/\lambda_0$. (Ref. 125.)

results obtained from eqn. (258) and that obtained from the exact expression given by Clarricoats[125] is shown in Fig. 62. The exact expression for α when $\bar{\mu} \neq 1$ is given in Appendix 2.

It is observed from Fig. 62 that the range of values of r_1/r_0 for which the thin rod perturbation is valid is much less for the attenuation coefficient than for the phase change coefficient. This is probably due to the fact that the guiding influence of the rod when determining the internal r.f. fields has been ignored. This affects the attenuation constant significantly, when the diameter of the rod is small.

15. Dielectric Post in Rectangular Waveguide

The problem is treated as one of discontinuity in a waveguide. The presence of a discontinuity generates a reflected wave and gives rise to a storage of reactive energy in the vicinity of the discontinuity due to the excitation of higher-order evanescent waves. If the dominant H_{01} mode is incident on the obstacle from

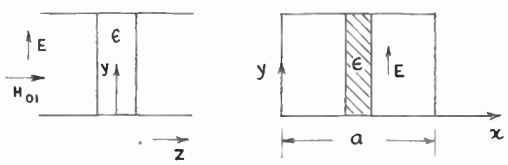

Fig. 63. Dielectric post in rectangular guide.

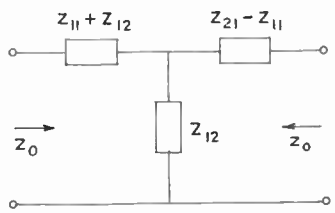

Fig. 64. Equivalent circuit of a rectangular guide containing a dielectric post. (Ref. 99.)

both directions with arbitrary amplitudes, the effect of the obstacle is then to generate a far field, consisting of scattered or reflected field and it also produces entirely local fields arising from the excitation of the exponentially attenuated higher-order modes. A complete description of the obstacle would need consideration of both fields in detail. Since from a practical point of view we are interested in the propagation of energy by the waveguide, it is necessary to consider the effect of the obstacle only on the propagating mode. It is also evident that any discontinuity, such as a post when introduced into the guide disturbs the cylindrical symmetry of the system about the axis. So it is no longer possible to derive the entire field from a single Hertz vector. Several authors[36, 99, 149–151] have treated the problem of discontinuity in a waveguide. The method of approach and the results obtained by Schwinger[99] is discussed below. The dielectric post is placed in the y-direction in a rectangular guide (Fig. 63) and is excited by H mode. As the electric field is only in the y-direction, the problem reduces to a two-dimensional scalar problem.

If the incident electric field is denoted by $\phi^{in}(x, z)$ and $G(x, z; x', z')$ represents the Green's function such that $-jkc\mu G$ is the y-component of the electric field at (x, z), due to a unit current filament in the y-direction at (x, z), then the electric field at any point (x, z) in the guide is given by the following integral equation[99]:

$$\phi(x,z) = \phi^{in}(x,z) + (\varepsilon - 1)k^2 \int \phi(x',z')G(x,z;\,x',z')\mathrm{d}s \qquad \text{.....(260)}$$

where ϕ satisfies the equations

$$(\nabla^2 + k^2)\phi = 0 \qquad \text{outside the dielectric}$$

$$(\nabla^2 + k^2\varepsilon)\phi = 0 \qquad \text{inside the dielectric}$$

and G satisfies the inhomogeneous wave equation

$$\left(\frac{\partial^2}{\partial x^2}+\frac{\partial^2}{\partial z^2}+K^2\right)G(x,z;\ x',z')=-\delta(x-x')\delta(z-z') \qquad \text{.....(261)}$$

where

$$\int \delta(x-x')\mathrm{d}x=\begin{cases}1 & \text{if the interval } x_1x_2 \text{ contains } x'\\ 0 & \text{if the interval } x_1x_2 \text{ does not contain } x'\end{cases}$$

Similarly, for $\delta(z-z')$. $K(x, z)$ is $jkc\mu$ times the polarization current density $J_p(x, z)$ in the dielectric. The above integral equation leads to

$$G=\frac{\mathrm{j}}{a}\sum_{n=1}^{\infty}\frac{\sin\frac{n\pi x}{a}\sin\frac{n\pi x'}{a}}{K_n}\exp\left[\mathrm{j}K_n|z-z'|\right] \qquad \text{.....(262)}$$

where

$$K_n^2=k^2-\left(\frac{n\pi}{a}\right)^2$$

Representing the electric field as the sum of even (ϕ_e) and odd (ϕ_o) functions about the $z = 0$ plane and letting

$$\begin{aligned}\phi_e^{in}&=\psi_e(x,z)\\ \phi_o^{in}&=\psi_o(x,z)\end{aligned} \qquad \text{.....(263)}$$

the integral equations are for the even and odd cases respectively

$$\begin{aligned}\psi_e(x,z)&=-\phi_e(x,z)+(\varepsilon-1)K^2\int G_e'(x,z;\ x',z')\phi_e(x',z')\mathrm{d}s'\\ \psi_o(x,z)&=\phi_o(x,z)+(\varepsilon-1)K^2\int G_o'(x,z;\ x',z')\phi_o(x',z')\mathrm{d}s'\end{aligned} \qquad \text{.....(264)}$$

where $\phi_e(x, z) = \phi_e(x, -z)$ corresponds to a magnetic wall closing the guide at $z = 0$ plane, and $\phi_0(x, z) = -\phi_0(x, -z)$ corresponds to an electric wall closing the guide at $z = 0$ plane. The modified Green's function in the even and odd cases are

$$G_e'=-\frac{1}{K_a}\sin\frac{\pi x}{a}\sin\frac{\pi x'}{a}\left(\sin K|z-z'|+\sin K|z+z'|\right)+$$
$$+\frac{\mathrm{j}}{a}\sum_{n=2}^{\infty}\frac{\sin\frac{n\pi x}{a}\sin\frac{n\pi x'}{a}}{K_n}\left[\exp\left(\mathrm{j}K_n|z-z'|\right)+\exp\left(\mathrm{j}K_n|z+z'|\right)\right] \qquad \text{.....(265)}$$

$$G_o'=-\frac{1}{K_a}\sin\frac{\pi x}{a}\sin\frac{\pi x'}{a}\left(\sin K|z-z'|-\sin K|z+z'|\right)+$$
$$+\frac{\mathrm{j}}{a}\sum_{n=2}^{\infty}\frac{\sin\frac{n\pi x}{a}\sin\frac{n\pi x'}{a}}{K_n}\left[\exp\left(\mathrm{j}K_n|z-z'|\right)-\exp\left(-\mathrm{j}K_n|z-z'|\right)\right] \qquad \text{.....(266)}$$

The impedance relations are

$$\frac{1}{Z_{11}+Z_{12}}=\frac{2\mathrm{j}}{ka}(\varepsilon-1)K^2\int\psi_e\phi_e\mathrm{d}s' \qquad \text{for the even case} \qquad \text{.....(267)}$$

and

$$Z_{11}-Z_{12}=\frac{2\mathrm{j}}{ka}(\varepsilon-1)K^2\int\psi_o\phi_o\mathrm{d}s' \qquad \text{for the odd case} \qquad \text{.....(268)}$$

When put in the variational form, the impedance relation for the even case is

$$\mathrm{j}(Z_{11}+Z_{12})\frac{(\varepsilon-1)K^2}{ka}=-\frac{\int\phi_e^2(x,z)\mathrm{d}s'-(\varepsilon-1)K^2\iint\phi_e(x,z)G'(x,z;\ x',z')\phi_e(x',z')\mathrm{d}s\,\mathrm{d}s'}{\left(\int\phi_e\psi_e\,\mathrm{d}s\right)^2} \qquad \text{.....(269)}$$

Similarly for the odd case.

If we consider the case of a circular cylindrical post of radius R with its centre at $(x = x_0)$ $z = 0$, and write

$$\phi_e = \sum_{m=0}^{\infty} A_{2m} \cos 2m\theta J_{2m}(\sqrt{\varepsilon}kr) + A_{2m+1} \sin (2m+1)\theta J_{2m+1}(k\sqrt{\varepsilon}r) \quad \text{.....(270)}$$

$$\phi_o = \sum_{m=0}^{\infty} B_{2m} \cos (2m+1)\theta J_{2m+1}(k_o\sqrt{\varepsilon}r) + B_{2m} \sin 2m\theta J_{2m}(k_o\sqrt{\varepsilon}r) \quad \text{.....(271)}$$

where A_m and B_m are coefficients determined from the requirement that the impedance element be stationary. The impedance relations derived from the variational integrals for the even and odd cases are[99]

$$Z_{11}+Z_{12} = j\frac{a}{\lambda_g}\operatorname{cosec}^2\frac{\pi x_0}{a}\left[\left(\log\frac{2a}{\pi R}\sin\frac{\pi x_0}{a}\right)-2\sin^2\frac{\pi x_0}{a}-\frac{1}{4}\left(\frac{2\pi R}{\lambda}\right)^2+2\sum_{n=2}^{\infty}\sin^2\frac{n\pi x_0}{a}\times\right.$$
$$\left.\times\left(\frac{1}{\sqrt{n^2-\left(\frac{2a}{\lambda}\right)^2}}-\frac{1}{n}\right)+\frac{J_0(y)}{[J_0(x)xJ_0(y)J_1(x)-yJ_0(x)J_1(y)]}\right] \quad \text{.....(272)}$$

$$Z_{11}-Z_{12} = j\frac{a}{\lambda_g}\sin^2\frac{\pi x_0}{a}\frac{\left(\frac{2\pi R}{a}\right)^2}{\frac{1}{2}x^2\frac{J_1(y)}{J_1(x)xJ_0(x)J_1(y)-yJ_0(y)J_1(x)}} \quad \text{.....(273)}$$

where $x = \dfrac{2\pi R}{\lambda}$ $\qquad y = x\sqrt{\varepsilon}$

The complex impedances Z_{11} and Z_{12} represent the values of the shunt and series arms of the equivalent circuit in Fig. 64. It may be noted that for large values of $\varepsilon/\varepsilon_0$, resonant effects occur, so that the field is concentrated largely inside the post. The representation as an equivalent circuit is accurate if R is not very large and $\varepsilon/\varepsilon_0$ is not very large. The characteristic impedance of the guide has been taken to be unity. For an obstacle with real dielectric constant, the above relations are valid, provided jZ_{11} and $-jZ_{12}$ are replaced by X_{11} and X_{12} respectively. Numerical computations for X_{11}/Z_0 and X_{12}/Z_0 have been made for a centered post $(x/a = 0{\cdot}5)$ with real dielectric constant $(\varepsilon'' = 0, \varepsilon' = \varepsilon/\varepsilon_0)$ and for a wavelength $\lambda = 1{\cdot}4\,a$ and are tabulated by Marcuvitz.[97]

[To be continued] *(Paper No. 1000/2).*

Part III, which includes the References and Bibliography, will be published in the December issue.

STANDARD FREQUENCY TRANSMISSIONS

(Communication from the National Physical Laboratory)

Deviations, in parts in 10^{10}, from nominal frequency for **October 1965**

October 1965	GBR 16 kc/s 24-hour mean centred on 0300 U.T.	MSF 60 kc/s 1430–1530 U.T.	Droitwich 200 kc/s 1000–1100 U.T.	October 1965	GBR 16 kc/s 24-hour mean centred on 0300 U.T.	MSF 60 kc/s 1430–1530 U.T.	Droitwich 200 kc/s 1000–1100 U.T.
1	− 150·7	− 150·3	− 6	17	− 149·2	− 148·8	0
2	− 150·3	− 150·5	− 5	18	− 149·1	− 150·2	+ 1
3	− 150·3	− 150·3	− 4	19	− 150 8	− 151 2	0
4	− 150·1	− 151·2	− 3	20	− 150 4	− 151 0	− 1
5	− 151·4	− 151·3	− 3	21	− 150·5	− 150·3	0
6	− 150·8	− 151·5	− 3	22	− 150 9	− 151 0	0
7	− 151·2	− 150·9	− 2	23	− 150 8	− 150·4	0
8	− 150·7	− 150·4	− 2	24	− 150 1	− 150 2	0
9	− 150·0	—	0	25	− 150·5	− 150 2	0
10	− 149 8	− 149·4	0	26	− 150·5	− 151·0	− 1
11	− 149·4	− 149·9	+ 1	27	− 151·0	− 150 7	− 1
12	− 149·3	− 150·7	0	28	− 151·1	− 151 5	− 2
13	− 150·1	− 150·3	+ 1	29	− 150·7	− 150·3	− 1
14	− 150·3	− 150·5	+ 1	30	− 150·3	− 150·5	0
15	− 150·2	− 149·9	0	31	—	—	—
16	− 149·6	− 148·9	+ 1				

Nominal frequency corresponds to a value of 9 192 631 770 c/s for the caesium F,m (4,0)–F,m (3,0) transition at zero field.

U.D.C. 621.372.837.3

Switching Criteria for Waveguide Ferrite Devices

By

J. HELSZAJN, M.S.E.E.
(*Associate Member*)†

Summary: A microwave ferrite device becomes a switch when actuated by a pulsed magnetic field. Because of the changing magnetic field, eddy currents are induced in the waveguide walls which results in a certain degree of shielding. In this paper, a criterion is given for the shielding effect of the waveguide walls to sinusoids to meet the switching response in the time domain when the field is applied through a long solenoid. It is also shown that the criterion can be obtained from inductance measurements. In this way the switching response can be specified in terms of the frequency response, thereby greatly facilitating design.

List of Symbols

$\bar{E}$	electric field strength (V/m)
$\bar{H}$	magnetic field strength (A/m)
$\bar{J}$	current density (A/m^2)
$\bar{D}$	electric flux density (C/m^2)
μ_0	permeability of air (H/m)
μ_r^a	relative incremental permeability of the composite ferrite waveguide cross section
μ_r^b	relative incremental permeability of the composite ferrite-solenoid cross-section
H_i	longitudinal magnetic field strength inside (A/m) waveguide
H_o	longitudinal magnetic field strength outside waveguide (A/m)
ρ	specific resistance (Ω-m)
a	radius of round waveguide (m)
b	radius of solenoid (m)
d	thickness of round waveguide (m)
e	height of rectangular waveguide (m)
f	width of rectangular waveguide (m)
g	thickness of rectangular waveguide (m)
i_a	induced current in waveguide (A)
i_b	solenoid current (A)
i_0	solenoid current at zero frequency (A)
V	stepped voltage
N	number of turns on solenoid
k	mutual coupling coefficient between waveguide and solenoid
L_b	solenoid inductance (H/m)
L_a	waveguide inductance (H/m)
$L(\omega)$	apparent input inductance of solenoid (H/m)
R_a	waveguide resistance (Ω/m)
R_b	solenoid resistance (Ω/m)
$\psi(\omega)$	magnetic flux through section (wb)
t_0	time constant of waveguide (s)
ω_0	radian frequency at the 3-dB point of the amplitude response

1. Introduction

In modulating microwave ferrite devices with externally applied magnetic fields, eddy currents are induced in the ferrite housing. When the magnetic field is pulsed, these eddy currents cause the time it takes for the magnetic field inside the waveguide to reach its final value to lag on that of the solenoid current pulse producing it. On the other hand, for alternating magnetic fields, the ferrite housing becomes opaque as the modulating frequency is increased. A number of schemes are available to make the waveguide transparent to the modulating pulse. These techniques include thin aluminium coatings on plastic waveguides, the use of waveguides made of silver-loaded epoxy, and other such schemes.[1] For longitudinal fields helical windings for the waveguide walls have been used to eliminate completely the shielding effect. In general, however, it is difficult to assess the contributions of the various parts of the ferrite housing to the pulse response, particularly if we are dealing with transverse field devices; and should the response be unsatisfactory, it is not always clear what steps would be taken to remedy the situation.

Because the specification of such ferrite modulators often relate to the switching speed this paper will

† Microwave Associates Inc., Burlington, Mass., U.S.A.

consider the relation between the shielding effect of round and rectangular waveguides to the sinusoid and pulse responses. Such a correlation between the pulse response and the frequency response is often employed in servo analysis.[2] Experience with servo systems indicates that the rise-time of a stepped function can be accurately described by the 3-dB point of the amplitude response in the frequency domain.

The shielding effect of cylindrical shells to alternating magnetic fields at any frequency for the case when the external magnetic field is at a great distance from the cylinder has been treated by King.[3] The shielding equation of such a waveguide holds when the external field makes any angle with the axis of the waveguide. The shielding of transverse fields has also been dealt with elsewhere.[4] The low-frequency approximation of King's exact shielding equation has been derived separately by Lyon[5] for a thin cylinder in a longitudinal field. Our conclusions will therefore be valid for both transverse and longitudinal field devices.

In this paper we shall derive a differential equation for the thin waveguide which relates the magnetic fields inside and outside the waveguide. By solving this equation for sinusoid and stepped exciting functions we will relate the 3-dB point of the amplitude response to the time it takes for the field inside the waveguide to reach 63% of its final value. The latter time we shall term the time-constant of the waveguide, which we will find is simply the ratio of the low-frequency inductance to resistance of the cylinder. We will also show how to measure the shielding effect when we modulate the ferrite device through a solenoid.

Also, with the help of the well-known transformer equations,[6] we will give the switching time in terms of the time-constants of the drive circuit and that of the ferrite housing. This will allow us to specify the 3-dB frequency of the ferrite housing to meet the switching specification. We will also show that all the information needed to specify the switching performance and the shielding effect can be obtained from inductance measurements in the frequency domain. The paper concludes with a comparison between the experimental data obtained on an absorption type ferrite modulator[7] and that indicated by theory. An Appendix gives an equation for the switching power needed to actuate ferrite devices in terms of the switching time and the circuit parameter.

2. Shielding Effect of Round and Rectangular Waveguides

2.1. *Thin Cylindrical Waveguide of Infinite Length in a Longitudinal Field*

In order to determine the relation between the frequency and time responses we derive a differential equation which relates the magnetic fields inside and outside the waveguide. We then solve this equation when the exciting magnetic field is a sinusoid and a stepped function. To do this, we consider a cylindrical waveguide immersed in a magnetic field parallel to the axis of the waveguide as shown in Fig. 1. One of Maxwell's equations in the m.k.s. system is

$$\nabla \times \bar{E} = -\mu_r^a \mu_0 \frac{\partial \bar{H}}{\partial t}$$

By Stokes's theorem this becomes

$$\oint_c \bar{E} . \mathrm{d}\bar{l} = -\int\int_s \mu_r^a \mu_0 \frac{\partial \bar{H}}{\partial t} . \mathrm{d}\bar{s}$$

where $\mathrm{d}\bar{l}$ encircles $\mathrm{d}\bar{s}$ according to the right-hand rule.

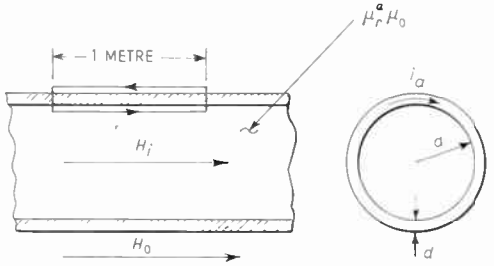

Fig. 1. Round waveguide section.

Applying this last equation around the section of radius a in Fig. 1 gives

$$2\pi a E = -\mu_r^a \mu_0 \pi a^2 \frac{\mathrm{d}H_i}{\mathrm{d}t} \qquad \ldots\ldots(1)$$

A second Maxwell equation is

$$\nabla \times \bar{H} = \left(\bar{J} + \frac{\partial \bar{D}}{\partial t}\right)$$

By Stokes's theorem, this becomes

$$\oint_c \bar{H} . \mathrm{d}\bar{l} = \int\int_s \left(\bar{J} + \frac{\partial \bar{D}}{\partial t}\right) . \mathrm{d}\bar{s}$$

For a good conductor, the displacement current density $\partial \bar{D}/\partial t$ is small compared to the conduction current density $\bar{J}$ and can be omitted. Applying the last equation to a closed rectangular path one metre long enclosing a portion of the surface current i_a in amperes gives

$$(H_i - H_o) = i_a \qquad \ldots\ldots(2)$$

From Ohm's law we also have for a section one metre long

$$\frac{E}{i_a} = \frac{\rho}{d} \qquad \ldots\ldots(3)$$

From eqns. (1) and (3) we obtain

$$i_a = -\frac{\mu_r^a \mu_0 a d}{2\rho} \cdot \frac{\mathrm{d}H_i}{\mathrm{d}t} \qquad \ldots\ldots(4)$$

Substituting eqn. (4) into (2) and rewriting gives

$$\frac{\mu_r^a \mu_0 ad}{2\rho} \cdot \frac{dH_i}{dt} + H_i = H_o \qquad \text{.....(5)}$$

The eddy currents induced in the ferrite material have been neglected because of the high resistivity of the ferrite.

2.2. *Thin Rectangular Waveguide of Infinite Length in a Longitudinal Field*

When modulating ferrite devices, we are often concerned not with round waveguides but with rectangular ones. If we repeat section 2.1 for a rectangular waveguide, we obtain

$$\frac{\mu_r^a \mu_0 e, g}{2\rho(e+f)} \cdot \frac{dH_i}{dt} + H_i = H_o \qquad \text{.....(6)}$$

3. Frequency and Time Responses

3.1. *Response in Frequency Domain*

To obtain a solution to eqn. (5) in the frequency domain, we let the exciting function have the form $H_o \sin \omega t$. This gives

$$\frac{\mu_r^a \mu_0 ad}{2\rho} \cdot \frac{dH_i}{dt} + H_i = H_o \sin \omega t \qquad \text{.....(7)}$$

The solution to the above differential equation is

$$H_i = H_o \cos\beta . \sin(\omega t - \beta) \qquad \text{.....(8)}$$

or

$$\left|\frac{H_i}{H_o}\right| = \cos\beta \qquad \text{.....(9)}$$

where

$$\tan\beta = \frac{\mu_r^a \mu_0 ad\omega}{2\rho} \qquad \text{.....(10)}$$

The last two equations are the same as the low frequency approximation of King's exact equation given by Lyon for sinusoidal excitation.

3.2. *Response in Time Domain*

To obtain a solution to eqn. (5) in the time domain, we solve the latter equation when H_o is a stepped field. The solution to this differential equation is

$$\frac{H_i}{H_o} = \left[1 - \exp\left(-\frac{2\rho t}{\mu_r^a \mu_0 ad}\right)\right] \qquad \text{.....(11)}$$

3.3. *Relation between Time and Frequency Domains*

From eqns. (9) and (10) we have $\left|\frac{H_i}{H_o}\right| = 0{\cdot}707$ when

$$\frac{\mu_r^a \mu_0 ad\omega_0}{2\rho} = 1 \qquad \text{.....(12)}$$

On the other hand, we notice from eqn. (11) that the internal field increases to 63% of its final value in time,

$$t_0 = \frac{\mu_r^a \mu_0 ad}{2\rho} \qquad \text{.....(13)}$$

We further note that for the waveguide, the low frequency resistance and inductance per metre is given by

$$R_a = \frac{2\pi a\rho}{d} \qquad \text{.....(14)}$$

and

$$L_a = \mu_r^a \mu_0 \pi a^2 \qquad \text{.....(15)}$$

Hence, $\mu_r^a \mu_o ad/2\rho$ is simply the ratio of the low frequency inductance to resistance of the waveguide.

Combining eqns. (12) and (13) we have

$$t_0 = \frac{1}{\omega_0} \qquad \text{.....(16)}$$

The last equation says that by measuring the response of such a waveguide in the frequency domain, and noting the 3-dB frequency, we obtain the time-constant of the waveguide. This is the procedure that we shall adopt in this paper.

3.4. *Response in Frequency Domain when External Field is Applied Through a Long Solenoid Connected to a Constant Current Generator*

When the external magnetic field is produced by a solenoid wound around the waveguide as shown in Fig. 2, the field at the centre of the waveguide is given by

$$H_i = Ni_b - i_a \qquad \text{.....(17)}$$

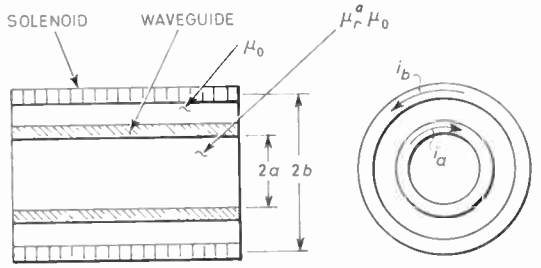

Fig. 2. Waveguide with solenoid.

To obtain the currents i_a and i_b, we must solve the well-known transformer equations. The shielding effect of the waveguide can be obtained quite simply, however, by connecting the solenoid across a constant current generator, thereby setting $i_b = i_0$ in eqn. (17). When we do this, eqn. (17) becomes

$$H_i = Ni_0\left(1 - \frac{i_a}{Ni_0}\right) = H_o\left(1 - \frac{i_a}{Ni_0}\right) \qquad \text{.....(18)}$$

To obtain the ratio i_a/Ni_0, we apply Kirchhoff's law to the waveguide. This gives

$$0 = -j\omega Mi_0 + \left(\frac{2\pi a\rho}{d} + j\omega\mu_0 \mu_r^a \pi a^2\right) i_a \qquad \text{...(19)}$$

We also have

$$M^2 = k^2(N^2\mu_0\mu_r^a\pi a^2)(\mu_0\mu_r^b\pi b^2)$$

$$k = \frac{a}{b}$$

In this section, we let $\mu_r^b = \mu_b$ by assuming a tightly-wound solenoid, although in a later section we shall relate these two quantities.

Substituting the above into eqn. (19) gives

$$\frac{i_a}{Ni_0} = \sin^2\beta(1+\mathrm{j}\cot\beta) \qquad \text{.....(20)}$$

Introducing this last equation into eqn. (18) gives

$$\left|\frac{H_i}{H_o}\right| = \cos\beta$$

where

$$\tan\beta = \frac{\mu_r^a\mu_0 ad\omega}{2\rho}$$

Hence, by making the current through the solenoid independent of frequency with the help of a large resistance in series with the coil, we have a means of measuring the shielding effect given by eqns. (9) and (10). Specifically, the 3-dB frequency of any structure can be obtained by modulating the ferrite device and displaying the detected r.f. output on a scope for constant solenoid current.

3.5. *Response in Time Domain when External Field is Applied Through a Long Solenoid*

To do this we must obtain i_a and i_b from the transformer equations for a stepped voltage. The transformer circuit equations are

$$L_b\frac{\mathrm{d}i_b}{\mathrm{d}t} + R_b i_b - M\frac{\mathrm{d}i_a}{\mathrm{d}t} = V \qquad \text{.....(21)}$$

$$-\frac{M\,\mathrm{d}i_b}{\mathrm{d}t} + L_a\frac{\mathrm{d}i_a}{\mathrm{d}t} + R_a i_a = 0 \qquad \text{.....(22)}$$

From these circuit equations we have[6]

$$i_b = \frac{V}{R_b}\left\{1-\mathrm{e}^{-at}\left(\cosh bt + \frac{a}{b}\cdot\frac{1-\gamma}{1+\gamma}\cdot\sinh bt\right)\right\} \qquad (23)$$

$$i_a = \frac{-V}{R_a}\cdot k\sqrt{\frac{L_a}{L_b}}\cdot\frac{a}{b}\cdot\frac{2}{1+\gamma}\cdot\mathrm{e}^{-at}\sinh bt \qquad \text{.....(24)}$$

where

$$a = \left(\frac{R_b}{L_b}\right)\cdot\frac{(1+\gamma)}{2\gamma(1-k^2)}$$

$$b = \left(\frac{R_b}{L_b}\right)\cdot\frac{[1+\gamma^2+2\gamma-4\gamma(1-k^2)]^{\frac{1}{2}}}{2\gamma(1-k^2)}$$

$$\gamma = \frac{R_b}{L_b}\Big/\frac{R_a}{L_a}$$

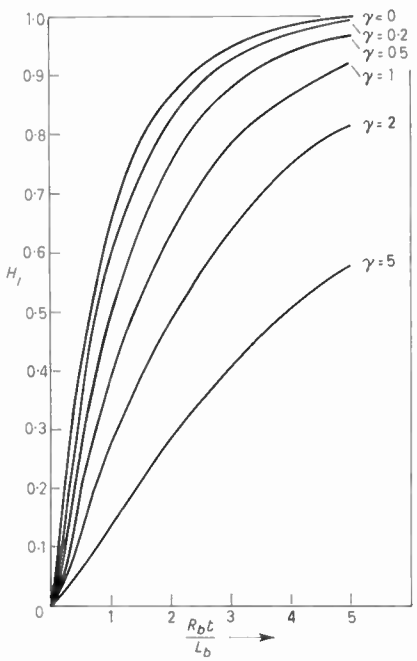

Fig. 3. Time response of magnetic field inside waveguide for $k = 0{\cdot}90$ and parametric values of γ.

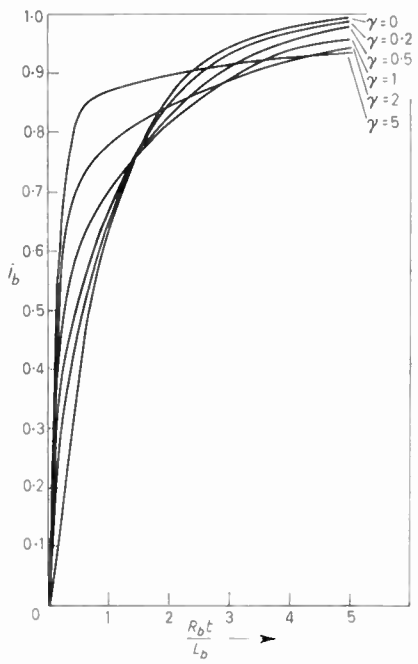

Fig. 4. Time response of solenoid current for $k = 0{\cdot}90$ and parametric values of γ.

We also have

$$V = i_0 R_b$$

$$\frac{V}{R_a} \cdot k \cdot \sqrt{\frac{L_a}{L_b}} = i_0 \cdot \frac{R_b}{R_a} \cdot k \cdot \sqrt{\frac{L_b}{L_a}} \cdot \frac{L_a}{L_b} = i_0 N\gamma$$

Substituting for i_a and i_b from eqns. (23) and (24), eqn. (17) gives the total magnetic field inside the cylinder.

$$\frac{H_i}{H_o} = \left[1 - e^{-at}\left(\cosh bt + \frac{a}{b}\sinh bt\right)\right] \quad \ldots(25)$$

The relation between H_i and $R_b t/L_b$ is given graphically in Fig. 3 for parametric values of γ and $k = 0{\cdot}90$. In Fig. 4, the relation between i_b and $R_b t/L_b$ is shown for comparison.

For γ different from zero, the time it takes for the magnetic field inside the cylinder to reach its final value is increased. The time it takes the solenoid current to reach its final value, on the other hand, is decreased.

Figure 3 may be used to obtain the value of γ and, hence, the 3-dB frequency to meet the desired switching response for given mutual coupling.

More generally, eqn. (25) can also be obtained by solving eqn. (5) when the exciting function has the form of the current i_b.

3.6. *Measurement of Mutual Coupling Coefficient and Incremental Permeability*

In order to specify completely the switching performance, we need to know the mutual coupling coefficient between the solenoid and the waveguide. This can be obtained from inductance measurements. Also, to correlate the experimental and theoretical data, we must know μ_r^a. The latter can be related to μ_r^b which can also be obtained from inductance measurements. These permeabilities were previously assumed equal for a tightly wound solenoid.

In making measurements on the inductance and shielding effect, it soon became apparent that the incremental permeability of the ferrite material and, hence, the incremental inductance, was important. Incremental permeability depends on both direct and alternating current magnetization. Hence, a certain amount of non-linearity is introduced thereby.

The mutual coupling coefficient between the solenoid and the waveguide can be obtained from the ratio of the inductance of the solenoid at zero frequency and at infinite frequency.

From Fig. 2, the total flux through the section when the frequency is low enough so that the eddy currents in the waveguide can be neglected is

$$\phi(0) = [\mu_0 \pi(b^2 - a^2) + \mu_r^a \mu_0 \pi a^2] N i_0 \quad \ldots\ldots(26)$$

From the above equation and the definition of inductance, we have

$$L(0) = \mu_0 N^2 \pi b^2 [1 + k^2(\mu_r^a - 1)] \quad \ldots\ldots(27)$$

or

$$L(0) = \mu_0 N^2 \pi b^2 \mu_r^b \quad \ldots\ldots(28)$$

From eqns. (27) and (28), we also have

$$\mu_r^b = 1 + k^2(\mu_r^a - 1) \quad \ldots\ldots(29)$$

This gives the relation between μ_r^a and μ_r^b in terms of k. At very high frequencies, the flux through the waveguide is zero. This gives

$$\phi(\infty) = [\mu_0 N \pi(b^2 - a^2)] i_0 \quad \ldots\ldots(30)$$

From this equation we obtain

$$L(\infty) = \mu_0 N^2 \pi b^2 (1 - k^2) \quad \ldots\ldots(31)$$

Taking the ratio of eqns. (28) and (31) gives

$$\frac{L(\infty)}{L(0)} = \frac{(1 - k^2)}{\mu_r^b} \quad \ldots\ldots(32)$$

The ratio of the zero frequency inductance with and without the ferrite in the waveguide gives μ_r^b, and k is obtained with the help of eqn. (32).

4. Measurement

4.1. *Ferrite Modulator*

The experimental investigation was carried out on an absorption-type, reciprocal ferrite modulator. This modulator consists of two ferrite slabs centrally located in a standard W.R. 90, aluminium alloy waveguide. Between the ferrite slabs a thin resistance card of 60 ohms/square is inserted in the plane perpendicular to the input r.f. electrical field. The ferrite used was R151, a commercially available magnesium manganese material. The ferrite shape was 3·5 in (8·9 cm) long with $\frac{7}{8}$ in (2·225 cm) tapers to give a good impedance match to the empty rectangular waveguide; the cross section used was 0·300 in × 0·300 in (0·76 × 0·76 cm). The ferrite was biased

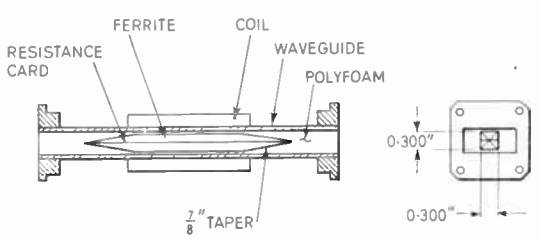

Fig. 5. Microwave ferrite modulator.

with a longitudinal field applied through a $1\frac{7}{8}$ in (4·765 cm) long solenoid wound with 850 turns of No. 27 wire (14·2 mils ≃ 0·36 mm; approximately 28 S.W.G.). The modulator used is shown in Fig. 5.

The modulator has been analysed in terms of coupled waves.[8] In the absence of a magnetizing field, the r.f. energy is transmitted without loss. In the magnetized state, the r.f. energy is attenuated. This loss phenomenon is due to the transfer of r.f. energy between the incident polarization and another perpendicular to it because of the transfer effect of the off-diagonal component of the tensor permeability of the ferrite material; the attenuation constant of the perpendicular polarization is large because of the resistance card. When modulating such ferrite devices with an alternating magnetic field, a direct biasing field is required. This was obtained with the help of a C-magnet. Figure 6 shows a typical loss curve versus applied field for the ferrite modulator on which is superimposed the modulating and biasing fields.

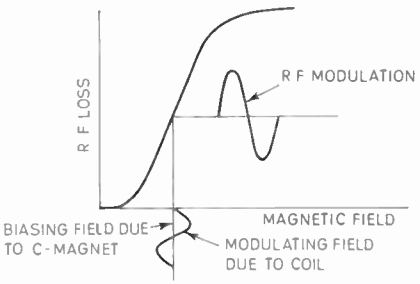

Fig. 6. R.f. modulation versus direct and alternating current magnetization for ferrite modulator.

4.2. *Measurement of Shielding Effect*

Figure 7 shows the shielding effect of the W.R. 90 waveguide for two positions of the C-magnet corresponding to relative incremental permeabilities of 3·65 and 3·32.

For the rectangular waveguide, eqn. (6) gives

$$\frac{\mu_r^a \mu_0 efg\omega_0}{2\rho(e+f)} = 1 \qquad \text{.....(33)}$$

The waveguide used was fabricated from an aluminium alloy, type 356, in the TG condition (7% Si, 0·3% Mg). For such a waveguide we have

$f = 2{\cdot}286 \times 10^{-2}$ metres

$e = 1{\cdot}016 \times 10^{-2}$ metres

$g = 0{\cdot}1220 \times 10^{-2}$ metres

$\rho = 4{\cdot}420 \times 10^{-7}$ ohms-metre

$\mu_0 = 4 \times 10^{-7}$ henrys/metre.

This gives $\mu_r^a f_0 = 1285$ c/s compared to the measured quantities of 1900 c/s and 2150 c/s. The corresponding waveguide time-constants are 0·305 ms and 0·246 ms.

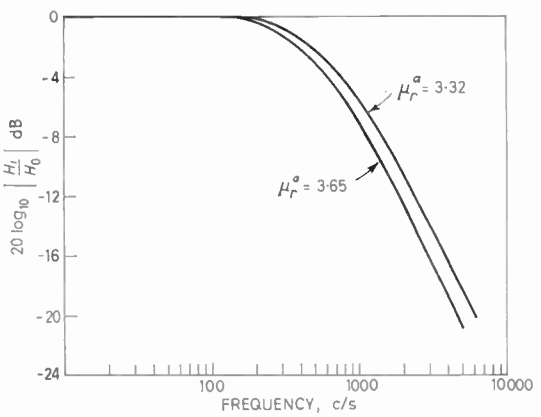

Fig. 7. Shielding effect of W.R. 90 rectangular waveguide.

4.3. *Shielding Effect from Inductance Measurements*

At low frequencies, we also have from the transformer equations

$$L(\omega) = L_b[1 - k^2 \sin^2 \beta] \qquad \text{.....(34)}$$

This last equation is valid as long as the current density throughout the waveguide is constant. At the 3-dB frequency, eqn. (34) becomes

$$L(\omega) = L_b \left[1 - \frac{k^2}{2}\right] \qquad \text{.....(35)}$$

Hence, with the help of eqns. (32) and (34), all the information required to specify the switching performance and the shielding effect can be obtained.

Figure 8 shows the incremental inductance for various direct current magnetizations obtained by biasing the ferrite modulator with a C-magnet. These readings were obtained using a General Radio Type 650-A, impedance bridge.

In Table 1 the relative incremental permeabilities obtained from eqn. (29) are tabulated for various positions of the C-magnet from the modulator. The corresponding 3-dB frequencies obtained with the help

Table 1

Tabulated values of μ_r^b, μ_r^a, f_0 and $\mu_r^a f_0$, versus position of C-magnet from modulator

Position of C-magnet	μ_r^b	μ_r^a	f_0	$\mu_r^a f_0$
½ in	1·17	1·28	1350 c/s	1730 c/s
1 in	1·22	1·36	1200 c/s	1640 c/s
2 in	1·47	1·78	920 c/s	1635 c/s
2½ in	2·00	2·65	580 c/s	1540 c/s
3 in	2·40	3·32	440 c/s	1460 c/s
4 in	2·60	3·65	400 c/s	1455 c/s

of eqn. (34) and the product $\mu_r^a f_0$ are likewise tabulated. We note that the agreement between the calculated and measured values of $\mu_r^a f_0$ becomes better as μ_r^a increases.

In section 3.3 we showed that the 3-dB frequency for a long waveguide is simply the ratio of the low frequency resistance to inductance of the waveguide. When the waveguide is short the inductance per unit length is in general less than that given by eqn. (15). This is particularly true when the relative incremental permeability is small. The measured 3-dB frequencies of short waveguides will therefore be larger than the calculated ones. This is consistent with the measured data obtained from the two methods used. A more accurate expression for the 3-dB frequency may be obtained by introducing the proper low-frequency inductance formula of the short waveguide into eqn. (13).

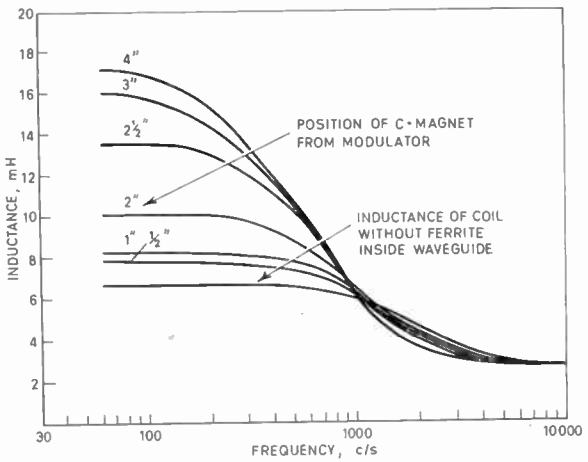

Fig. 8. Incremental inductance versus position of C-magnet.

When the coil was rewound over $3\frac{1}{2}$ in length, the 3-dB frequency obtained from inductance measurement on the waveguide without the ferrite inside was 1800 c/s compared to 2000 c/s for the $1\frac{7}{8}$ in long coil.

The measured mutual coupling coefficient k was 0·775.

5. Conclusions

The shielding effect of waveguides at the 3-dB frequency has been noted to be consistent with the low-frequency assumption whereby the induced eddy currents in the waveguide walls are uniformly distributed. Using this assumption a differential equation relating the field inside the waveguide to the outside was obtained. With the help of this latter equation, the 3-dB frequency was shown to determine the time-constant of the waveguide. The more difficult case was then solved, in conjunction with inductance measurements, when the magnetic field is applied through a solenoid. This was done in terms of the time-constants of the waveguide and solenoid circuit.

The 3-dB frequency, and hence the waveguide time-constant, was obtained from measurements on shielding effect and inductance. These are consistent with the assumption of a long waveguide.

6. Acknowledgment

The author gratefully acknowledges Dr. J. D. Bruce of the University of Santa Clara, and Mr. J. Q. Owen of the Raytheon Company, for their many helpful discussions. The author also wishes to thank the University of Santa Clara for permission to publish this paper.

7. References

1. G. S. Uebele, "High speed ferrite microwave switch", *I.R.E. Natl Conv. Rec.*, **5**, Part I, pp. 227–34, March 1957.
2. Z. J. Jelonek and G. I. Boomer, "A correlation between the transient and frequency responses in servomechanisms", *J. Brit. I.R.E.*, **18**, pp. 101–14, February 1958.
3. L. V. King, "Electromagnetic shielding at radio frequencies", *Phil. Mag.*, Ser. 7, **15**, pp. 201, February 1933.
4. J. Laplume, "Shielding effect of a cylindrical tube placed in a uniform magnetic field perpendicular to its axis", *Annales de Radioélectricité*, **1**, No. 1, pp. 65–73, July 1945.
5. W. Lyons, "Experiments on electromagnetic shielding at frequencies between one and thirty kilocycles", *Proc. Inst. Radio Engrs*, **21**, No. 4, pp. 574–90, April 1933.
6. D. K. McCleery, "Introduction to Transients", (Wiley, New York, 1961).
7. F. Reggia, "A new broad-band absorption modulator for rapid switching", *Trans. I.R.E. on Microwave Theory and Techniques*, **MTT-9**, No. 4, pp. 343–9, July 1961.
8. J. Helszajn, "Coupled-wave description of the absorption-type ferrite modulator," *The Radio and Electronic Engineer*, **29**, No. 2, pp. 129–132, February 1965.

8. Appendix

Switching Power Needed to Actuate Ferrite Devices

In calculating the switching power, we will assume that the form of the current through the coil is that due to a simple series LR-circuit, i.e., $\gamma \ll 1$.
For series LR-circuit, we have

$$V = i(t)R + L\frac{\mathrm{d}i(t)}{\mathrm{d}t} \qquad \text{.....(36)}$$

Instantaneous power is

$$Vi(t) = i^2(t)R + Li(t)\frac{\mathrm{d}i(t)}{\mathrm{d}t} \qquad \text{.....(37)}$$

where $i^2(t)R$ is power dissipated in the series resistance, and $Li(t)\ \mathrm{d}i(t)/\mathrm{d}t$ is the rate at which energy is being stored in the coil.

For a step voltage, eqn. (36) has a solution of the form

$$i(t) = i_0[1-\exp(-Rt/L)] \quad \text{.....(38)}$$

From eqn. (38) we have

$$\frac{di(t)}{dt} = \frac{i_0 \exp(-Rt/L)}{L/R} \quad \text{.....(39)}$$

Rewriting eqn. (37) in terms of (38) and (39)

$$Vi(t) = i_0^2 R[1-\exp(-Rt/L)] \quad \text{.....(40)}$$

From eqn. (38), solving for R, we have

$$R = \frac{L}{t} \ln\left(\frac{1}{1-\frac{i(t)}{i_0}}\right) \quad \text{.....(41)}$$

Substitute for R in eqn. (40)

$$Vi(t) = \frac{Li_0^2}{t} \cdot \ln\left(\frac{1}{1-\frac{i(t)}{i_0}}\right) \cdot [1-\exp(-Rt/L)] \quad (42)$$

This gives the switching power in terms of the energy stored in the magnetic circuit, the switching time, and a function which depends upon the switching point and the number of time constants it requires to reach it.

For a round solenoid one metre long, we have,

$$Li_0^2 = \mu_0 \mu_r^b \pi_b^2 H_0^2 \quad \text{joules} \quad \text{.....(43)}$$

Substituting (43) into (42) gives the switching power in watts in terms of the switching volume:

$$Vi(t) = \frac{\mu_r^b \mu_0 \pi_b^2 H_0^2}{t} \cdot \ln\left(\frac{1}{1-\frac{i(t)}{i_0}}\right) \cdot [1-\exp(-Rt/L)] \quad \text{.....(44)}$$

Manuscript first received by the Institution on 5th February 1965 and in final form on 21st April 1965. (Paper No. 1007).

Seismic Research Programme

The underground explosion, fired by the U.S. Atomic Energy Commission on Friday, 29th October, at Amchitka Island in the Aleutians, was well recorded by four U.K.A.E.A.-type seismological array stations in Scotland, Canada, India and Australia. (These arrays are described in the paper "British Seismometer Array Recording Systems" which starts on the opposite page.) The experiment's purpose was to see if an underground explosion, in a seismic and geologically complex area, gave anomalous recordings which would lead to mislocation or misidentification of the event.

To detect the anomalies, if any, it was necessary to record the event on several arrays which were well distributed round the event. The well-established arrays in Canada (Dominion Observatory) and Scotland (Eskdalemuir) were therefore complemented by two new arrays which were installed in association with the Atomic Energy Establishment at Trombay, India, and with the Australian National University in Canberra. The recordings of the Amchitka explosion will be processed at the U.K.A.E.A.'s seismological laboratory at Blacknest, near Aldermaston.

Meanwhile, the four arrays will continue to record earthquakes from the Aleutian Islands in order to provide material for comparative studies. They will be operated and maintained by the countries concerned, duplicate recordings being sent to U.K. for data processing.

The operating agencies for the overseas arrays have also expressed their interest in using the arrays for research on earthquakes and the physics of the earth's interior, and it is likely that the arrays will continue to record for several years for this purpose.

U.D.C. 550.341

British Seismometer Array Recording Systems

By

C. G. KEEN, B.Sc.,

J. MONTGOMERY (*Associate Member*),

W. M. H. MOWAT,

J. E. MULLARD (*Associate Member*)

AND

D. C. PLATT †

Presented at a Symposium on "Modern Techniques for Recording and Processing Seismic Signals" held in London on 13th May 1964.

Summary: The requirements for a seismic recording system are stated for sites with a noise level of the order of 1 mμm displacement at a frequency of 1 c/s.

Two methods developed for the transmission of the electrical outputs from seismometers distributed over a large array to a recording centre in the field are described. The first method involves direct transmission of the amplified signals, and the second uses amplitude modulated tones. The methods used for remotely calibrating the seismometers and associated field amplifiers are described. Problems of lightning and animal damage to cables are discussed.

An outline of the instrumentation used in the recording centre is given. The signals are recorded on a primary 24-track magnetic tape. The system also includes a secondary tape deck, and an eight-channel pen recorder, controlled by an on-line correlator. Details are given of the timing system, including the pulse code adopted, and the method of measuring and correcting errors relative to G.M.T.

1. Introduction

The seismic systems with which this paper is concerned have been developed primarily for research into the detection and identification of distant underground nuclear explosions.[1, 2] Explosion signals are often of low amplitude, and may be masked by the ambient seismic noise. The signal/ambient seismic noise ratio may be improved by summing the outputs of an array of seismometers covering an area of a few kilometres in diameter. If the dimensions of the array are increased to 20 km and above, the array may be used as a filter to select teleseismic signals from a particular direction and apparent velocity of propagation along the earth's surface. This requires the signals to be recorded individually, so that they can be phased on playback to correspond to the required signal.

An example of a teleseismic array is shown by Fig. 1, and comprises two perpendicular arms, each having ten seismometers spaced 2·5 kilometres apart. In addition, there is a cluster of up to 36 seismometers covering an area of about 2·5 km diameter. The recording instruments are housed in the station laboratory. The site for this is chosen as close as possible to the point of intersection of the two lines, subject to satisfying the requirements of access, power supply and communication. There may thus be up to 55 seismometers in the complete system, the furthest being perhaps 30 km from the laboratory.

The outputs from all the seismometers are recorded continuously. Those from the seismometers in the arms are recorded individually. The seismometers in the cluster are divided into sub-clusters, and summed outputs from these are recorded separately. Coded time pulses corrected to a world standard are also recorded.

A single channel of such a system requires: (1) a seismometer housed in a weatherproof pit in such a way that the instrument is mechanically coupled to unweathered bedrock, (2) a low noise preamplifier, also in the pit, to raise the signal level above noise generated or induced in the system, (3) a means of transmission to the laboratory, and (4) a suitable recording system. In addition, there is a requirement for remotely calibrating the seismometer and preamplifier.

The method chosen for transmitting the signals to the recording laboratory has a bearing on the cost, complexity and reliability of the array system. Therefore, two methods which have been used are described in detail. These are a direct transmission system (Fig. 2) and an amplitude-modulated audio carrier (tone) system (Fig. 4). Four experimental stations were installed using the direct system, namely, Salisbury Plain (U.K.), Pole Mountain (U.S.A.), Eskdalemuir (U.K.) and Yellowknife (Canada). The

† U.K. Atomic Energy Authority, Atomic Weapons Research Establishment, Aldermaston, Berkshire.

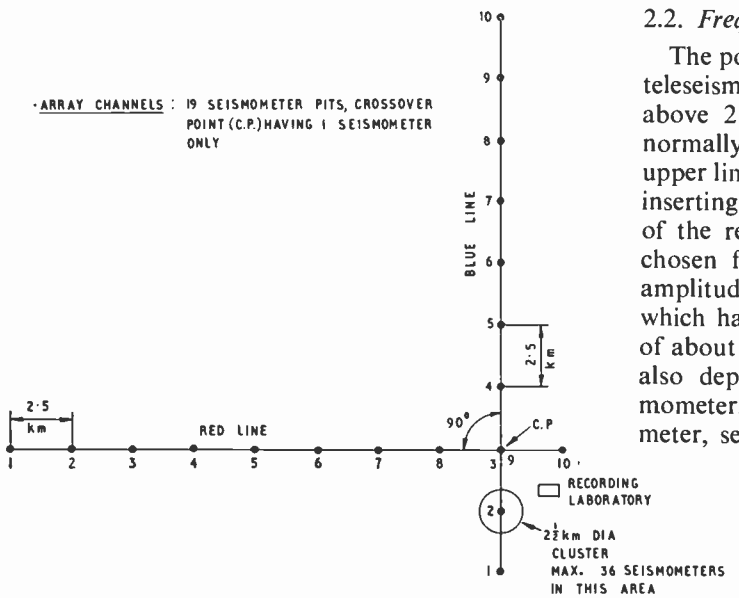

Fig. 1. 2·5 km 21-channel seismic array.

station at Yellowknife now uses the tone system, and any future stations are likely to be planned on similar lines. Apart from the different methods of transmission, the instrumentation in the station laboratories is similar at all stations.

2. System Requirements

2.1. *Noise*

An array site is chosen with a number of factors in mind. Assuming that the logistic, geographical and geological requirements can be satisfied, the further outstanding requirement is that the seismic background noise particle velocity throughout the array should be less than 10^{-6} cm/s r.m.s. in the main frequency band of interest, namely 1 to 2 c/s. At very quiet sites, the seismic noise level in this band may sometimes be as low as 10^{-7} cm/s r.m.s. velocity. This corresponds to a displacement of $10^{-7}/2\pi f$ cm r.m.s., i.e. 10^{-8} cm r.m.s. at 1·6 c/s, assuming simple harmonic motion for the sake of illustration.

The Willmore Mk. II seismometer has become standard for the systems being considered, and has a velocity transducer with a sensitivity of 3·5 volts per cm/s, with a 3300-Ω coil and 5600-Ω damping resistor. Under these conditions, the damping factor is 0·6. With a noise velocity of 10^{-7} cm/s r.m.s. the output from the seismometer would be 0·35 μV r.m.s.

It was specified that noise generated within the system due to all causes should be less than half this value, namely 0·18 μV r.m.s. referred to the input of the preamplifier within a narrow bandwidth of 1 to 2 c/s.

2.2. *Frequency Response*

The power spectrum of the seismic body waves from teleseismic events usually decreases at frequencies above 2 c/s and a system passband of 0–5 c/s will normally suffice. However, it was decided that the upper limit should be higher to cater for nearer events, inserting filters as required during replay and analysis of the records. A low frequency limit of $\frac{1}{3}$ c/s was chosen for the recording system to avoid excessive amplitudes being recorded from microseismic noise, which has a spectrum sharply peaked at a frequency of about $\frac{1}{6}$ c/s. The overall low frequency response is also dependent on the natural period of the seismometer. The period of a Willmore Mk. II seismometer, set up as a vertical component instrument, is adjustable over the range 0·6 to 3 seconds. It is normally set to 1 second, in order to provide additional discrimination against microseismic noise.

2.3. *Dynamic Range*

The largest signal required to be recorded is $0{\cdot}5 \times 10^{-4}$ cm/s peak, corresponding to about magnitude m6 for teleseismic events at Great Circle distances of 4500–10 000 km (40 deg to 90 deg). The corresponding output from the seismometer specified in section 2.1 is 175 μV peak. The ratio of this to the required system noise gives a dynamic range of 57 dB, in the band 1 to 2 c/s.

3. Direct Transmission System

3.1. *Head Amplifier*

A head amplifier is necessary at the instrument pit to raise the level of the signal above stray pick-up on the cable conveying it back to the recording laboratory. A directly-coupled balanced amplifier circuit is used employing two transistor stages in cascade followed by an emitter follower which is directly connected to the line. The transistors are all operated in low current conditions in order to achieve low noise. The input impedance is approximately six times higher than the 5600-Ω seismometer damping resistance, which is connected directly across the input, thus insuring that the seismometer damping is constant. The amplifier has an in-phase rejection of 80 dB. The output impedance is approximately 5000 ohms, and the voltage gain is seventy times. The noise, bandwidth and dynamic range meet the requirements laid down in

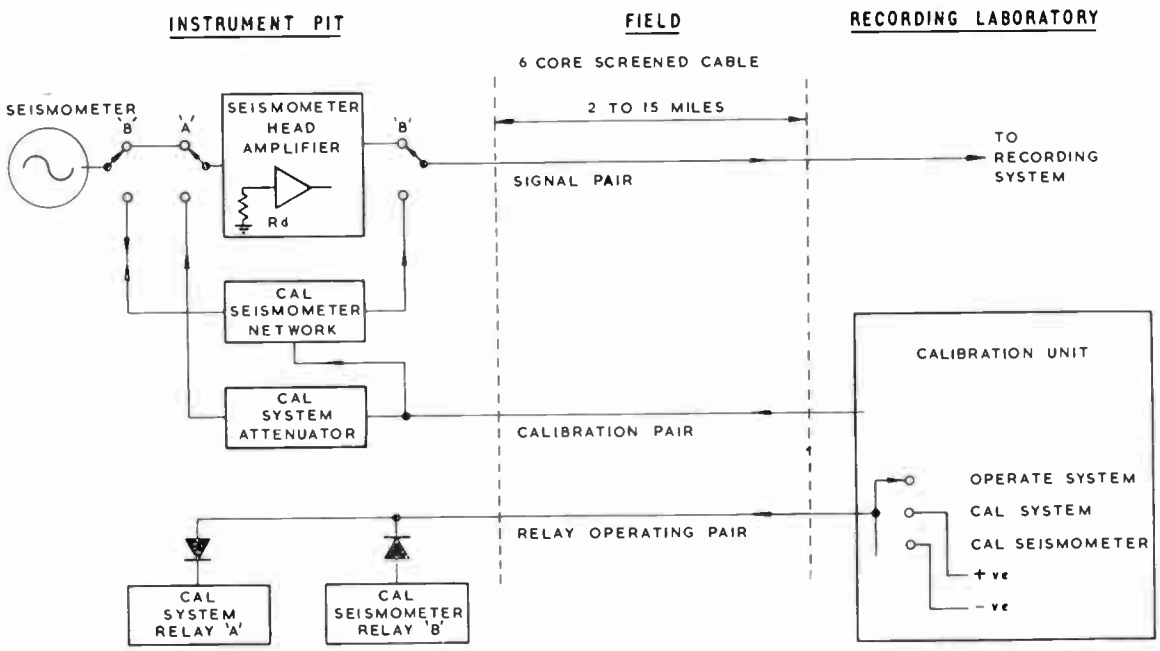

Fig. 2. Direct transmission system.

sections 2.1 and 2.2. A watertight case houses the amplifier, together with calibration relays and circuits.

Mercury cells are used to power the amplifiers, and are soldered directly into the circuit to avoid the use of spring contacts. The latter were used previously but had produced variable voltage drops, causing unreliable operation. The current drain from each cell is less than 200 μA, resulting in a life of better than six months. This is reasonable as routine maintenance is carried out at each instrument pit twice a year.

3.2. *Seismometer Calibration*

The sensitivity of the seismometer is measured by injecting a known step function of current into the coil which deflects the mass. The current produces a pen deflection d on a paper chart monitor (Fig. 3). After equilibrium is reached the current is removed. The mass then undergoes a series of damped oscillations about the rest position, resulting in a corresponding output voltage waveform of maximum amplitude A_0 (measured on the same paper chart recorder and corrected for the loss due to damping during the first quarter of a cycle). The ratio A_0/d and the natural period $2\pi/\omega_0$ of the seismometer are measured on the paper chart record, and from these values, and a knowledge of the velocity transducer coil resistance R_s and the seismometer mass M, the sensitivity constant K_s of the seismometer can be calculated. When connected to a damping resistance R_d, the modified seismometer sensitivity K_s' is given by

$$K_s' = \frac{R_d}{(R_d+R_s)} K_s = \frac{R_d}{(R_d+R_s)} \sqrt{\omega_0 M R_s \frac{A_0}{d}}$$

The above method is carried out in practice as follows. The head amplifier and damping resistance are disconnected and the seismometer connected through a T-network to the pair of signal conductors in the field cable. The calibration pair is also connected into the T-network so that line leakage will not damp the seismometer. All this switching is achieved by a relay energized from a negative voltage source at the laboratory, and from here also the step function of current is injected into the calibration pair. The whole calibration is carried out at a level to minimize the effect of seismic background signals on the calibrating waveforms.

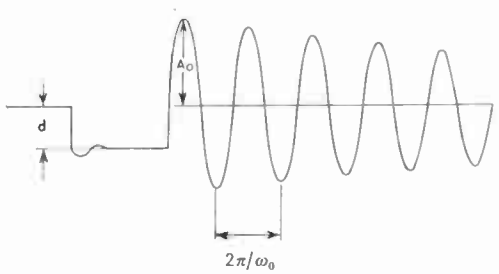

Fig. 3. Seismometer calibration waveform.

3.3. *System Calibration*

Calibration of the complete recording system (Fig. 2) is made by applying a known voltage step to the head amplifier. A positive voltage is applied from the laboratory to the 'calibrate system' relay. This switches the input of the head amplifier from the

seismometer to the 'calibrate system' attenuator. Appropriate known step voltages, of sufficiently high level to overcome any noise that may be picked up by the cable, are then transmitted from the calibration unit to the attenuator, thus calibrating the complete system.

3.4. *Choice of Cable*

To meet the electrical requirements of the system, six cores are required for each pit. Two of these, which carry the signal from the head amplifier, have to be individually screened to reduce pickup from external sources. The conductors are not required to carry a heavy current, therefore a light cable can be used provided that it has sufficient mechanical strength.

The mechanical requirements vary depending on whether the cable is to be buried, surface run, or elevated on poles. At some sites burying the cable is out of the question because of the rocky nature of the terrain. Laying cables on the surface is the cheapest but also the method most liable to damage. This method is only used if the installation is of a temporary nature, or if it is necessary to prove the seismological suitability of the site before the installation is made permanent. This can then be achieved by burying the cable or raising it on tripods or poles. The Salisbury Plain, Pole Mountain and original Yellowknife installations were made using a standard unarmoured p.v.c. sheathed cable, with 6 individually screened polythene-insulated cores. At Eskdalemuir, where the cable is buried, a special unarmoured heavy-duty, watertight landcable is used, having 26 cores, including 4 screened pairs. This cable was designed making use of experience gained in oil prospecting. It is suitable for burial in waterlogged ground. A useful practical feature is the provision of external telephone tappings connected to one of the pairs.

3.5. *Performance of the System*

The system was used for short periods on Salisbury Plain, Pole Mountain and at Yellowknife, and has been in operation for two years at Eskdalemuir. It is sensitive to low insulation resistance between conductors, and some trouble has been encountered due to ingress of water into the cables.

The original installation at Pole Mountain was made using unarmoured cables laid on the surface. This proved to be unsatisfactory because animals, such as rabbits and elk, gnawed the cable, causing considerable damage. Later the cables were buried, which nearly eliminated this problem. Electrical storms were prevalent during the summer, and local lightning strikes induced large surge voltages into the cables. These often burnt out transistors, and other components in the head amplifier unit. More extensive damage occurred at times, a number of seismometer coils being burnt out, and some lengths of the field cable permanently damaged. It was not uncommon for the whole array to be out of action after a severe storm.

At Eskdalemuir, where the cables are buried to a depth of between 6 and 18 inches, the performance of the system has been satisfactory except, once again, during periods of lightning activity. Lightning protection equipment has been installed and has resulted in an improvement. However, direct strikes of the cable are likely to remain a hazard.

An unarmoured cable system was laid on the surface at Yellowknife during the autumn of 1962, and the station became operational later the same year. The cables suffered some damage from the attacks of animals, but these ceased with the onset of the cold weather. The installation worked well throughout the winter, although the animal damage recurred when the thaw set in. The damaged cables were then replaced by armoured cables, and a new transmission system introduced.

4. The Amplitude Modulated Tone Transmission System

4.1. *Factors leading to the Development of the Tone System*

This system (Fig. 4) was developed as an alternative to the direct transmission system. Among the advantages obtained are:

(*a*) A considerable saving in the cable costs for an array. A 25 km teleseismic array may contain up to 270 miles of cable using the direct system. The cost of using an armoured cable with 6 individually-screened cores is likely to be over £50,000. Various alternatives to the direct system were considered, one being the use of a single coaxial cable to connect all the instruments in one arm of the array. But this method would necessitate fairly complex equipment at the instrument pits, conflicting with the requirement for a simple field equipment giving maximum reliability for the long periods when the array might be inaccessible. Further, damage to this cable might result in the loss of information from all the seismometers in that arm of the array. However, the overriding consideration was the problem of supplying power to the field equipment.

At this time a source of supply of a semi-armoured cable, "Spiral-Four", became available at a relatively low cost. In order to make use of this cable, which contains only four cores, the transmission system had to be redesigned. A method using amplitude modulation of a carrier in the audio frequency range was considered to be the most suitable. To obtain further economy, it was decided to use a single cable for each

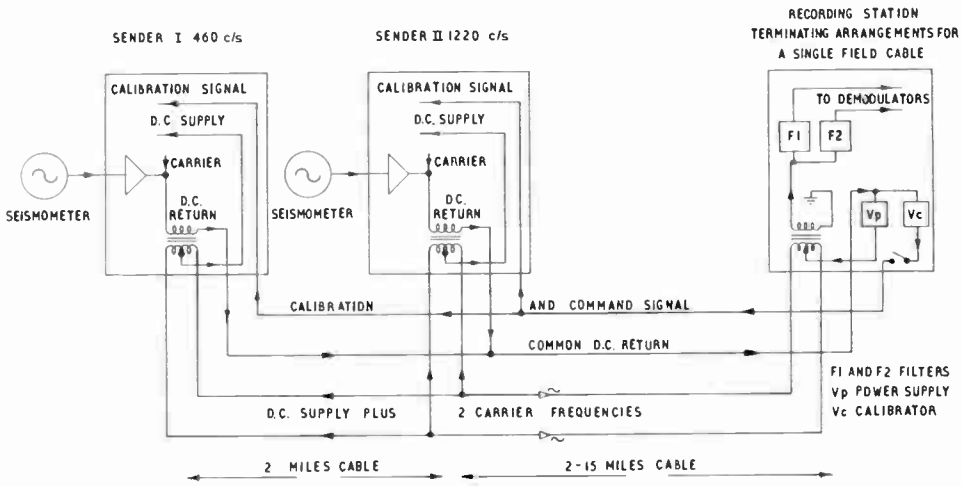

Fig. 4. Amplitude modulation transmission system.

pair of adjacent instrument pits. This almost halves the quantity of cable required. Using this system, the cost of the cable for the example considered above is reduced to below £10,000.

(*b*) Improved lightning protection (Sect. 3.5). The transistors in the terminal equipment of the direct system are directly connected to the cables and have suffered frequent damage during electrical storms. The audio-frequency line transformers used in the tone system (Sect. 4.2) protect the transistors from low level, in-phase line surges. Lightning protection devices at the line terminals limit the higher voltage surges.

(*c*) Increased tolerance to electrical leakage in the field cables, typically caused by moisture entering through sheath punctures. The impedance of the tone system is much lower than that of the direct system, being limited by the characteristic impedance of the cable to about 600 ohms. Furthermore, the signal pair is a.c. coupled.

The disadvantages with the tone system are that the field instruments must be calibrated in pairs and that damage to one cable renders two instrument positions unserviceable. Further increase in the number of instruments sharing a single cable is not possible due to the excessive loss which would be incurred in the power supplied to the field equipment by means of the cable.

4.2. *A Brief Description of the System*

Figure 4 shows that one pair of cores in the common field cable carries the modulated tones from a pair of instrument pits. The two tones, 460 c/s and 1220 c/s, are modulated with the seismic information. Amplitude modulation was chosen, principally because the simple circuits involved could be expected to function for long periods without attention. The line is transformer-coupled to the instrumentation at both ends. Direct current to operate the field instrumentation is fed to the transformer centre-tap at the laboratory end and extracted from the centre-taps at the pits. The power supply return is by way of the third of the four cores. The fourth core carries the command signals to operate the calibration circuits, with the return by way of the third core.

The tone sender comprises three basic elements, namely, an oscillator, a d.c. amplifier and a modulator.

The oscillator uses a single grounded-base transistor in a bridged-T circuit,[4] providing a stable output about 0·5 V of drive, the output being passed through a clipping stage to the modulator. The main factors influencing the choice of carrier frequencies were as follows:

(*a*) The upper frequency should not be so high as to cause excessive attenuation on the longest cables, and the lower frequency should be sufficiently high to avoid demodulation and carrier ripple problems.

(*b*) Their spacing should be wide so that simple filters can be used.

(*c*) There should be no cross-modulation products in the seismic frequency band.

(*d*) They should not be harmonically related.

Balanced electrical signals from the seismometer are fed to the d.c. amplifier, the first two stages being run at low collector currents in order to keep transistor generated noise to a minimum. Long-tail pairs are used in these stages, giving an in-phase rejection of 44 dB. To simplify biasing arrangements, p-n-p and n-p-n transistor stages are used alternately. The output is taken unbalanced to a further stage of amplification before passing to the modulator,

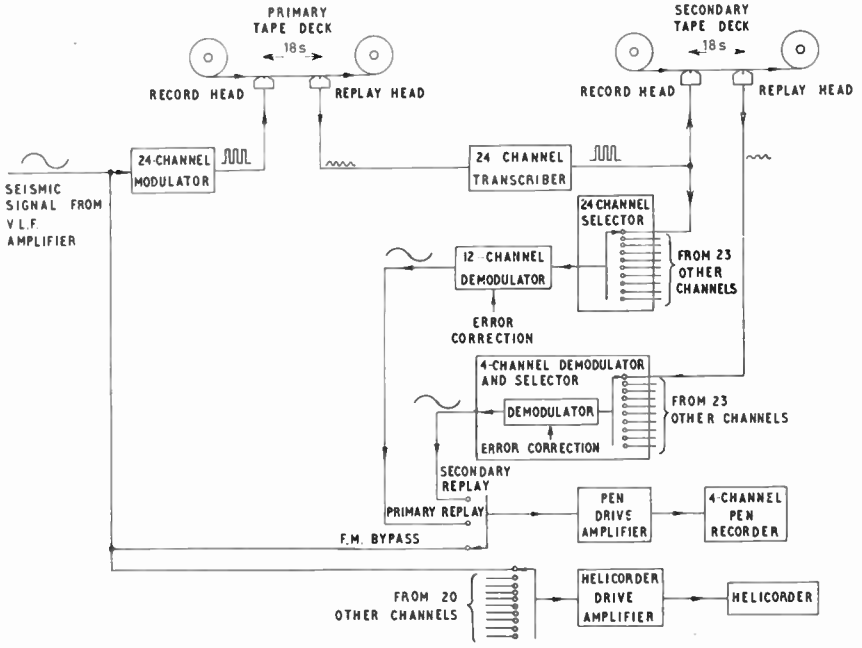

Fig. 5. One channel of the 24-channel f.m. recording system.

matching being obtained with an emitter follower stage. The gain of the d.c. amplifier is 60 dB ± 3 dB and the equivalent input noise voltage is less than 0·2 μV r.m.s. in the band 1 to 2 c/s.

A clipper modulator is used. The voltage is dependent upon the sum of the carrier and modulating signals, limited in one direction by a Zener diode clamp. A transformer supplies a balanced, symmetrical waveform to the line. Power supplies are stabilized with a two-stage Zener diode arrangement.

The principles of the methods used for calibrating the seismometer and subsequent recording system are the same as described in sections 3.2 and 3.3. Due to the reduced number of cores available in the field cables, a triggered bi-stable circuit is necessary in the sender to generate the current step required to deflect the seismometer mass for the seismometer calibration. For calibrating the subsequent system, step variations are made in the calibration line current and these are applied, as calibrating voltage pulses, to the d.c. amplifier.

A system is in the early experimental stage which would provide precisely known physical accelerations to the seismometer. If successful, this method will give a single overall calibration.

At the recording station the two carriers are filtered into separate channels. The crosstalk rejection is greater than 40 dB. This is acceptable and does not conflict with the requirement of 57 dB dynamic range for the system, since the signal levels in the two channels are similar for any given event. The modulated carrier signals from all pits are amplified to a common level to compensate for the losses in the field cables, which differ with the frequencies and cable length used. The modulated tones are passed through demodulators, the outputs being from emitter follower stages.

5. Recording System

The outputs of the transmission systems are fed to multi-channel v.l.f. amplifiers. These have balanced or unbalanced inputs and a gain variable over the range 20 to 77 dB, with a maximum linear output of ± 5 V. They also include an optional notch filter tuned to eliminate interference from the a.c. mains.

The signals are recorded on a magnetic tape deck which accommodates reels containing 7200 ft of 1-inch wide tape. Direct recording and frequency modulation are more economical in the use of tape than pulse width modulation or digital recording. Of the two former, frequency modulation recording was chosen in order to achieve the desired linearity and dynamic range. The f.m. carrier packing density (900 cycles/inch) and recording speed (0·3 in/s) were chosen to be compatible with the standards used by the participants in the American *Vela Uniform* seismological research programme, thus facilitating interchange of data. This speed is unnecessarily high for the signal bandwidth, but it does enable a better signal/noise ratio to be obtained with playback in real time. At 0·3 in/s, the carrier frequency is 270 c/s

and each reel of tape lasts for three days. The maximum frequency deviation is ±33·3%, corresponding to a modulator input of ±5 V. There are 24 recording tracks equally spaced across the width of the tape and these are produced by two 12-track heads mounted so that the tracks are interleaved. Of the 24 channels available, 21 are used for seismic information, one for time, and two for error correction for reducing the noise arising from wow and flutter.

The overall frequency response of the f.m. system is flat from d.c. to 10 c/s, is 6 dB down at 15 c/s, and is governed by low-pass filters in the demodulator. The signal/noise ratio is 47 dB, increasing to 60 dB when the band is restricted to 1 to 2 c/s.

Figure 5 shows that the 21 seismic outputs from the main v.l.f. amplifier, plus one time signal, are fed into a 24-channel frequency modulator. The two error correction channels have short-circuited inputs. The outputs are fed to the record heads on a tape deck. A pair of twelve-channel replay heads is mounted a little over 5 inches further along the tape path from the record heads. At 0·3 in/s there is a delay of 18 seconds between the record and replay signals. After incurring this delay, the signals from the replay heads are fed into a transcriber which amplifies and shapes the f.m. signals, and feeds the record heads of a second deck. The transcriber output also feeds a selector unit, where any three channels, plus time, may be selected for demodulation into analogue form and subsequent display on a four-channel pen recorder. The selector unit also selects the cluster, outer pits and time channels to be fed through a 12-channel demodulator to the triggered display, described in section 6, and arranges for the appropriate error correction to be applied to each channel.

The four-channel pen recorder is used to check the daily calibration of the recording system. It is also useful as a test instrument, there being three main systems which it can monitor. Firstly, it can be set to the 'f.m. bypass' position, to monitor the outputs from the v.l.f. amplifiers directly, thereby checking the operation of the field transmission system. Secondly, it can be set to 'primary replay', where it monitors the output of the primary tape deck. Finally, it may be set to 'secondary replay', which monitors the output of the secondary tape deck. In this position, the outputs of the secondary deck are fed through a four-channel selector and demodulator to the four-channel pen recorder. Thus, using the four-channel pen recorder, a fault in any particular part of the system can be readily identified.

A permanent continuous record of the output of one selected seismometer is required, as a visual monitor of the events recorded on the tape. This is provided by a 'Helicorder', which is a continuously-running pen recorder, with a heat-sensitive recording paper chart wrapped around a slowly-rotating drum. The heat pen and galvanometer assembly are slowly moved across the width of the paper, resulting in a helical trace providing a 24-hour record. 'Slow code' timing pulses, illustrated by Fig. 8, are mixed with the signal.

In the f.m. system, the modulators and demodulators have to be set up for correct centre frequency and deviation. This is carried out using a f.m. test set, which supplies positive, negative or zero d.c. levels for calibrating the modulators. The resultant output frequencies are measured on a built-in c.r.o. monitor by comparison with a crystal controlled frequency, using Lissajous figures. For the demodulators, various crystal controlled frequencies are injected into the demodulator, and the voltages produced are measured on a voltmeter.

6. On-Line Correlation

The information from the array of seismometers is continuously recorded on the primary 24-track magnetic tape recorder. As each tape becomes full, it is replaced and despatched to the main processing centre, together with the daily Helicorder charts and station log sheets. A station produces 122 magnetic tapes and 365 Helicorder records per year. This gives rise to two main problems.

Firstly, a lot of routine work is required at the processing centre to examine the Helicorder records and to list the times of occurrence of events of interest, referred to as 'event picking'. The method of displaying continuously the output of a single seismometer channel has the disadvantage that it does not exploit the capability of the array to improve signal/noise ratio. Low level events, which are worth processing using the full array, may remain undetected. In addition, the continuous paper records produced are, for reasons of cost and storage economy, restricted in dynamic range and paper speed.

Secondly, an appreciable amount of time is taken in the preparation of library tapes and tape loops for subsequent analysis. Consequently, a large backlog of original tapes may build up, thus making them unavailable for erasure and recirculation.

From the foregoing it is clear that some kind of automatic editing is desirable at the stations. This can be achieved by using a system which is triggered by a threshold detector. A simple amplitude discriminator, operating on the output from a single seismometer, is unsuitable, since it is too easily triggered by bursts of local noise, and does not have the signal to noise improvement of the summed array.

The scheme finally developed is shown in simplified form in Fig. 6. A number of seismometers, additional to those in the arms of the array, are arranged in a

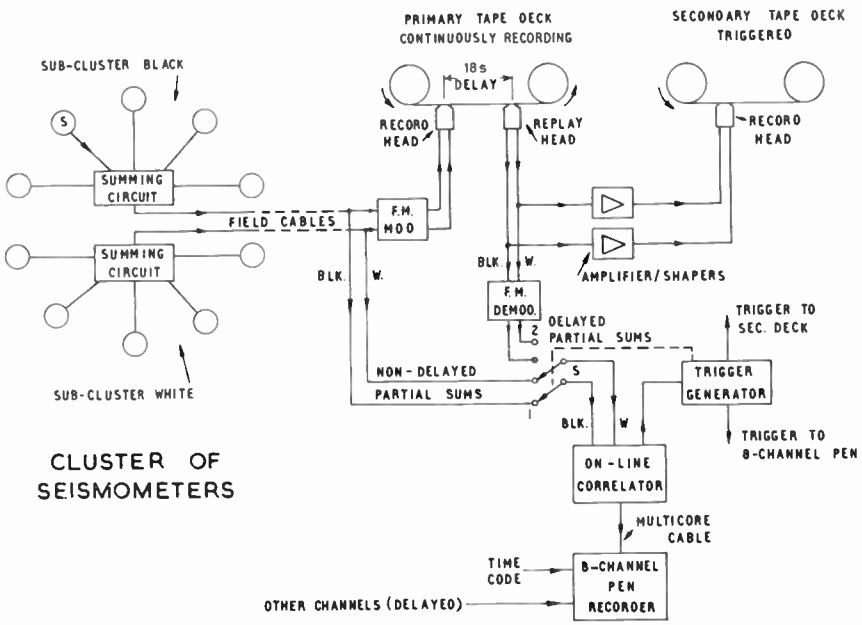

Fig. 6. On-line correlator system.

solid pattern or cluster. The purpose of this cluster is to provide a signal/ambient noise improvement without the necessity to phase the seismometer outputs.[6] The seismometers are divided into two sub-clusters labelled 'black' and 'white' in the figure. A typical overall diameter would be about 2·5 km, and the number of seismometers between 12 and 36. The output from each seismometer is fed to an adjacent standard d.c. head-amplifier (not shown), of the type used in the direct transmission system. The outputs from the head amplifiers are fed by cables to two central summing units. It is possible to calibrate the cluster instruments from the cluster centre. The outputs from the summing units are transmitted to the laboratory by one or other of the methods previously described.

The two sum signals ('partial sums') are supplied to frequency modulators and recorded on the primary tape, together with the signals from the main array. With switch S in the position shown, the partial sums are also fed to an on-line correlator. A description of this unit is given by Hutchins[5]; it comprises two automatic gain controlled (a.g.c.) amplifiers with narrow-band filters, a multiplier and an integrator. When the two partial sum signals are coherent and in-phase, the correlator output is positive. For non-coherent signals the output fluctuates about zero. When the correlator output reaches a sufficient positive value, it operates an external alarm and trigger circuit. This is a bistable multivibrator which has two adjustments, one to set the level at which the circuit trips, the other to determine the recovery or read-out time. The trigger circuit energizes a number of relays. One of these switches on the drive motors of the secondary tape deck and the eight-channel pen recorder, whilst another changes switch S to position 2. The input circuits of the correlator are thereby switched to the partial sum signals from the replay head of the primary deck. These are delayed by 18 seconds relative to the signals being recorded. The secondary tape deck and pen recorder attain normal speed in a few seconds. After the 18-second delay, the coherent signals recur, and are displayed on the pen recorder. A typical display includes the correlator output, the partial sums with a.g.c., the total sum without a.g.c. at two levels of sensitivity, time and other channels of interest such as the outer pits. The secondary tape deck records all the array channels, including the partial sums from the clusters. Due to the 18-second delay, the onsets of the events are recorded.

At the end of a preset read-out time, for example 2 minutes, the bistable alarm and trigger circuits reset, switching off the secondary deck and pen recorder motors, and returning the correlator inputs to the undelayed partial sum signals. If, at the end of the preset read-out time, the output from the correlator still exceeds the trip level, the system retriggers.

Hence, the secondary tape deck and eight-channel pen recorder record only coherent signals within the frequency band of interest. However, these will include some bursts of noise, since there will be occasions when the noise is in phase in the two channels for several cycles.

7. Timing System

A precision timing system is essential, since onset times of events must be measured accurately at a number of widely spaced stations so that the epicentres can be located.

The following is a brief description of a timing system developed to meet this requirement (Fig. 7). It uses solid-state devices throughout and normally operates from a 230 V 50 c/s supply. However, a 'floating battery' standby system is incorporated which will continue to supply the power should the mains fail.

Reliability for relatively long unattended periods is a prime consideration, therefore a highly stable primary frequency standard (stability 1 part in 10^7) is used. With this accuracy, it is possible to contain any time error within the limits of $\pm 0{\cdot}1$ seconds over a period of ten days. Should corrections be found necessary, the primary clock can be advanced or retarded in discrete steps of 8 ms or 80 ms by fine and coarse controls.

A second clock, driven from an oscillator with a stability of 1 part in 10^5, quickly indicates any fault condition which may be developing in either standard.

The time coder which follows generates trains of pulses of coded widths. These are presented at four outputs, each of which can be switched independently to provide a fast or slow timing code in addition to regular timing pulses.

The timing codes are illustrated by Fig. 8. When the fast code is selected, a continuous train of one-second, ten-second and one-minute pulses are supplied. The five one-second pulses immediately following the minute pulse form a 5-bit binary code, indicating hours. The six one-second pulses immediately following the next ten-second pulse form a 6-bit binary code, indicating minutes. After the second ten-second pulse, a 5-bit binary code follows, indicating days. The '0' condition of the binary code is represented by a pulse of 0·1 second duration and the '1' condition by a pulse of 0·3 second duration. The time given by the code relates to the leading edge of the minute pulse. Selection of the slow code provides pulses at every $\frac{1}{2}$-minute, 5-minute and 1-hour interval, and an hour code is presented as a 5-bit binary code after each hour pulse. In this case, the coded time relates to the leading edge of the hour pulse. With each of

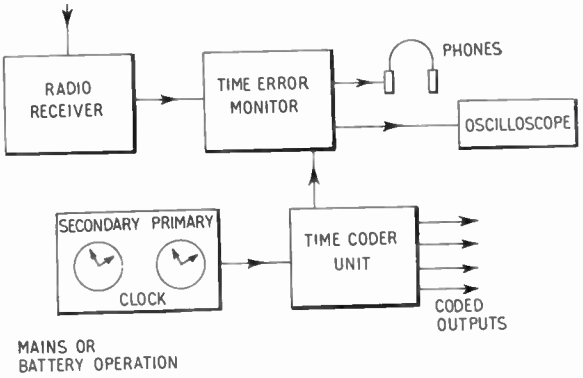

Fig. 7. Block diagram of timing system.

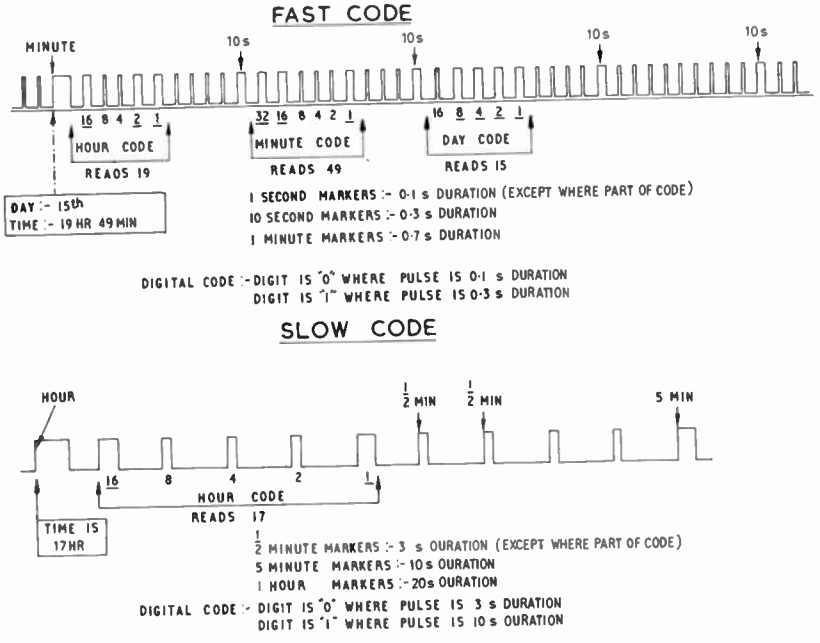

Fig. 8. Timing codes.

these codes, the first 'bit' is the most significant. Neons are used to indicate the '0' or '1' state of the binary scalers within the time coder, and in addition the time in hours and minutes is displayed numerically in decimal form.

A communications receiver is used to monitor standard time transmissions (e.g., MSF or WWV) and the signals are used as a time reference. In conjunction with the time error monitor, which uses selected gate circuits synchronized to the time coder unit, they form an accurate system calibrator. Errors between the primary standard and the broadcast signal can be measured within the range $-0{\cdot}5$ second to $+0{\cdot}5$ second, to an accuracy of ± 10 ms.

A coarse switch can select a gate period of 100 ms duration from 5 periods on either side of the leading edge of the 1 second pulse from the coder unit. The selected gating pulse is used to produce a 100 ms dead period in the broadcast signal supplied to the headphones. It is thereby possible to select a particular 100 ms gate which will mask the receiver time pip. The fine switch enables a 10 ms burst of 2 kc/s tone to be strobed over the selected 100 ms period. The strobing is achieved by means of a variable delay generator, with a 20 ms overlap at the beginning and end of the period. The broadcast pip and the internally generated 2 kc/s pip are monitored with headphones, and the strobe control adjusted until they coincide.

A trigger socket permits the use of an oscilloscope as an alternative monitoring device.

An added refinement takes the form of a high-pass filter with a cut-off frequency of 750 c/s, and a low-pass filter with a cut-off frequency of 1250 c/s. These can be used independently, or as a combined band-pass filter centered on 1000 c/s. They are useful in reducing background noise and interference in the radio signal when reception conditions are poor.

8. Conclusions

The direct-coupled system, described in this paper, has been in operation at Eskdalemuir since June 1962. Initial susceptibility of the calibration system to leakage between cores within the field cable was reduced considerably by a.c. coupling the calibration lines at the head amplifier. The system has since performed satisfactorily, with the exception that the transistors in the units connected to the ends of the field cables are prone to lightning damage.

The tone system has been in use at Yellowknife since December 1963. Its main advantage over the direct-coupled system lies in cable economy, since it requires only two pairs of cores instead of three per cable, and a single cable for two pits. It is also much less affected by cable leakage. It is too early to compare susceptibility to lightning damage of the two systems. Lightning protectors were installed at Eskdalemuir, and reduced the incidence of damage to equipment during 1964. They were installed in the tone system at Yellowknife in the latter part of 1964. Damage occurred earlier in the year to many of the senders.

Triggered recording systems were operated at Eskdalemuir and Yellowknife during 1964, but the associated clusters are only now being put into operation. The Eskdalemuir triggered system, operating from eight seismometers in the main array, trips reliably from all events which can be seen on the chart displaying the summed output of the same seismometers. In order to reduce variability in the number of noise trips, it was found necessary to incorporate a long-term differentiator between the correlator and the threshold trigger. This variability occurred due to changing noise characteristics.

The frequency modulated tape recording system has operated satisfactorily, although some drop-outs have occurred during records of interest. Digital recording is still being considered for future systems, especially where a triggered tape deck is used which permits economy of tape. Such a system could be arranged to provide automatically edited digital library tapes in the correct format for a digital computer.

9. Acknowledgments

The authors wish to thank the U.K.A.E.A. for permission to publish this paper, and to acknowledge the contributory work of other staff at the Atomic Weapons Research Establishment. In particular, Mr. W. Hutchins was responsible for the design of the timing and correlator systems, and Mr. R. W. Brown (now of Canadian Marconi Co. Ltd.) was closely concerned with the design of the tone transmission system.

10. References

1. H. I. S. Thirlaway, "Earthquake or explosion", *New Scientist*, **18**, p. 311, 9th May 1963.
2. F. E. Whiteway, "The recording and analysis of seismic body waves using linear cross arrays", *The Radio and Electronic Engineer*, **29**, No. 1, pp. 33–46, January 1965.
3. J. R. Truscott, "The Eskdalemuir seismological station", *Geophys. J. Roy. Astronom. Soc.* **9**, No. 1, pp. 59–68, October 1964.
4. E. T. Emms, "A novel single transistor RC oscillator", *Electronic Engng*, **32**, No. 390, pp. 506–8, August 1960.
5. W. Hutchins, "A real time seismic data analyser and its associated event selector", *The Radio and Electronic Engineer*. (To be published.)
6. F. E. Whiteway, "The use of arrays in earthquake seismology". (To be published.)

Manuscript first received by the Institution on 31st March 1965 and in final form on 22nd July 1965. (Paper No. 1008/EA23).

U.D.C. 656.7.05:681.38

Simulation of the European Air Traffic Control System

By

J. G. COCHRAN, B.Sc., (*Graduate*)†

AND

E. J. PRESTON, M.A., M.Sc.†

Presented at a Joint I.E.R.E.-I.E.E. Symposium on "Simulators for Training Purposes" held in London on 21st April 1964.

Summary: A notably comprehensive and sophisticated air traffic control simulation system based on a powerful digital computer is due to be supplied to Eurocontrol in 1966. The operational facilities provided are outlined, followed by a discussion of the functions, equipment and computer programs, and a detailed description of some of the engineering problems. These include the flicker-free display on cathode-ray tubes and on a large screen of large quantities of simulated radar, synthetic and tabular data, and the simulation of realistic radar displays and comprehensive telecommunication facilities. Some possible uses of the system are also discussed.

1. Introduction

The Eurocontrol Association, the international air traffic control organization with responsibilities for control of civil aircraft at higher altitudes throughout Western Europe, awarded a contract early in 1964 for the supply of a notably comprehensive and sophisticated air traffic control simulator system based on a powerful digital computer. This equipment is due to be installed at the Eurocontrol experimental centre at Bretigny, near Paris, during 1966.

The system is intended to be used to study the complex air traffic control problems and procedures associated with control of European air traffic during the next 10–20 years in as realistic an environment as possible. Procedures to be tried will be based initially on manual procedural control methods using primary surveillance radar coverage over the whole area, supplemented by full secondary radar facilities. The various functions of the system have already been outlined in this Journal.‡

It is not possible to discuss in this paper all parts of the system in detail. After outlining the system in terms of operational facilities provided, the functions of the simulator will be discussed under the following headings:

(*a*) Simulation of aircraft movements.

(*b*) Simulation of primary and secondary radar display of those movements.

(*c*) Simulation of a.t.c. procedures for satisfactory control of all the aircraft concerned.

The equipment and computer program facilities to be provided for these purposes will be described. The solutions adopted to some particular problems which arise in engineering such a complex system will be discussed in detail. These include the problems of producing a large screen display of the complete air situation as it changes in 'real time', and of arranging flicker-free display of simulated radar, synthetic plan position and alpha-numeric tabular data on cathode ray tubes without over-loading the computer. Other notable problems include the simulation of fixed and moving clutter echoes, and of comprehensive telecommunication facilities both between different controllers and by v.h.f. radio between controller and aircraft pilots.

Finally some of the purposes for which the system will be used by Eurocontrol personnel will be discussed.

2. Operational Facilities

The system will permit the simultaneous simulation of up to five different control sectors, jointly controlling up to 300 aircraft flying in an area covered by up to six simulated primary and six simulated secondary surveillance radars. In order to allow as much flexibility as possible in arranging the equipment for experiments to simulate a variety of different control situations, the system is built up from a series of modules. These are:

(*a*) 20 procedural (P) modules, each with a flight progress board showing up to 5 columns of 20 flight progress strips.

(*b*) 11 radar (R) modules, 8 with a 16-in diameter p.p.i. display arranged vertically, and 3 with a

† Plessey Radar Limited, Tolworth Division, Surbiton, Surrey.

‡ "Radar simulator for air-traffic control", *The Radio and Electronic Engineer*, **27**, No. 4, p. 276, April 1964.

horizontal 21-in diameter display. Five 16-in monitor radar displays will also be provided.

(*c*) 10 control (C) modules, with a keyboard.

(*d*) Telephone, teleprinter and r.t. communications switching modules, each capable of simulating actual communications between controllers and pilots using up to 50 different radio frequencies, and between the consoles of different controllers. Each R module will have telephone and associated selection keys incorporated in the control desk.

(*e*) One 'large screen' display for use by the control supervisor, able to show by selection either any single simulated radar video or a synthetic plan display of the complete area, as a 6 ft square picture.

(*f*) 20 'pilots' modules, each with a keyboard and c.r.t. tabular display, suitable for 'operating' up to 15 simulated aircraft from each position, inserting aircraft data into the system and interrogating the computer as required for information on each flight. These facilities are interlinked by the central computer system, together with the radar simulators, video maps and clutter simulators, video distribution and display drive equipment.

Each radar display may show either simulated primary and secondary radar video from any of the six radars, with inter-scan markers for inter-console marking and range and bearing measurements; or, if selected, a purely synthetic display with alpha-numeric labels generated by the computer. Inter-console marking is achieved by means of a tracking ball control; it is possible to communicate in this way, via the computer, with controllers using either the same or a quite different radar, provided that the geographical overlap permits. This is made possible by the ability of the computer to carry out the necessary calculations and to present interscans which are asynchronous with respect to the radar video.

The supervisor will be able to listen in to r.t. conversations on any of the 50 radio frequencies, either during an exercise or during replay of recorded messages, and to simulate r.t. failures or vary the background noise on each channel. He will also have a separate telephone system to talk to pilots, controller and computer room personnel. In addition to the large projection display he will have computer input/output equipment similar to that of the pilots, and two monitor radar displays.

The complete installation will be in air-conditioned accommodation on a single level, with separate rooms for computer, video equipment, pilots, controller and supervisor.

3. Functions of the Simulator

3.1. *Simulation of Aircraft Movements*

The system will simulate the movement of up to 300 controlled aircraft, together with a considerable number of others not under direct control, as seen by the six simulated radars. At the beginning of each exercise, basic data on all aircraft tracks must be stored in the computer. This will normally be done in the form of two separate inputs for each aircraft:

(*a*) A flight plan of the usual type, giving estimated times, separating points and heights, and

(*b*) A 'computer track plan', giving actual time and place of take-off, actual height and route, and actual place of landing.

The second plan allows simulation of diversions, gross pilot errors, military flights without flight plans, etc.

During the exercise the computer will determine all aircraft positions relative to the appropriate radars at the time when each is illuminated by each radar, after simulating aircraft behaviour in a realistic manner, and it will initiate position reports when the designated beacons are approached. For this purpose it will interpret and follow all piloting instructions on course, speed, height, rate of turn, etc., whenever these are made, and obtain the correct heading of each aircraft taking account of the track plan together with simulated errors in the navigational system in use, errors in navigation of the aircraft by the pilot and winds. Each of these errors will be reproduced as realistically as possible. For example different rules will be applied according to the navigational aid in use by the aircraft (VOR, DME, HARCO, etc.) and the magnitude of the error introduced will be determined according to the stored accuracy of the aid and the effect of random variations (determined from random number generation).

3.2. *Simulation of Radar Display*

Each of the six simulated radars consists of a primary surveillance radar with suitable facilities (m.t.i. etc.) and parameters (p.r.f. beamwidth, rotation rate, pulse width, range) which are stored in the computer and may be varied over a wide range from one exercise to the next; this is together with a secondary surveillance radar with up to 4 modes of interrogation. In both cases the horizontal and vertical radiation diagrams are stored by the computer and used to determine for each controlled aircraft at each antenna rotation the probability of detection, number of radar returns (if any) allowing for random fading, brightness on the display, and the range and azimuth at start and end of each illumination. The only significant simplication introduced by the simulation is that all

the echoes on one target during a particular illumination must have the same intensity. One other limitation on overall flexibility is that while two of the radars are completely independent and asynchronous, the remaining four have the same rotation rate, beamwidth and synchronization. Their geographical positions may of course be varied from one exercise to another.

Primary radar video for each aircraft is then generated in real time for each radar. Before display at all control positions which have selected the radar concerned, this video is mixed with signals produced by a fixed clutter simulator and video map generator, a background noise generator and (in the case of the two main radars) a moving echo generator. The method of operation of these devices, based on flying-spot scanners, is described elsewhere.†

Secondary radar returns are decoded according to each controller's selection of mode/code combinations and displayed in analogue form as appropriate 'bracket' symbols at the correct range and azimuth. Each controller will be able to carry out active decoding of any aircraft track using his tracking ball and keyboard. The appropriate code data may then be written on his display adjacent to the radar return of the track selected.

3.3. *Simulation of A.T.C. Procedures*

With the modules of equipment listed in section 2 (Operational Facilities), it is clearly possible to set up exercises to simulate the procedures involved in controlling aircraft from a number of different a.t.c. centres in an exceptionally realistic environment. The most difficult problem here is to make available for r.t. transmission all the data normally available within each aircraft. In this case each human 'pilot' has to deal with up to 15 aircraft, and his principal function is to act as intermediary ('binary to voice converter') between the computer and controller for providing such data.

The pilot's keyboard will contain function keys, digits and letters for entering flight data into the system. The tabular display will show the call-signs of all aircraft he is operating, together with any data requested by the pilot from the computer store. This may be data such as current flight level which has been requested by a controller or a position report, or any check on stored data on a particular aircraft.

Any message input to the system will also be shown on the tabular display at the bottom, as a check read-out before being generally released to the system as new data. Identification of any particular aircraft as the subject of an input message is simplified by the use of eight keys arranged beside the corresponding call-signs on each side of the tabular display. By this means the selection of one key only is sufficient to define the aircraft concerned.

† loc. cit.

4. Description of Equipment Operation

4.1. *System Considerations*

A description will be given of some of the system features of the display system and its interface with the TR4 computer and buffer store.

At an early stage in the systems design it had been decided to buffer the TR4 computer from the display system in order to reduce the significant load that would otherwise have been placed on the TR4 output in delivering data continuously to a large number of synthetic and tabular displays to obtain flicker-free presentation. Preliminary calculations showed that this task might absorb 27% of the computer's duty cycle alone. In addition the buffer store interface units could be used to transfer keyboard and rolling ball data from the display systems to the TR4, thus avoiding the use of special input/output channels between each keyboard and the computer and allowing the transfer to take place in a time-saving fashion.

4.2. *Transfer of Data Between the Computer and the Buffer Store*

The timing is divided into 40 ms periods by means of a timing circuit in the buffer store. At the commencement of each period the buffer store commences input of data to the computer and when the buffer store signals that input of data is complete, the computer immediately commences the output of data. Data for different parts of the buffer store are put out as separate blocks of data and each such block of data is preceded by an instruction word and has its own start and stop phase. The total amount of data transmitted in any one period is limited to 200 computer words to avoid the possibility of over-running the 40 ms period. On the completion of the output of data, the computer instructs the buffer to put in data, when it is ready and this instruction is answered when the buffer timing circuit dictates.

4.3. *The Buffer Store*

The buffer store accepts digital data from the computer in the computer's time-scale and presents this data to the tabular displays and synthetic radar displays in their required time-scale. It also provides inputs of rolling ball and keyboard data, through the buffer store distribution, to the computer.

A block diagram of these functions is shown at Fig. 1.

The store itself is a general-purpose device with the following facilities:

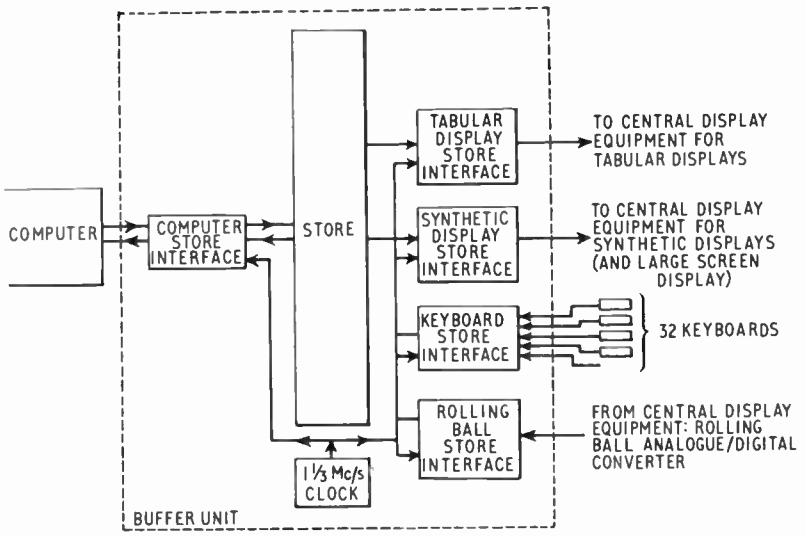

Fig. 1. Buffer unit block diagram.

(*a*) A queue to handle multiple inputs and outputs.

(*b*) A very simple repertoire of instructions for reading and writing one word at a time.

The machine operates as a stored instruction machine with the allocation of storage under the control of the programs, the instructions being inserted prior to the start of an exercise.

The computer and other devices are connected to the store via 'interfaces', which are all different and are specially made to deal with their attached equipments. These interfaces and the store are designed so that they run asynchronously from separate clocks, which has the advantage of keeping the system flexible so that further additions can be made later.

The store itself contains 4096 25 bit words, the last bit being used as a marker. The store has a read-write cycle of 6 μs and operates in synchronism with a clock frequency of 1⅓ Mc/s, allowing 8 micro-steps to be completed within the 6 μs cycle time.

Operation occurs when a demand is made by an ancillary, an ancillary being defined as anything external to the buffer store itself, such as the computer and interface units. The demand enters a queueing system, where it is dealt with according to its priority—for instance, requested synthetic plan data has a higher priority than tabular data. When the buffer store is answering a demand it will not accept another until that demand is satisfied. In view of this, the action taken in response to any demand is arranged

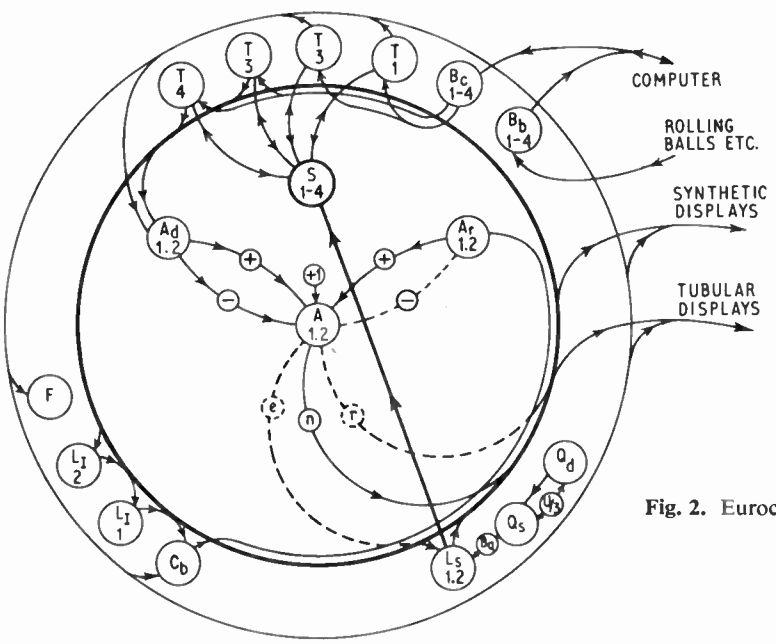

Fig. 2. Eurocontrol buffer—basic machine.

to be short, thus ensuring that low priority demands do not stifle the system.

Referring to the data flow diagram (Fig. 2), a demand enters the demand staticizor, Qd, which is a register with one bit per ancillary. The output from Qd passes to the queuer demand suppression register, Qs, also with one bit per ancillary. This contains a gating arrangement that suppresses all but the most significant bit. Having thus selected the highest priority demand, inverse transfer occurs from Qs to Qd to cancel that demand.

The selected demand passes to an address decoder Bq, which selects an address from the address register Ls. Ls drives the address in the store S that contains the instruction defining detailed action. This instruction passes through the access register, T_1, T_2, T_3, T_4, which handles all data or instructions passing to or from the store, S. The outputs from the access register T pass down the two data highways represented by the two circles, to the instruction register, which consists of:

(*a*) The function register F, (6 bits) which defines the type of operation to be carried out, and drives the instruction matrix (not shown).

(*b*) The address register L_1, (12 bits) which defines the address on which the instruction is to operate. It drives the address part of the store via gates in order to allow the choice of address between this register and the queue address decoder Bq.

(*c*) The count register Cb, (12 bits) which can be used:

(i) to define the number of words to be operated on in a block, or

(ii) to define the separation of words in a sequence, or

(iii) to define an ancillary among a number.

Outputs from the instruction register pass down both data highways and are extracted to the synthetic drive and tabular drive via cable matching and driving circuits.

The adder A, (12 bits) is a full parallel adder with the facility to add or subtract unity from a number passed through it. The adder is connected to the output of the count register Cb, and may increase the count or add it to the address from L. It is also connected to the output of the access register T. Connections shown dotted are provided but are not required for this application.

Data transfer between the computer and buffer is effected via the buffer register Bc in the interface unit. The buffer register Bc gains access to the store S through the access register T. Stored rolling ball and keyboard data is transferred to the computer when required through the buffer register Bb.

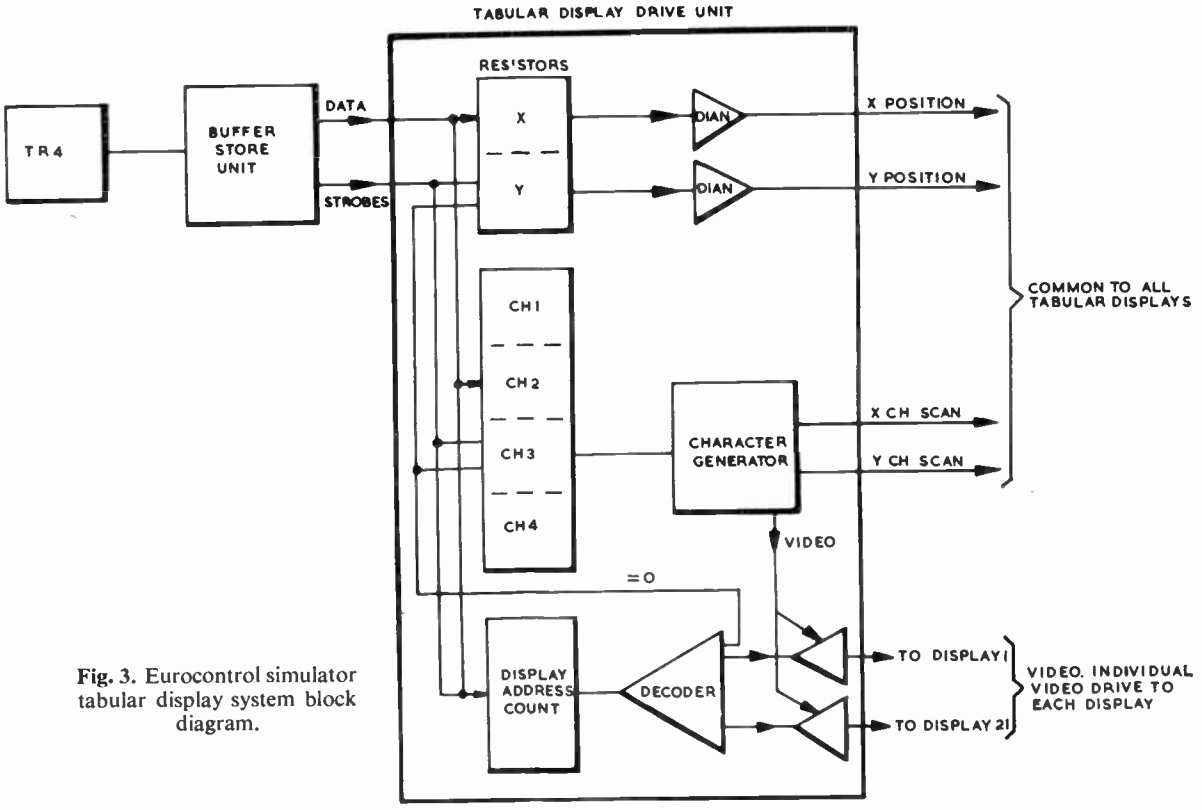

Fig. 3. Eurocontrol simulator tabular display system block diagram.

4.4. *Tabular Display System*

A description will be given of the organization of the tabular display system: the actual engineering principles involved are not described although somewhat similar systems have been described elsewhere. The system block diagram is shown at Fig. 3.

The data to be displayed are passed from the computer to the buffer unit at 40 ms intervals, and the format of the data in the buffer store is shown in Table 1. The basic unit of tabular data is a 4-character group, each character being defined by 6 bits, thus a 4 character group occupies one buffer store location of 24 bits.

Table 1

Tabular display data format in buffer store

Store address	Contents	State of count
AD	4 characters for tabular display 1	21
AD + 1	4 characters for tabular display 2	20
AD + 2	4 characters for tabular display 3	19
AD + 3	4 characters for tabular display 4	18
.		
.		
.		
.		
.		
AD + 20	4 characters for tabular display 21	1
AD + 21	X, and Y positional data	0
AD + 22	4 characters for tabular display 1	21
.		
.		
.		
.		
.		
AD + 1054	4 characters for tabular display 21	1
AD + 1055	X and Y positional data	0
		Marker detected
		Reset store address to AD
		Reset count to 21 and recycle

The tabular display presentation consists of 12 lines, each line containing four 4-character groups, and there are, therefore, 48 character group positions to be defined; each position is defined by 4 bits in the X axis and 5 bits in the Y axis and is contained in one buffer word only.

The data are passed from the buffer store to the tabular display drive on receipt of a 'call' from the tabular display drive unit. Two words of data are passed upon receipt of each call: the first word is the count part of the buffer instruction and if equal to 0 defines the second word as positional information.

If the count part of the instruction is not equal to 0 the second word is a 4-character group, and the count defines the address of the tabular display viewing unit on which the characters must be displayed.

Referring to Table 1 the cycle of events will be as follows:

1st call: Address = AD + 1055, Count = 0, and end of tabular marker detected.

The count part of the buffer instruction will define that the following data is positional information.

The data from address AD + 1055 will give an output for positional information.

The marker will be detected and will reset the instruction address to AD, and the count to 21.

2nd call: Address = AD, Count = 21.

The count part of the buffer instruction will define the display on which the following 4-character group will be displayed.

The data from address AD will be used as a 4-character group.

3rd call: Address = AD + 1, Count = 20.

The count part of the buffer instruction will define the display on which the following 4 character group will be displayed.

The data from address AD + 1 will be used as a 4-character group.

The sequence continues to

23rd call: Address = AD + 21, Count = 0.

The count part of the instruction will define the following data as positional information.

The data from address AD + 21 will give positional information. The count = 0, will be reset to 21.

This routine will be continually repeated, the tabular displays thus cycling through the storage block allocated to them.

The sequence of events is therefore:

(1) Set X and Y positions on all displays.
(2) Write characters on display 21.
(3) ,, ,, ,, ,, 20.

and on to

(23) Write characters on display 1.
(24) Reset X and Y positions on all displays.
(25) Write characters on display 21.
etc.

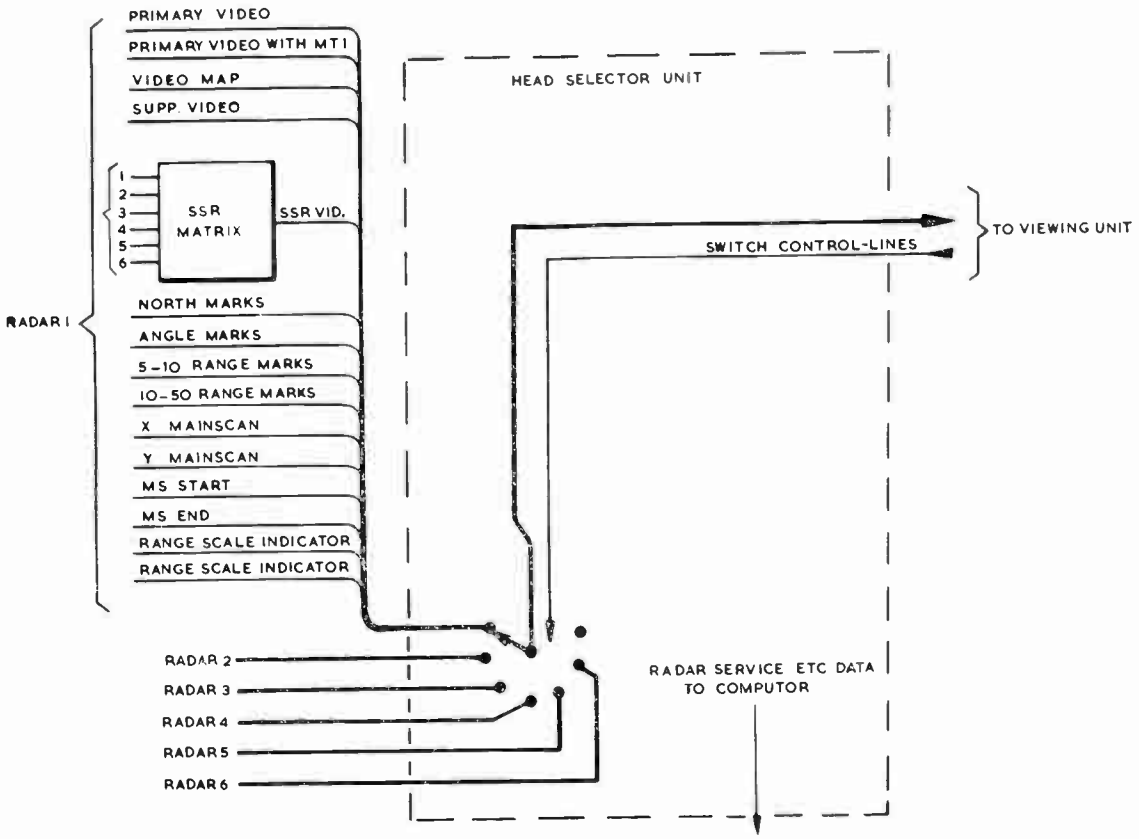

Fig. 4. Radar selection block diagram.

The maximum time to write a complete picture on 21 displays assuming an average buffer queueing time of 8μs is 117·3 ms, thus giving a maximum paint rate of 8·5 c/s.

The data from the buffer unit is passed to the display drive unit via a 24-bit highway and is stored in registers according to its function.

The X, Y positional registers drive all the tabular displays (see Fig. 3) via digital to analogue converters.

The character registers drive the character generators, which provide 'character scan' and 'character video' waveforms; the 'character scan' waveforms drive all displays, but the character video waveform is switched to the selected display only via the display address register, and therefore all displays scan the characters, but only the selected display has video 'bright-up'.

4.5. *The Radar and Synthetic Picture*

As has been mentioned radar and synthetic pictures are provided at all the controller's viewing units, the monitor viewing units and at the large screen display.

The method of driving a controller's viewing unit only is described. The radar and synthetic pictures will be considered separately.

4.5.1. The radar picture

The radar simulator generates simulated radar signals from six individual radar stations, comprising both primary and secondary radar.

The radar signals are derived from individual 'aircraft words' generated by the computer, and in addition the simulator also generates associated synchronizing and rotational waveforms. These waveforms are converted within the main scan generator and timer into the required scan waveforms for the displays, and these waveforms together with the radar simulator video waveforms are connected to a head selector unit. These connections are shown at Fig. 4.

The function of the head selector unit is that of a 7-position 15-pole switch, and it is driven from radar service selection controls in the controller's console control panels. Six of the seven positions of the switches may be used to select one of the six available radars; the seventh position is used to select the synthetic picture, and in this position there is no output of radar data from the head selector. The

selected radar signals are connected to the controller's console, when selection of the required video is carried out with manual controls.

Within the viewing unit certain categories of synthetic pictures are electronically switched in during normal radar pictures. The synthetic pictures concerned are:

(1) Inter-console marking symbols.
(2) Micro-tabular display: this is a display of a small amount of tabular data near the south edge of the c.r.t. of each controller's viewing unit and is intended to be used for the display of s.s.r. codes and modes.
(3) Range and bearing line.
(4) Local rolling ball symbol.

The generation of these synthetic pictures is described together with the synthetic picture.

4.5.2. The synthetic picture

The synthetic picture is composed of two groups of synthetic data: Group I are Synthetic Tracks which are generated within the computer, namely:

(1) Synthetic aircraft positions and data.
(2) Inter-console marking symbols.
(3) Micro-tabular display.

Group 2 are synthetic tracks originating from sources outside the computer. These are generated within the display system and are:

(4) Range and bearing lines
and
(5) Rolling ball markers.

A system block diagram of the synthetic display drive unit is shown at Fig. 5.

Upon receipt of a call from the synthetic drive, the buffer unit will output three 24-bit words for a track message. This track message may be a symbol/vector combination, or a four-character group, and can be specified for one individual display, or be categorized for displays allocated to a category group. The three 24-bit words are staticized in three of the four registers shown in Fig. 5, the choice of the symbol vector or '4-character group' register being made in this case by the state of bit 16 of the first word.

The X and Y positional co-ordinates are converted to analogue voltages and distributed to all viewing units: the symbol/vector or character group registers

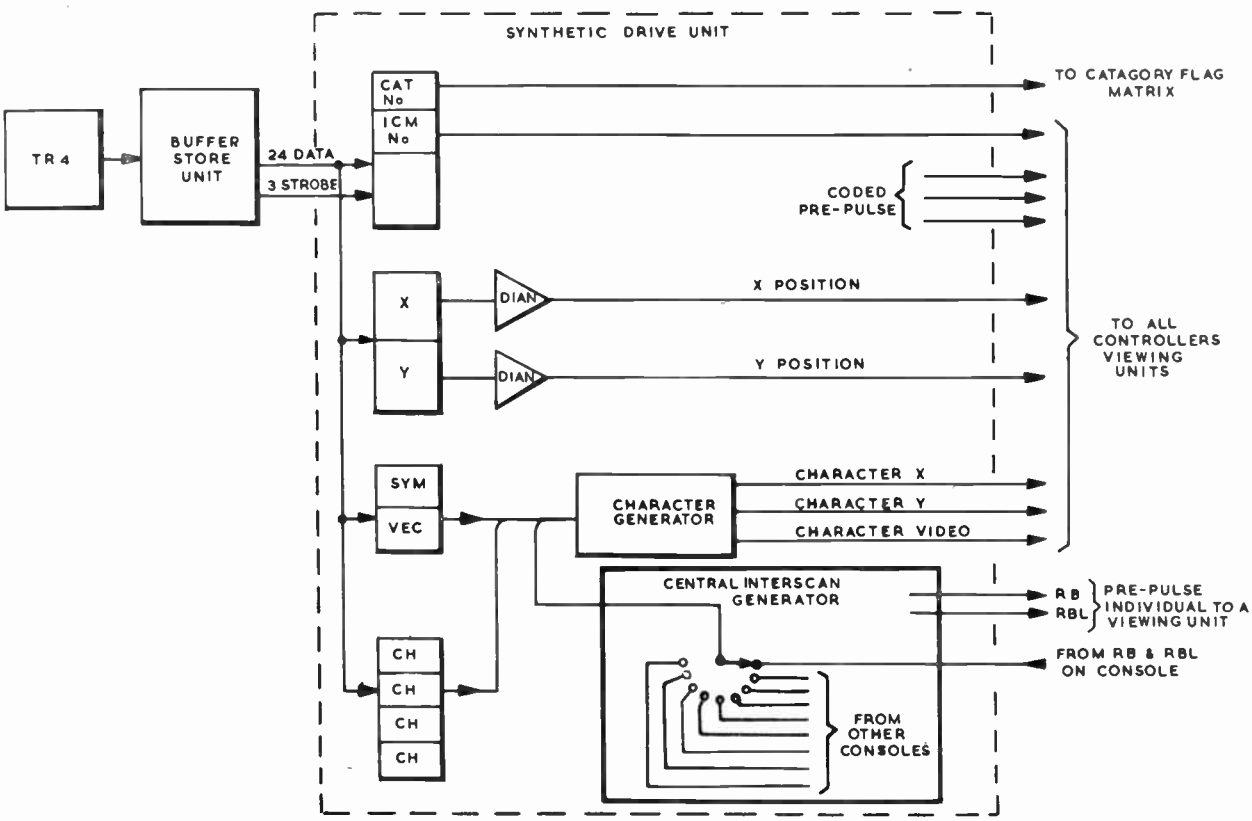

Fig. 5. Synthetic drive system block diagram.

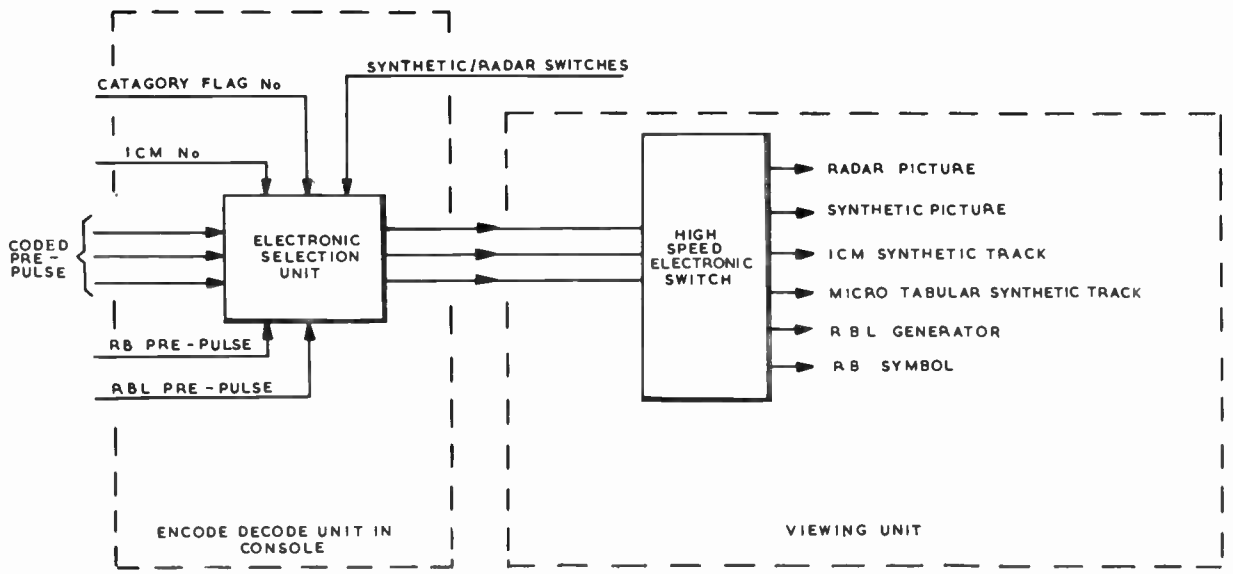

Fig. 6. Showing the selection method in the console with block diagram of the viewing unit.

drive the character generator which produces character X and Y deflection waveforms, and video brilliance waveforms which are fed to all viewing units.

The synthetic drive unit also includes a central interscan generator: this unit on receipt of an end of synthetic picture pulse from the buffer unit sequentially scans all rolling balls and range and bearing line inputs from control positions. This central interscan generation uses the synthetic drive character generator for forming the symbols and the output of the character generator is fed to all viewing units. The individual viewing unit to which this data is to be addressed is selected by a pre-probe line which connects to the electronic selection unit in the console. (See Fig. 6.)

The sequence of operations performed by the synthetic drive unit is therefore as follows:

(1) Calls buffer.

(2) Accepts three 24-bit data words and reads out the output of a track.

(3) Repeats (1) and (2) until all tracks have been read, when the end of the synthetic picture pulse is fed out by the buffer.

(4) Inhibits call to buffer, and scans range and bearing line inputs, feeding the range and bearing line outputs to their respective displays.

(5) Scans the rolling ball inputs and feeds rolling ball marker outputs to their respective displays.

(6) Repeats cycle from (1) above.

As described above all viewing units are fed with the positional X, Y waveforms and the character X, Y and video waveforms, the selection from the viewing unit being carried out by an electronic switch unit within each console and a high speed electronic switch within each viewing unit. (See Fig. 6.)

5. Programming

Four sets of computer programs are being provided with the simulator. These are:

(1) Preparation program for the exercises.

(2) Real-time system operation programs.

(3) Analysis program for analysing the results of exercises.

(4) Replay program to enable reconstitution of an exercise from recorded data.

It will be clear from what has been said that the tremendous flexibility of the system which stems from the program control of all basic parameters of radars, aircraft, navaids, route structure, etc., requires correspondingly extensive facilities for easily programming and modifying the programs of the computer. The Telefunken TR4 computer programs are therefore offered together with a large number of service programs including an ALGOL compiler, a symbolic assembly program (SUSA), a 'translator' program for converting symbolic instructions to machine instructions on a one-for-one basis, and many test and diagnostic programs for debugging, etc.

5.1. *Preparation Program*

This arranges for values of all parameters to be input on punched cards and stored for using during the exercise, input, preliminary sorting and storage on magnetic tape of flight plans with conflict searches as

required, and preparation of all parts of the system including radar simulators and display buffer for the exercise.

5.2. *Real-Time Operation Program*

This consists of the following routines:

(*a*) Master control routine.

(*b*) Processing of manual input data.

(*c*) Production of radar data for all aircraft.

(*d*) Assembly of display data.

(*e*) Data recording and new flight plan processing.

(*f*) Test programs.

The master routine controls entries to the other five routines according to their priorities (i.e. the order given here) at appropriate times obtained from 1 second clock pulses or from externally derived interrupt signals. It also controls all input/output operations. Data recording for analysis and replay purposes is normally done every 2 minutes for all aircraft, on magnetic tape.

5.3. *Analysis Program*

This analyses the data recorded on magnetic tape for up to 20 complete exercises of up to 3 hours each.

5.4. *Replay Program*

This reconstitutes a previous exercise from the recorded data, by calculating and assembling all radar data and assembling data for synthetic displays and tabular displays, ready for output as in the original exercise.

6. Uses of the System

The system is intended to be used by Eurocontrol for studies of European a.t.c. systems: route structures, optimum siting and use of primary and secondary radar, and the exploitation of different types of navaids, can all be examined in a great variety of simulated conditions of traffic density and type as a result of the tremendous scope and flexibility of the simulator. In particular the problems posed by control of supersonic airliners mixed with subsonic and transonic aircraft may be investigated on a practical and realistic basis. The extensive statistical analysis and operational research facilities provided by the analysis programs can be used for *post mortem* studies and to optimize the route structure, radar siting, etc., for maximum efficiency.

A second valuable facility will be to simulate the co-ordination of a network of control centres under various traffic conditions, and to examine changes of control organization and procedure. This is made possible by modifying the layout of the various radar and procedural control and communications modules. Initially the procedures will be based on manual procedural control using surveillance radar, supplemented by full secondary radar facilities. However, the availability of new electronic techniques may be expected to cause gradual evolution of present day procedures towards a more automatic system in which ergonomic considerations and man-machine relationships will become of paramount importance.

A third useful and important field of the simulator could be in training air traffic controllers under a variety of conditions which could occur in operational situations (without any unfortunate effects on real aircraft and passengers). They will also be able to become thoroughly conversant with uses of secondary radar, and in due course with other new equipment such as flight plan processing systems, or the effects of different navaids. It seems clear that the advent of new aircraft and new techniques will produce significant problems in the sphere of training.

It has been noted that initially the simulated procedures will be based on existing control techniques using primary and secondary radar. However, Eurocontrol have stressed that the equipment must be designed from the outset with a view to extension to permit studies of semi-automatic control methods. Thus synthetic plan or tabular displays could be thoroughly tried out using all kinds of different presentations, simply by modifying the computer program.

It will be seen that this simulator represents a significant advance in a.t.c. technology and quite apart from its value in training controllers, promises to provide practical answers to many technical and operational questions that have been argued in principle for years. However it is still too early to forecast the results of the Eurocontrol experiments on the a.t.c. systems of the future.

7. Acknowledgments

The authors wish to thank Plessey Radar Limited and the Eurocontrol Association for kind permission to publish this paper. Thanks are also due to their colleagues who have helped with the preparation of this paper, and in particular to Mr. M. W. Gardner.

Manuscript first received by the Institution on 13th May, 1964 and in final form on 21st June, 1965. (Paper No. 1009/C82).

U.D.C. 511.11:681.3

A Computer Process for the Conversion of Binary-coded Decimal Numbers to Pure Binary Form

By

J. NUTTALL (*Graduate*)†

Summary: This note describes how the process of converting binary-coded decimal numbers to binary may be speeded up by reducing the number of additions necessary.

1. Number Representation

Numbers are represented in many large computers in binary form and as binary notation is not readily understood in everyday usage, it being too cumbersome, conversion processes between binary and decimal codes must be performed before the result of a computation can be understood.

The way in which decimal numbers are held in a computer's store, after input from a tape reader for example, is in the form of a binary code. These numbers are said to be in 'binary-coded decimal'. Often a binary-coded decimal number is directly related to the binary value of the character. For example its least significant four bits may be the actual binary value of that number and the most significant two digits (of a six-bit character say) may indicate that this is a number (or letter). For example, the least significant four bits of each of several characters which make up the number 1964, are:

0001, 1001, 0110, 0100

where the commas separate the characters.

2. Conversion

A common form of conversion is to multiply the left-most character by ten (in binary) and to add the next character to it. The result is then multiplied by ten and the next character added, and so on until the number is in binary form.

Now for each character we have one addition to multiply by ten (twice the number plus eight times the number) followed by a second addition to add the next character. Hence for an n digit number we perform $2(n-1)$ additions. For example, to convert the number 9874, proceed as shown in Table 1.

Table 1

1001,1000,0111,0100	Number 9874
1001	9×
1010	10
1001000	9×8
1001	9×2
1011010	90
1000	+8
1100010	98×
1010	10
1100010000	98×8
11000100	98×2
1111010100	980
0111	+7
1111011011	987×
1010	10
1111011011000	987×8
11110110110	987×2
10011010001110	9870
0100	+4
10011010010010	9874

A faster method

When counting in the decimal system a carry is taken to a column each time that the count in the column to its right would become ten. If however, the counting was being performed in the octal system a carry would be generated when the count in the column reached eight. Thus in order to convert a decimal to an octal number, for every unit in a column of a decimal number the total in the column to its right should be two greater for the equivalent octal number. For example:

$23_{10} = 27_8$ The suffixes denote the radix.

This is performed simply by multiplying the 2 in the left-hand column by 2 (in octal) and adding to the 3. Any carry from this addition is added in as normal.

† English Electric-Leo-Marconi Computers Ltd., Kidsgrove, Staffordshire.

For larger numbers this process is continued, conversion starting from the left (see Table 2).

Table 2

2756_{10}	2756	
	4	2×2 and shift
	3356	add
	66	2×33 and shift
Note that the arithmetic must be performed in octal.	4236	add
	1046	2×423 and shift
	5304_8	add

Now to convert a decimal number to binary it is only necessary to convert to binary-coded octal which is the same thing.

First of all consider a decimal number which has less than eight in any one column, e.g. 276. Coding this in binary-coded decimal it becomes 010,111,110 and this may be converted by working in binary as shown in Table 3.

Table 3

010,111,110	
0,10	shift 1st number 2 places right
011,011,110	and add
0,110,11	shift 1st two characters right
100,010,100	and add
	Hence the binary number.

The process requires one further refinement; it is obviously not possible to code 8 or 9 in three bits, neither can this 'overflow bit' be added to the next most significant number position initially as the number is still in the binary-coded decimal state and this will be a tens carry not an octal carry.

However, once the addition operation has been carried out on the associated sets of digits the carry may be added in. This 'carry' is therefore staticized separately until the completion of the addition, as shown in Table 4.

It is possible, however, to add the 'carry' in at the same time as its associated conversion addition. This can be accomplished with a normal three-input adder because there cannot be both a 'carry' from the fourth position of the binary-coded decimal character and a normal carry from the third position. If both

Table 4

789	
1 1	'carrys'
111,000,001	number
1,11	shift and add 1st character
1,000,110,001	add m.s. carry
1,001,110,001	shift and add next set of characters
10,011,10	
1,100,001,101	add
1,100,010,101	add 2nd carry

occurred, the binary character would be twelve, which is impossible (or wrong!).

If there is a 'carry' in the most significant position to start with (from such a number as 971 for example), then this carry is added in before any conversion, being treated thus because there is no associated conversion addition to the left. Any 'carry' is in fact added in during the addition of the character to the left of the one from which the 'carry' originated. Note that the characters must be shifted before this 'carry' is added.

The further example in Table 5 should make the process clear.

Table 5

9874	
1 1	'carrys'
001,000,111,100	number
1,001,000,111,100	add carry (OR-gate, not an addition)
10,01	shift 1st character
1,100,010,111,100	add (and carry)
11,000,10	shift
1,111,011,011,100	add
11,110,110,11	shift
10,011,010,010,010	add, forming binary number

Thus as the carry is added at the same time as a conversion addition an n digit number may be converted from decimal to binary with $n-1$ additions. The suggested conversion process is therefore twice as fast as the more conventional approach.

Manuscript first received by the Institution on 26th May 1964 and in final form on 3rd March 1965. (Contribution No. 86/C83).

I.E.C. PUBLICATIONS

The following publications have been issued by the International Electrotechnical Commission in recent months. Copies are obtainable from the Sales Department of the British Standards Institution, 2 Park Street, London, W.1.

IEC 68: 1964 'Basic environmental testing procedures for electronic components and electronic equipment'.

I.E.C. Publication 68 describes a standard general procedure for climatic and mechanical robustness tests designed to assess the durability under various conditions of use, transport and storage, of electronic components and electronic equipment. It is issued in the form of several booklets which are described below.

I.E.C. 68–1 Part 1: General 18*s.* 9*d.*

This gives a general description of the framework of the test procedure and how it is to be used.

I.E.C. 68–2 Part 2: Tests £3 12*s.* 6*d.*

This describes the different tests in detail and is issued in the form of separate booklets; each test is identified by a letter of the alphabet. For example:

I.E.C. 68–2–11 6*s.* 3*d*

This part describes Test Ka, which determines the resistance of a component to deterioration from salt mist. The test is intended mainly for evaluating the quality and uniformity of protective coatings, particularly for similar materials on a comparative basis.

I.E.C. 117–6: 1964. 'Recommended Graphical Symbols', Part 6: 'Variability, Examples of Resistors, Elements of Electronic Tubes, Valves and Rectifiers.' 33*s.* 9*d.*

This publication replaces the former Publications 35 and 42 which deal respectively with graphical symbols for heavy and light current electrical engineering. When complete, Publication 117 will include symbols for all branches of electrical technology. In order not to delay publication of available sections, it is being issued in parts as and when these are approved.

Part 6 contains some 85 symbols dealing with variability, examples of resistors, elements of electronic tubes, valves and rectifiers.

I.E.C. 151: 1964. 'Measurements of the electrical properties of electronic tubes and valves', Part 7: 'Measurement of equivalent noise resistance'. 10*s.*

Part 7 of the I.E.C. Publication 151 'Measurements of the electrical properties of electronic tubes and valves' gives methods based on current practice of measurement of equivalent noise resistance of electronic tubes and valves due to shot effect and partition noise.

I.E.C. 167: 1964. 'Methods of test for the determination of the insulation resistance of solid insulating materials'. 20*s.* 3*d.*

This publication describes procedures for determining rapidly the values of insulation resistance to give a general indication of quality, when great accuracy is not required. The rapidity of these methods is due to the ease with which the test specimens can be prepared.

The methods give values of resistance which include both volume and surface resistance. Consequently they do not give well-defined constants for materials, in contrast to the recommended methods of test for volume and surface resistivities given in I.E.C. Publication 93. However, empirical values which can be used for comparing the quality of different insulating materials are given. These values are very useful for determining the influence of moisture on hygroscopic insulating materials, in which conditioning appreciably modifies not only the insulating properties of the surface but also those of the body of the material.

I.E.C. 169: 1965. 'Radio-frequency connectors', Part 1: 'General requirements and measuring methods'. 60*s.*

The first part of I.E.C. 169 'Radio-frequency connectors' has recently been issued. It relates to connectors for r.f. transmission lines for use with electronic equipment and provides general requirements and measuring methods. It establishes uniform requirements for the electrical, climatic and mechanical properties as well as safety aspects; for test methods; for interchangeability and compatibility both between connectors and between connectors and cables; and for classification of connectors into groups according to their ability to withstand extremes of temperature and humidity.

This Recommendation is intended to be used in conjunction with other I.E.C. publications, such as Publications 68 (see above) and 96 'Radio-frequency cables.' Parts laying down detailed specifications for different types of connectors will be issued as they become ready.

I.E.C. 181: 1964. 'Index of electrical measuring apparatus used in connection with ionizing radiation'. 45*s.*

The aim of this index is to facilitate the study of the instruments by giving each a recognized title and clear definition. It covers measuring instruments currently manufactured, or likely to be so in the near future, and additions will be made to it as the need arises. As a general rule, the instruments mentioned do not include the terminal apparatus which supplies the information unless it forms an integral part of the apparatus.

In the field of control and safety of nuclear reactors, the Recommendation defines certain apparatus which does not belong to the category of electrical measuring instruments, but is included in view of the necessity of considering nuclear reactor instrumentation as a whole.

I.E.C. 194: 1965. 'Terms and definitions for printed circuits.' 11*s.* 8*d.*

This new I.E.C. publication contains 47 internationally agreed terms and definitions relating to printed circuits.

A Guide to International Recommendations

The British Standards Institution has published a separate catalogue of the publications of four international standards bodies—I.S.O. (International Organization for Standardization), I.E.C. (International Electrotechnical Commission), C.E.E. (International Commission on the Rules for the Approval of Electrical Equipment) and C.I.S.P.R. (International Special Committee on Radio Interference)—which expands and brings up to date to 30th June 1965 the relevant information in the current British Standards Yearbook.

The new catalogue includes a numerical list giving the title of each international publication, a brief summary of its contents and an indication of its relationship with the equivalent British Standard. A table shows in numerical order all British Standards to which there are corresponding international publications with the appropriate cross-references to these publications. The price is 7*s.* 6*d.* plus postage to non-members.

Radio Engineering Overseas . . .

The following abstracts are selected from Commonwealth, European and Asian journals received by the Institution's Library. Abstracts of papers published in American journals are not included because they are available in many other publications. Members who wish to consult any of the papers quoted should apply to the Librarian, giving full bibliographical details, i.e. title, author, journal and date of the paper required. All papers are in the language of the country of origin of the journal unless otherwise stated. Translations cannot be supplied.

SKY-WAVE DIRECTION FINDER

A directional antenna system and a visual-display direction finder based on the double-channel principle, which is discussed in a German paper, permits error-free direction finding of the ground waves in the presence of sky waves under anomalous polarization conditions and for different elevation angles. The method yields simultaneously the elevation angle of the sky wave and the directional sense of the incident waves. The screen displays obtained with visual-display radio direction finding of different transmitting stations are illustrated.

"A method for sky-wave error-free direction finding in the presence of ground and sky waves", H. Gabler and M. Wächtler, *Archiv der Elektrischen Ubertragung*, **18**, No. 11, pp. 657–62, November 1964.

END-FIRE ARRAY

A Canadian paper derives the directivity formula of a very long end-fire array made up of a continuous line of isotropic radiators by assuming a sine-modulated current amplitude along the axis and constant phase difference from element to element.

Sample calculations are given for an array of 40 wavelengths. The directivity of the array is found to depend on the phase velocity and the modulation coefficient; and the optimum directivity of this array is found to be greater than that of a Hansen-Woodyard array of the same length.

"Amplitude-modulated end-fire array", *Canadian Journal of Physics*, **43**, pp. 155–62, January 1965.

TELECOMMUNICATIONS IN AUSTRALIA

A recent Australian paper discusses the planning, design and operational features of a major Post Office project involving the reconstruction of over 1,000 miles of aerial trunk route between Port Augusta, South Australia, and Kalgoorlie, Western Australia. The project employs a number of constructional techniques not previously used in Australia. These methods, which have resulted in large savings in manipulative effort, are described and illustrated, and the electrical and mechanical design aspects of the project are discussed.

In addition, the telecommunication requirements between Perth and Eastern States are reviewed, and a description is given of the plans for the future provision of a new high-capacity broadband system between Perth and Adelaide. Such a system will provide adequate telephone, telegraph or data channels, plus a television relay channel when required.

"Telecommunication facilities between Western Australia and the Eastern States", F. I. C. Taylor, J. A. Huston, and G. E. J. Sayer, *The Journal of The Institution of Engineers, Australia*, **37**, No. 9, pp. 219, September 1965.

AUDIO FREQUENCY LEVEL MEASUREMENT IN BROADCASTING

The dynamic control of the audio-frequency programme signals in sound and television broadcasting is a subject which has never ceased to be controversial, especially as regards the choice of the really appropriate measuring instrument. A statistical study of the audio signal was undertaken by the Office de Radiodiffusion-Télevision Française in order to determine the basic principles of a more suitable instrument than those in current use.

A statistical law of general application has been derived from the results, which suggests clearly a parameter that has hitherto been ill defined and which it is proposed to call the *slope* of the signal. The unvarying nature of this parameter for a programme of a given type makes it possible to envisage a utilization of this idea for the automatic or semi-automatic determination of the dynamic range of a transmission. On the practical plane, the principles of an a.f. level indicator which effectively measures the energy by a counting process are given; a prototype of this instrument is being constructed.

"Statistical investigation of the audio signal with special reference to its dynamic control", J. Guillermin, *E.B.U. Review*, No. 88–A, pp. 250–59, December 1964.

MAGNETIC FREQUENCY DIVIDER

Electrical circuits comprising non-linear elements can be used for producing so-called subharmonic oscillations with a frequency which is the nth part of the input frequency (n is an integer number greater than 1). The network need not contain any active elements but in this case the occurrence of the subharmonic oscillation also depends on the initial conditions of the circuit.

The author of a German paper shows that this dependency can be avoided by using a special circuit which can be described by a third order non-linear differential equation, and quotes experimental results from circuits in which the input frequency is divided in a single step by $n = 2, 3 \ldots 15$. Such an arrangement can also be used to divide the frequency of pulses, as may be seen in oscilloscope pictures for a division by $n = 2$, 3 and 7.

"A magnetic frequency divider", E. Lüder, *Nachrichten Technische Zeitschrift*, **18**, No. 18, pp. 463–469 August 1965.

The June 1965 issue of *L'Onde Électrique* (Vol. 45, No. 459) is a special bi-lingual (French/English) edition. It is devoted to articles describing the installations in Broadcasting House in Paris (La Maison de l'O.R.T.F.), and also contains a 56-page review of the 1965 Paris Components Exhibition which was held in April.